First Stereoscopic 3D Measurements of Coronal Loops, Moss, Filaments, & CMEs

Markus J. Aschwanden
Jean-Pierre Wuelser, Jim Lemen, Nariaki Nitta, Anne Sandman
(LMSAL)
& G. Allen Gary (UAH)

STEREO Science Working Group #17
CALTECH, Pasadena, California, 13-14 Nov 2007

Contents :

(A) Triangulation and 3D reconstruction of active region loops

- A1) Image coalignment
- A2) Triangulation and 3D geometry
- A3) Image highpass filtering & loop definition
- A4) Loop tracing
- A5) Stereoscopic 3D coordinates and error of z(x,y)
- A6) Loop inclination, coplanarity, & circularity
- A7) Hydrostatic modeling
- A8) Magnetic modeling

(B) Outlook for 3D reconstruction of other EUV phenomena

- B1) Moss
- B2) Filaments and prominences
- B3) CMEs

Conclusions

May 2007

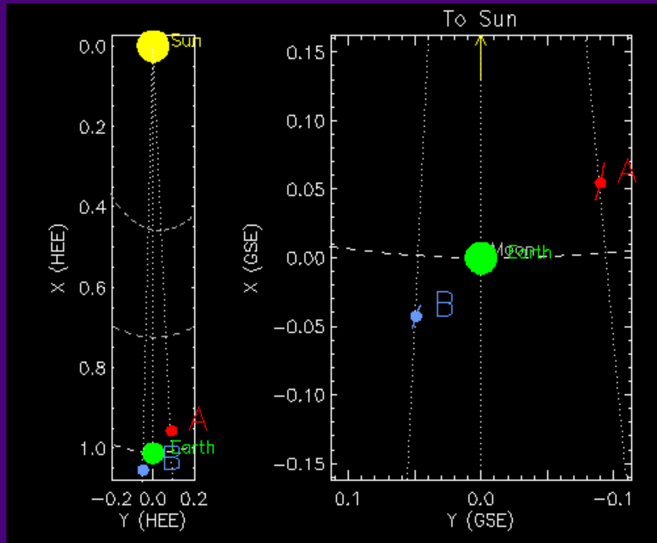

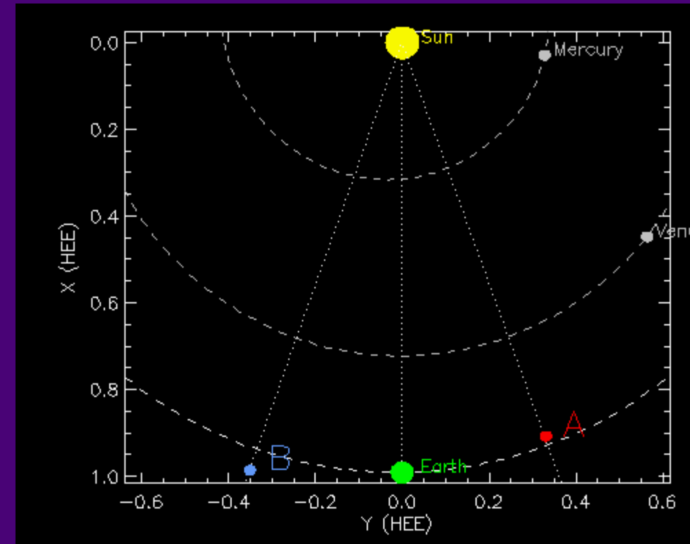

Nov 2007

STEREO A-B separation angles

(2007 is prime phase for small-angle stereoscopy)

Date	B (deg East)	A(deg West)	A-B(deg separation)
2007-Jan-1	0.151	0.157	0.009
2007-Feb-1	0.167	0.474	0.623
2007-Mar-1	0.169	1.061	1.229
2007-Apr-1	0.740	2.307	3.032
2007-May-1	1.888	4.213	6.089
2007-Jun-1	3.762	6.843	10.600
2007-Jul-1	6.196	9.810	16.004
2007-Aug-1	9.211	12.975	22.186
2007-Sep-1	12.525	15.871	28.396
2007-Oct-1	15.764	18.127	33.891
2007-Nov-1	18.830	19.744	38.574
2007-Dec-1	21.216	20.660	41.876
2008-Jan-1	22.837	21.182	44.018

Stereoscopic 3D Reconstruction Methods:

(a) Solar-rotation stereosocopy

(b) Two-spacecraft stereoscopy

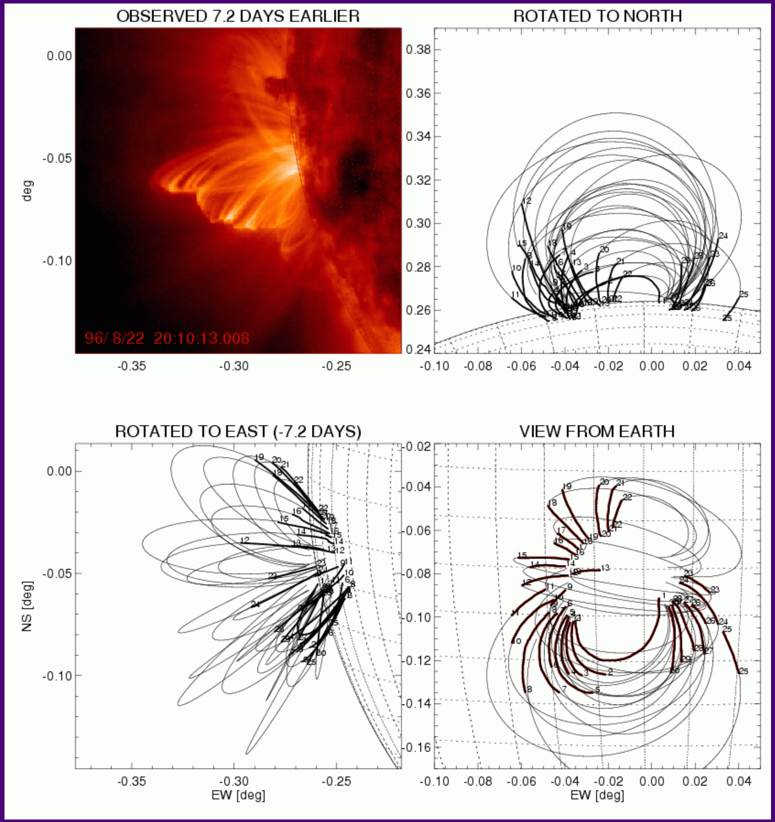

Aschwanden et al. (1999) - SoHO/EIT

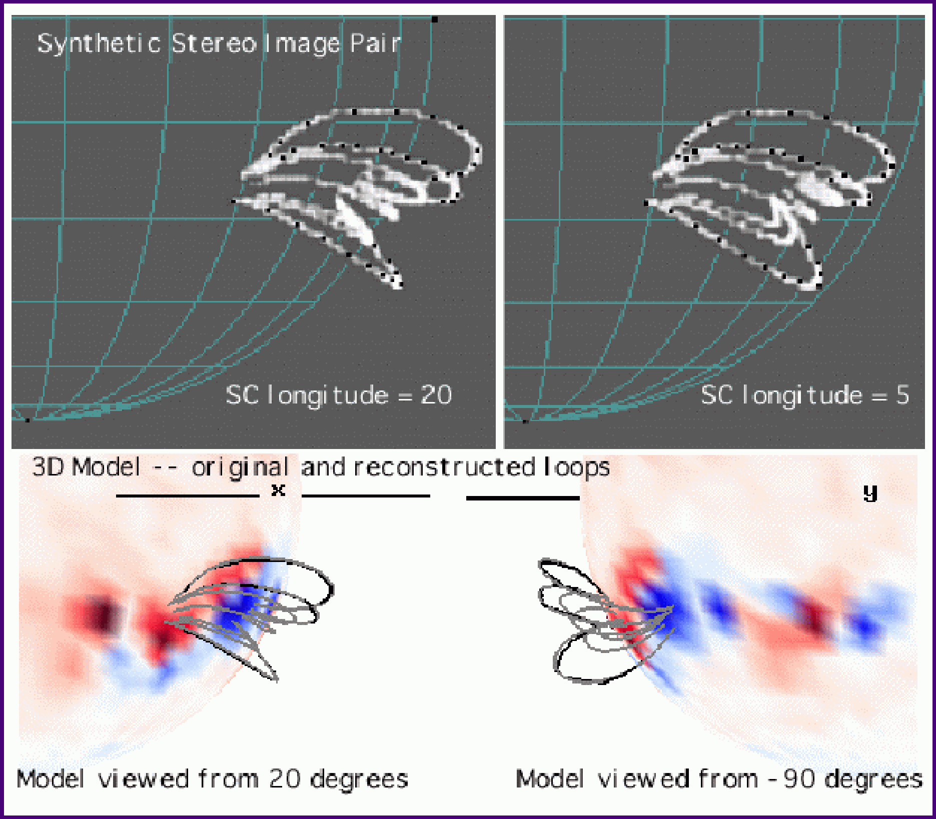

STEREO A+B (2007)

-Parallax measurement
as a function of time (>1 day)
-requires quasi-stationary loops

-Parallax measurements
simultaneously from 2 spacecraft
images at different positions

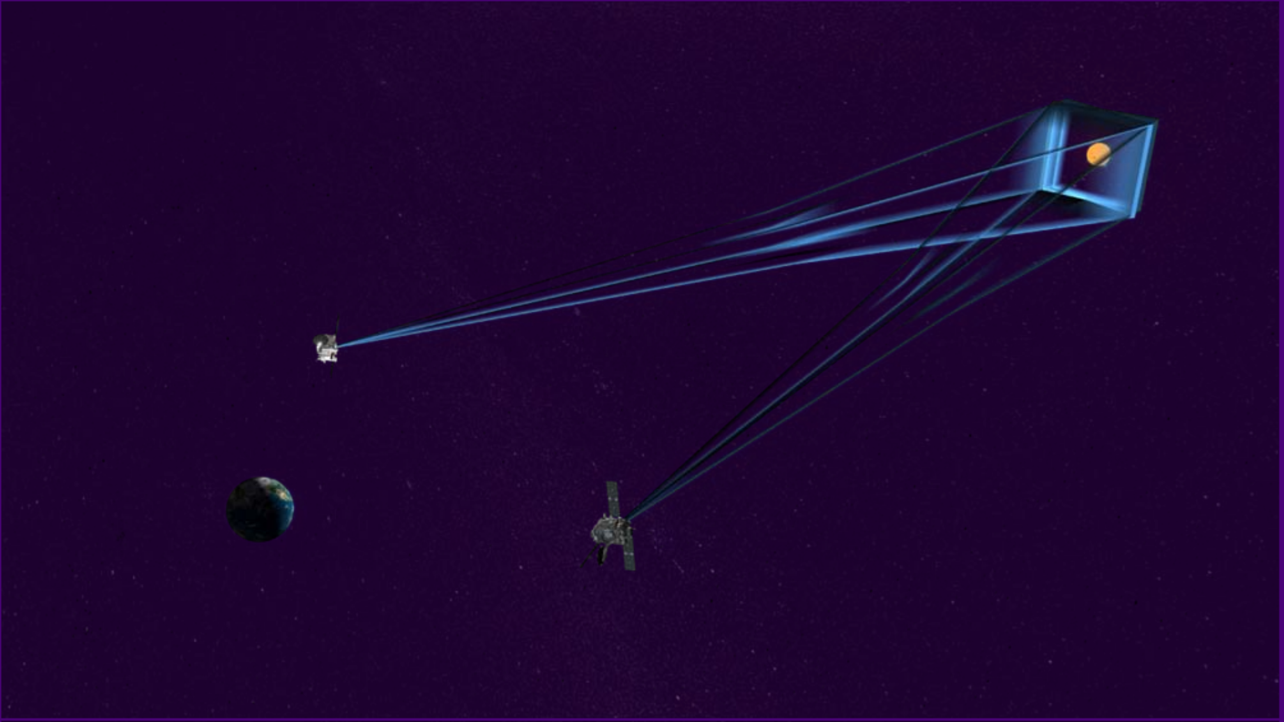

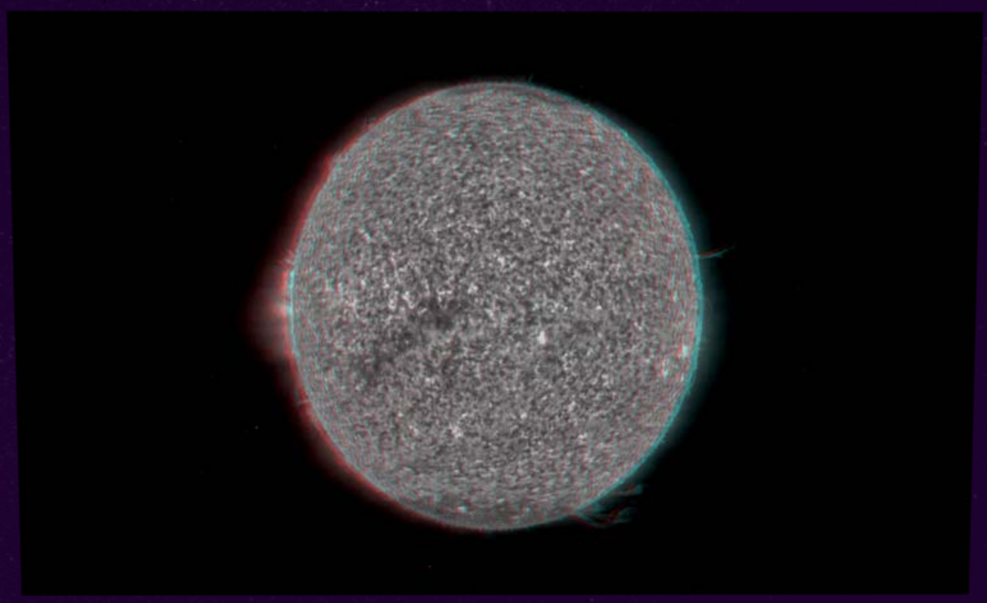

Data Analysis Steps:

Spacecraft A:
- distance to Sun d_A
- heliocentric longitude l_A
- roll angle r_A

Spacecraft B:
- distance to Sun d_B
- heliocentric longitude l_B
- roll angle r_B

Coaligment of images:
- rebin pixel sizes (dist. d_A)
- rotate image A by -r_A
- rotate image B by -r_B
  to ecliptic plane
  (epipolar stereoscopic plane)

SSW software (IDL routines)
See EUVI data analysis tools
with tutorials on
http://secchi.lmsal.com/EUVI/

A1) Image Coaligment

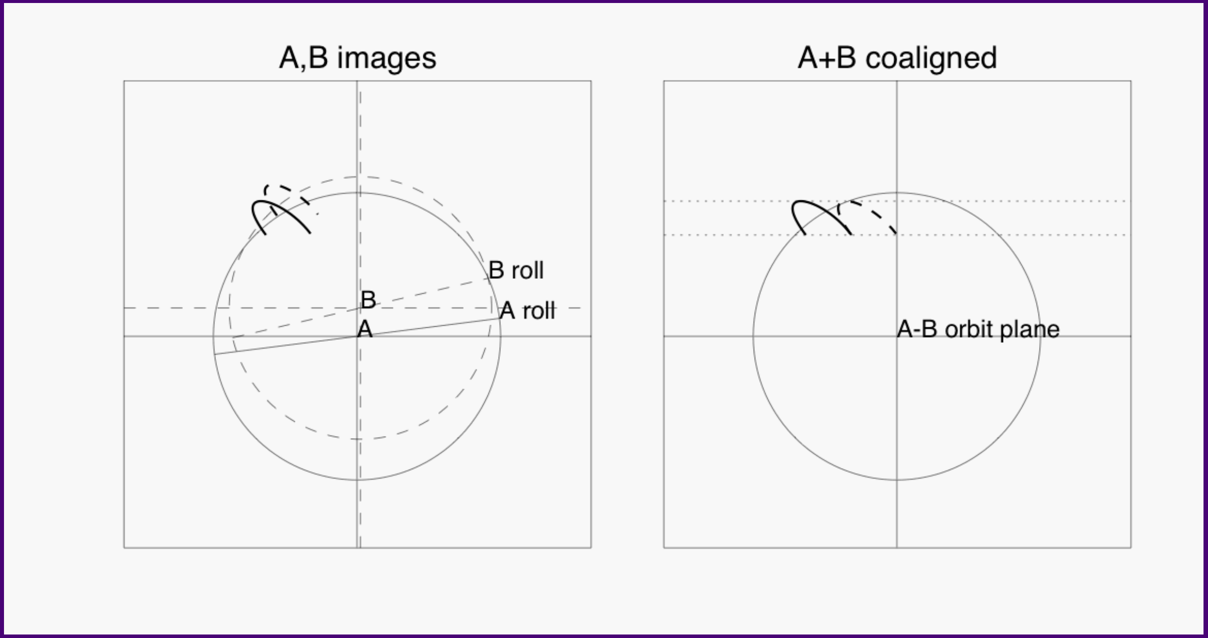

Spacecraft B:
- distance to Sun d_B
- heliocentric longitude l_B
- SC roll angle r_B
- Sun center offset x_B0

Spacecraft A:
-distance to Sun d_A
- heliocentric longitude l_A
- SC roll angle r_A
- Sun center coordinate x_A0

3 coalignment steps:
- rebinning both images to distance d_A
- coaligning Sun center to x_A0
- rotating images by roll angle into spacecraft A-B plane (epipolar stereoscopic plane)

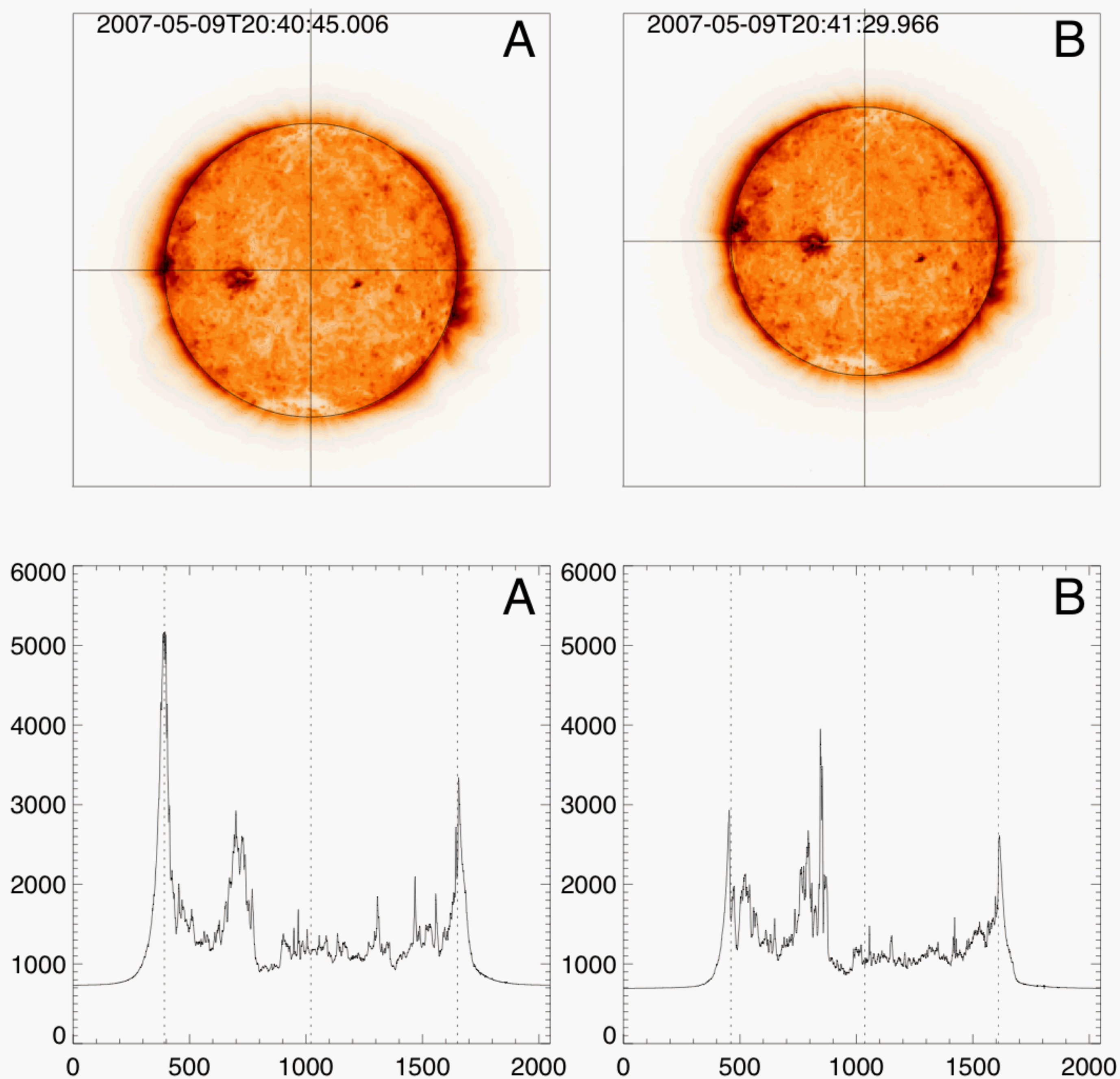

2007-05-09T20:40:45.006
A
2007-05-09T20:41:29.966
B
A
B
0
1000
2000
3000
4000
5000
6000
0
500
1000
1500
2000

2007 May 9, 20:40:45 UT, 171 A, STEREO-A, EUVI

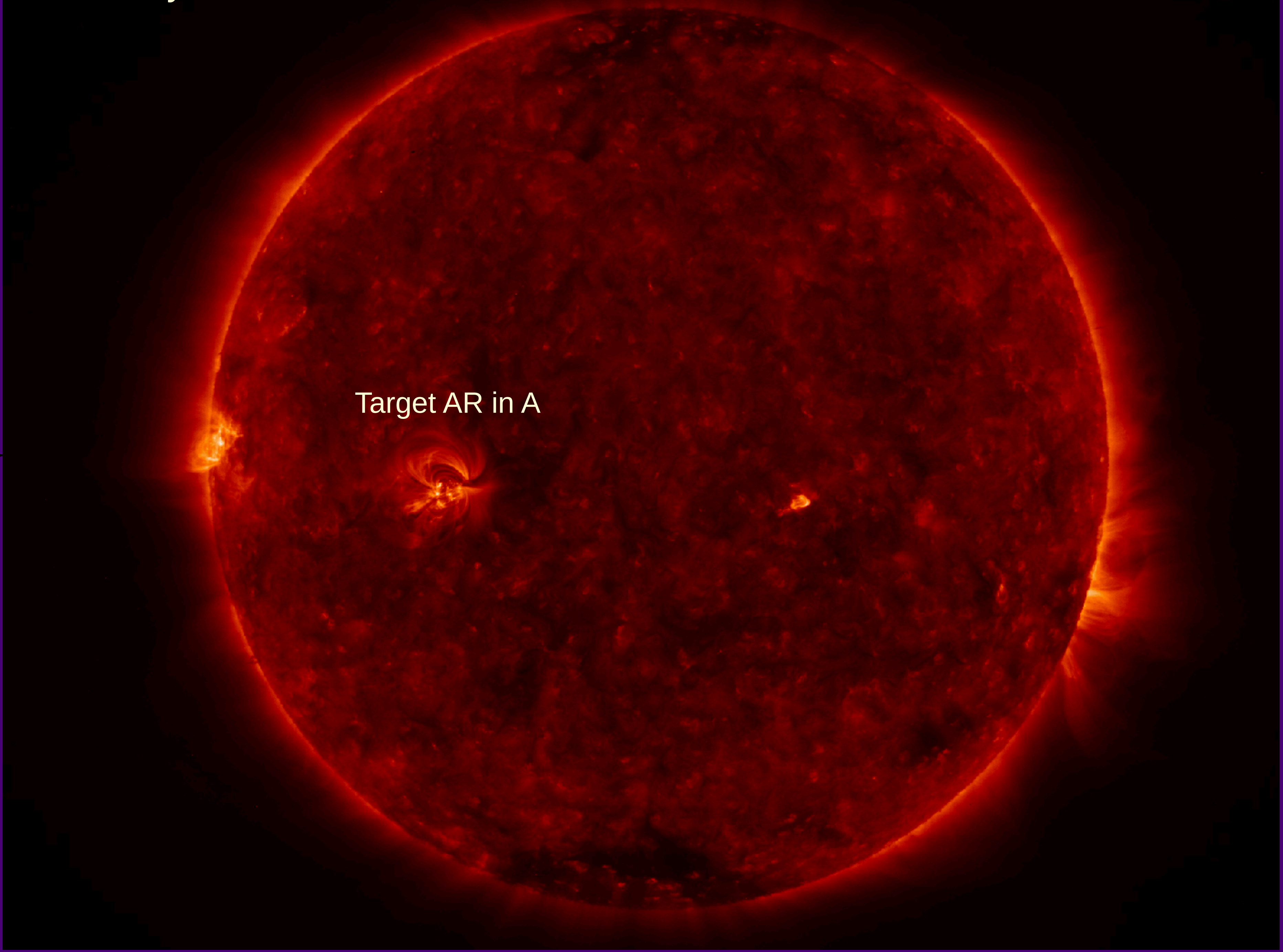

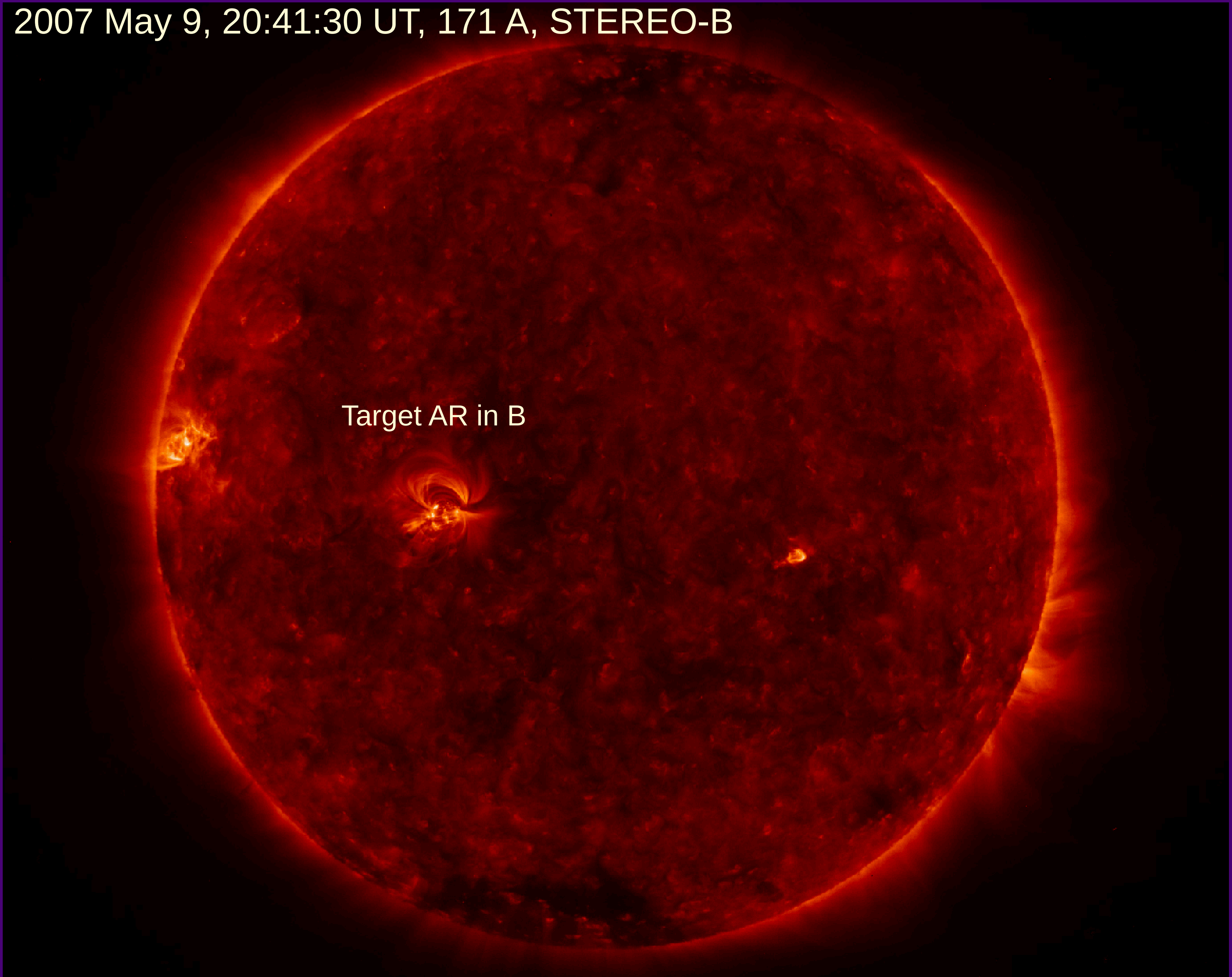
2007 May 9, 20:41:30 UT, 171 A, STEREO-B
Target AR in B

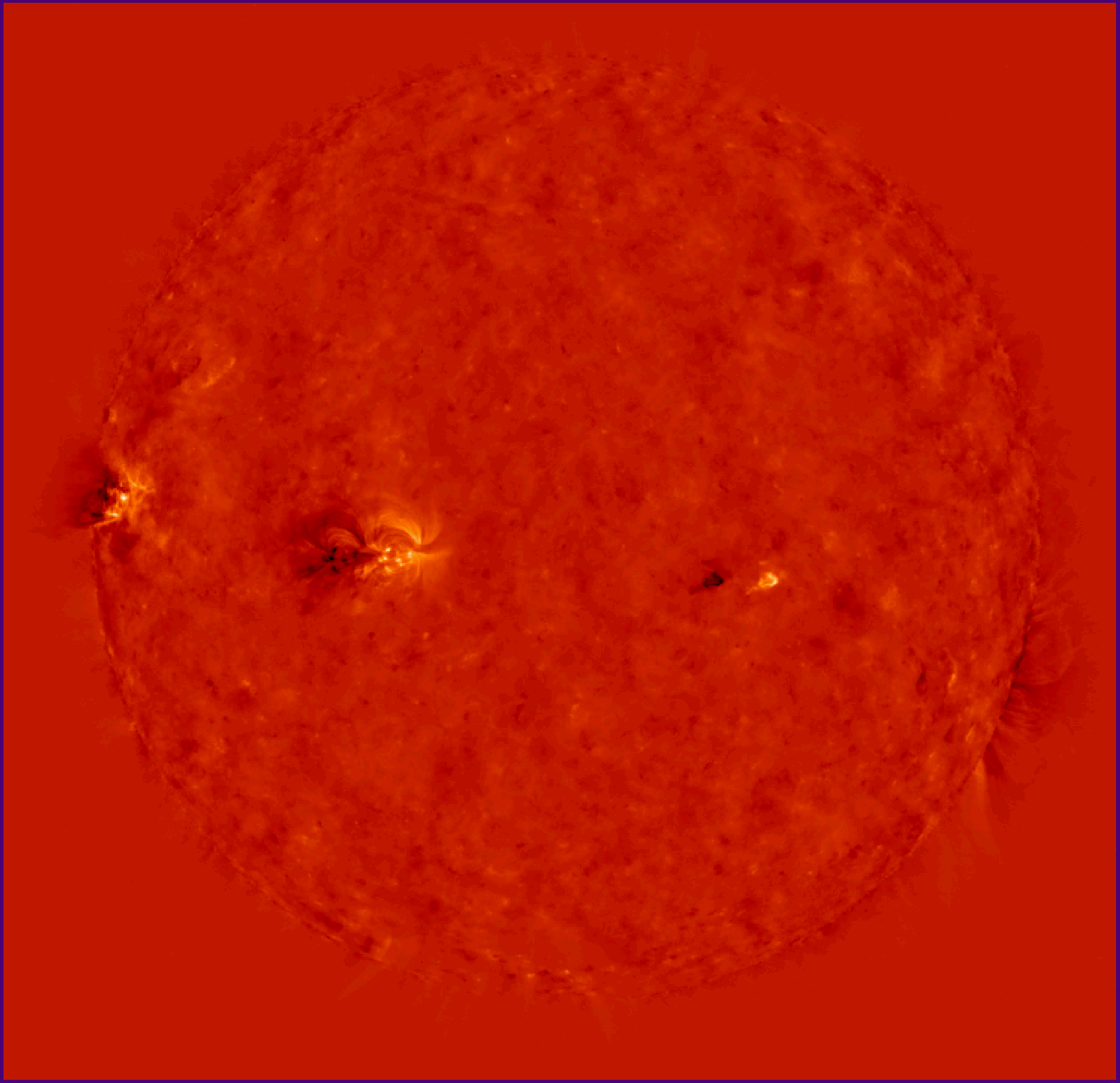

Difference of coaligned STEREO A-B images:

no gradients at limb visible if perfectly coaligned

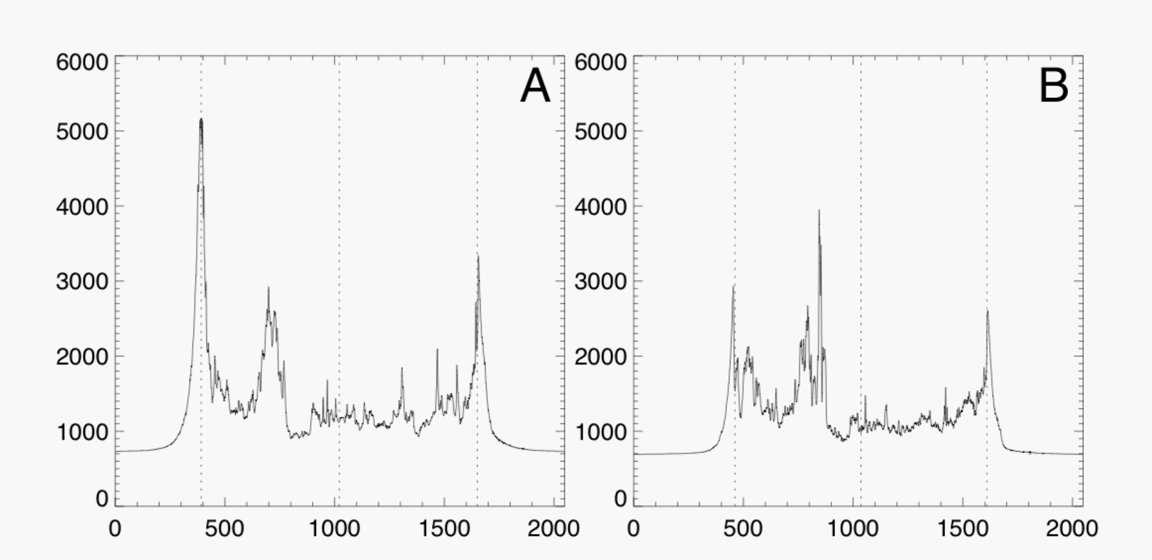

Coalignment testing
of offset dx and dy
by minimizing flux
differences at limb.

Result: dx=-0.11±0.03 pixel
dy=+0.24±0.20 pixel

d_roll = +1.0^0

d_roll = +0.0^0

d_roll = -1.0^0

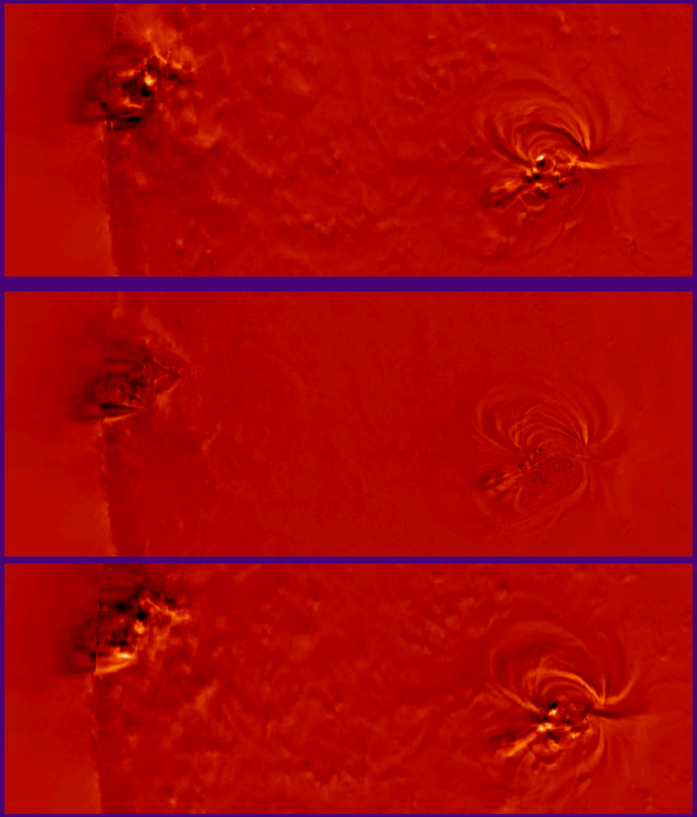

Coalignment testing
of roll angle offset
by minimizing flux
differences in
images rotated to
same stereoangle and by
varying relative roll angle.
(photospheric features
disappear).

Result: d_roll=0.01±0.05 deg

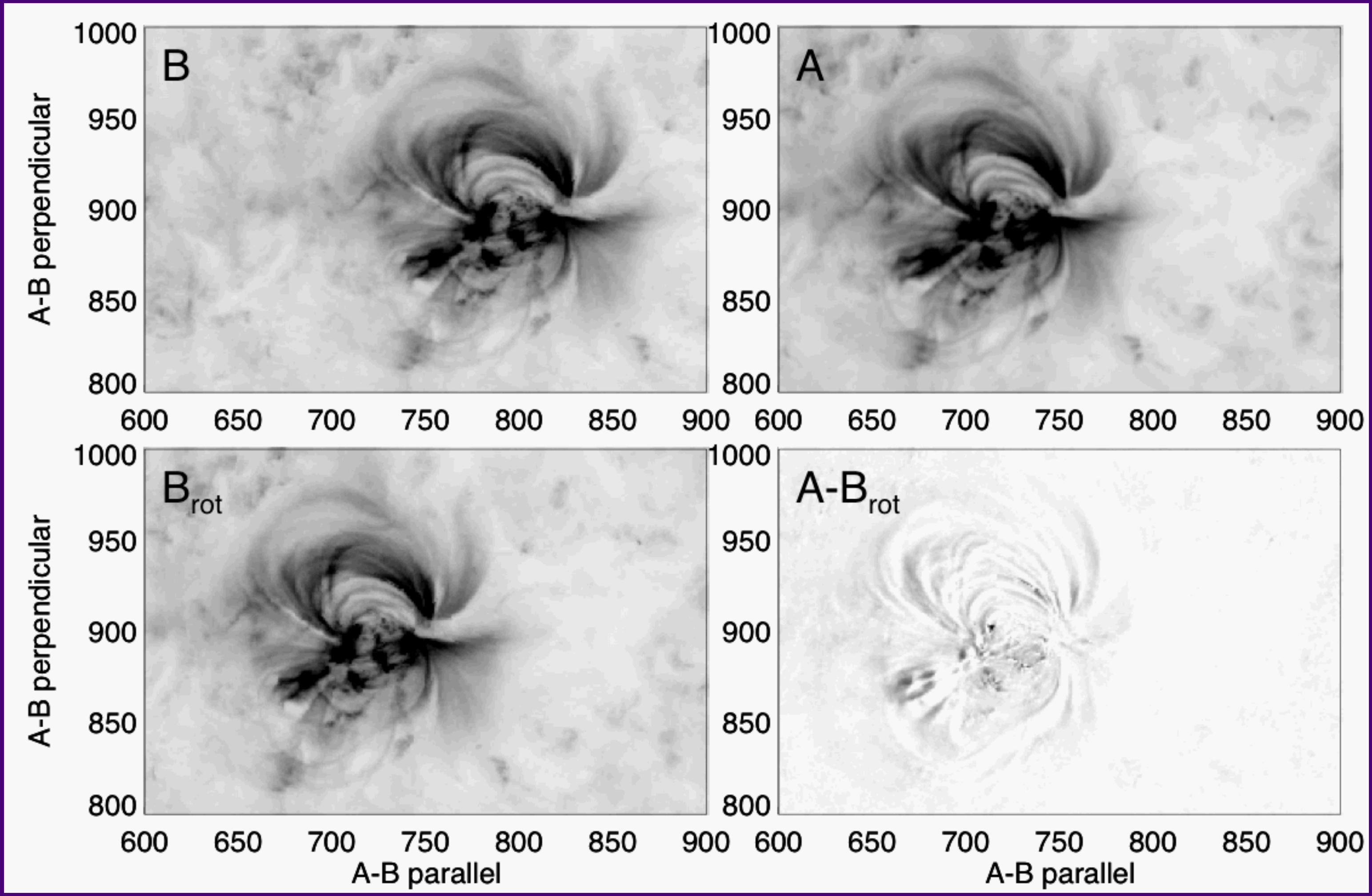

Coalignment test: Rotate image B to same stereo angle as image A and plot difference: photospheric features disappear.

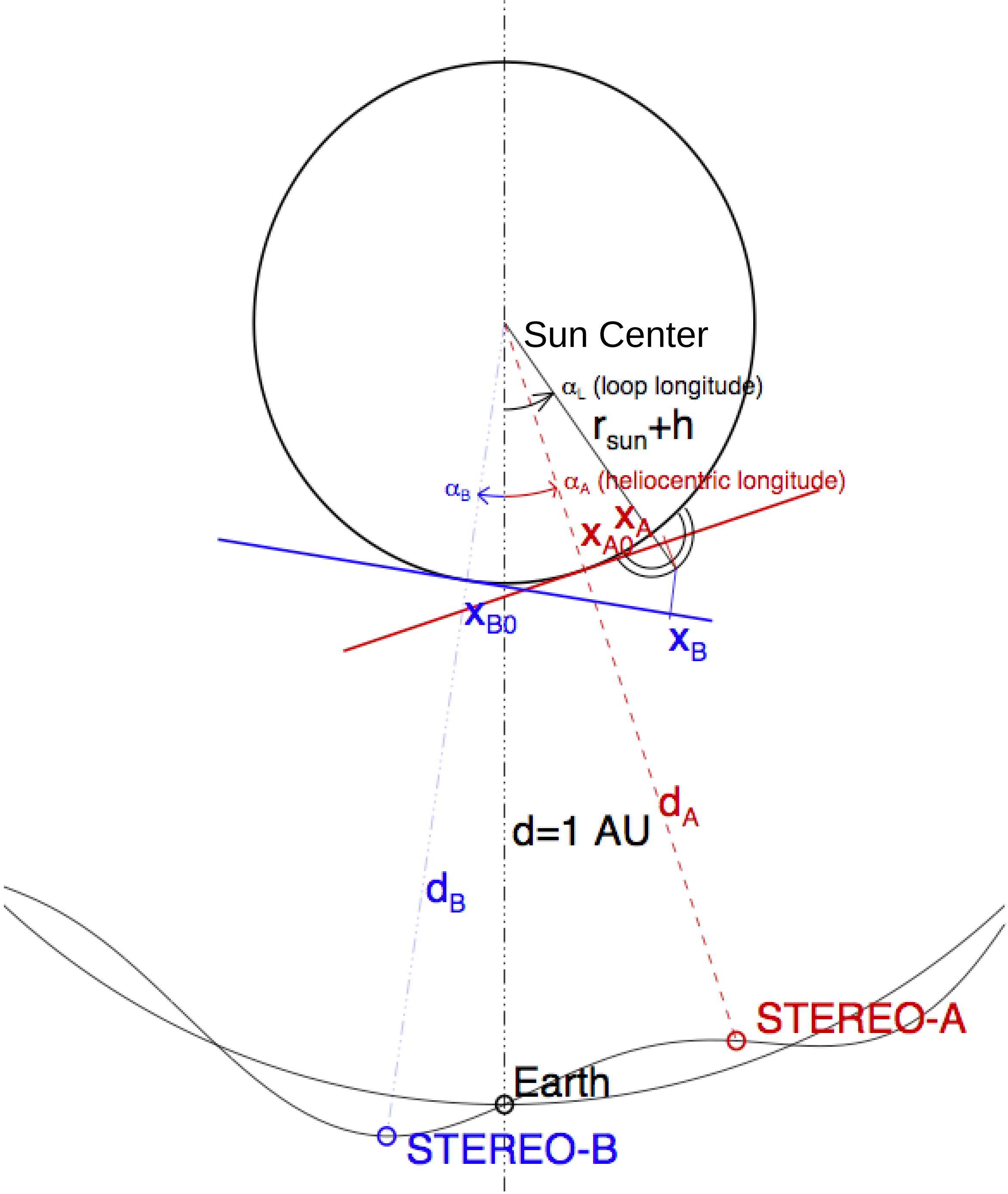

A2) Geometry of stereoscopic parallax

l_A = heliocentric longitude of loop
in STEREO-A image
l_B = heliocentric longitude of loop
in STEREO-B image
x_A = x-coordinate of loop in image A
x_B = x-coordinate of loop in image B
x_A0 = x-coordinate of Sun center in A
x_B0 = x-coordinate of Sun center in B
r_Sun = solar radius
h = altitude of loop location
α_A = heliocentric longitude of SC A
α_B = heliocentric longitude of SC B
α_L = heliocentric longitude of loop

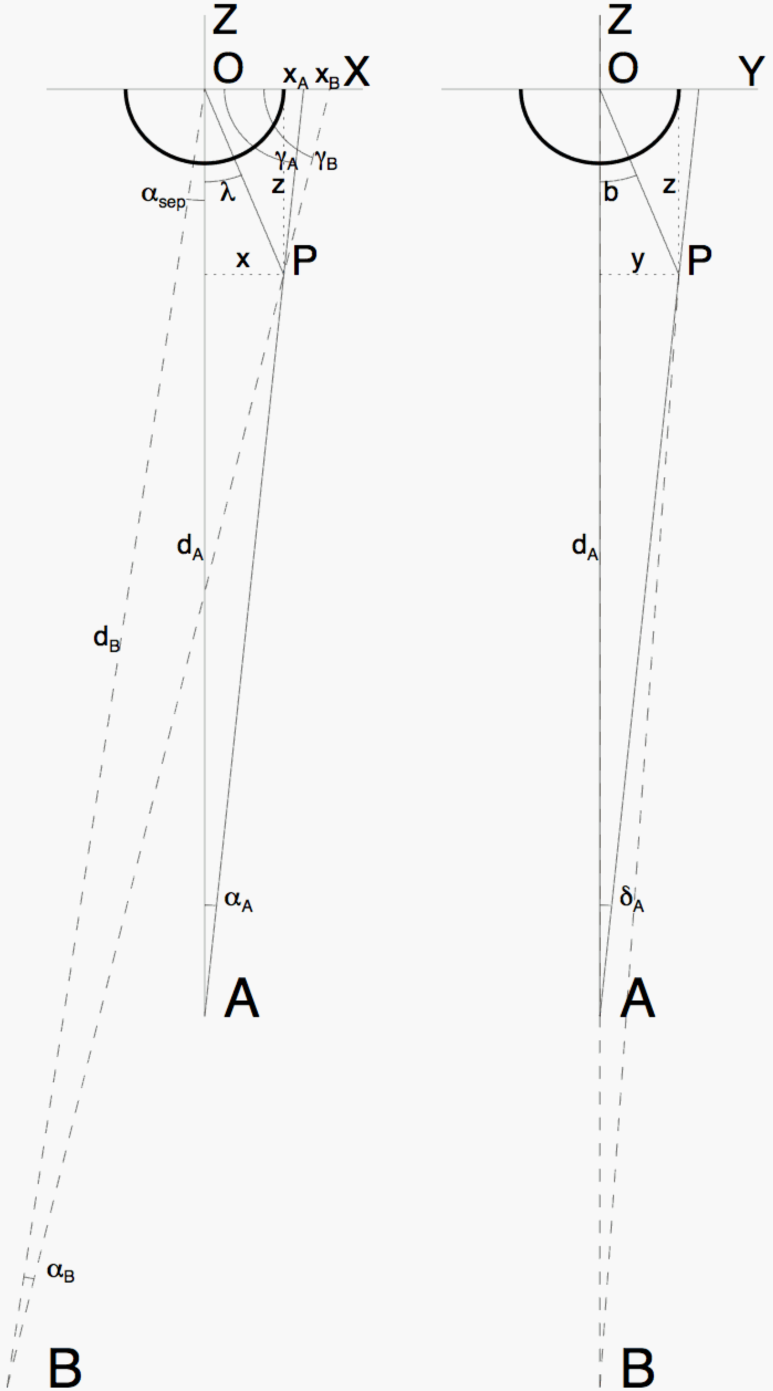

Observables:

d_A, d_B, α_A, α_B, δ_A, δ_B, α_{sep}

Trigonometric relations:

$$\gamma_A = \frac{\pi}{2} - \alpha_A$$

$$\gamma_B = \frac{\pi}{2} - \alpha_B - \alpha_{sep}$$

$$x_A = d_A \tan(\alpha_A)$$

$$x_B = d_B \frac{\sin(\alpha_B)}{\sin(\gamma_B)}$$

$$x = \frac{x_B \tan(\gamma_A) - x_A \tan(\gamma_B)}{\tan(\gamma_B) - \tan(\gamma_A)}$$

$$z = (x_A - x)\tan(\gamma_A)$$

$$y = (d_A - z)\tan(\delta_A)$$

$$r = \sqrt{x^2 + y^2 + z^2}$$

$$h = r - R_{\circ}$$

Calculated parameters:

x, y, z, r, h

A3) Image Highpass-Filtering and Loop Definition

Best S/N ratio, but widest loops

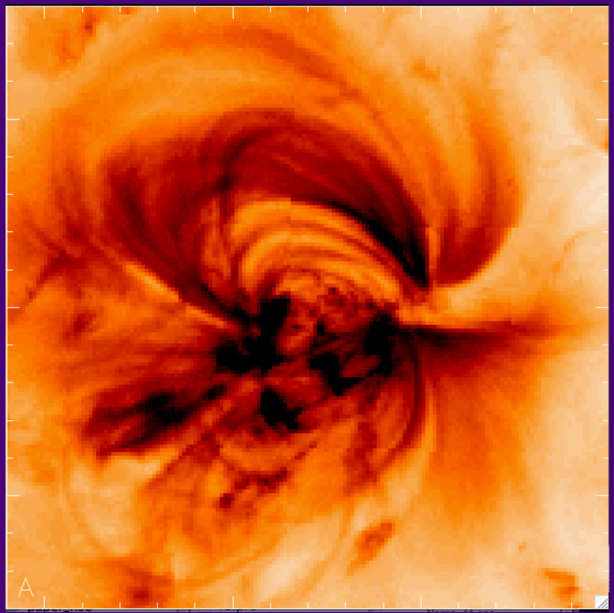

Unfiltered image (100% flux)

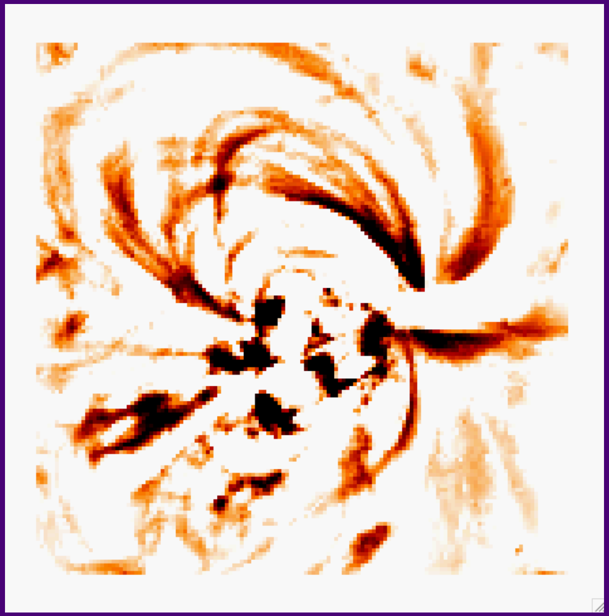

Higphass filter (w<21 pixel)

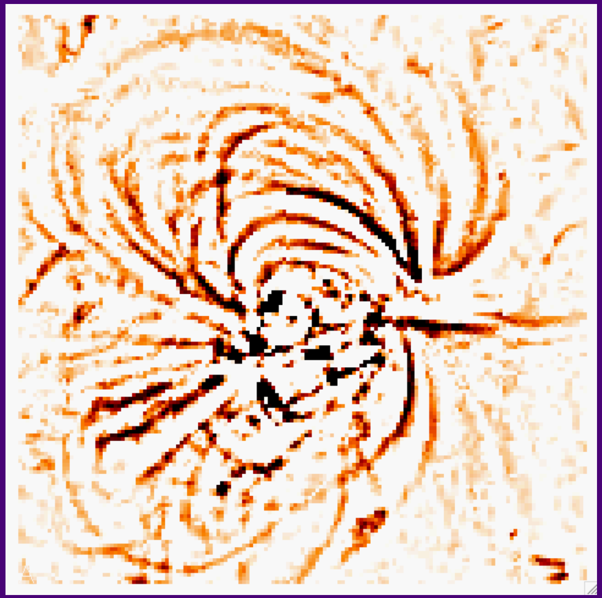

Highpass filter (w<7 pixel)

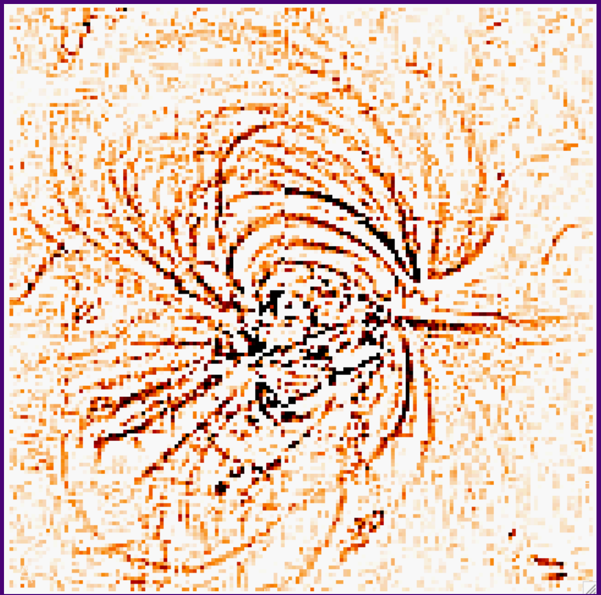

Highpass filter (w<3 pixel; 4% flux)

Lowest S/N ratio, but narrowest loops

Coaligned STEREO image pair A+B with FOV of AR

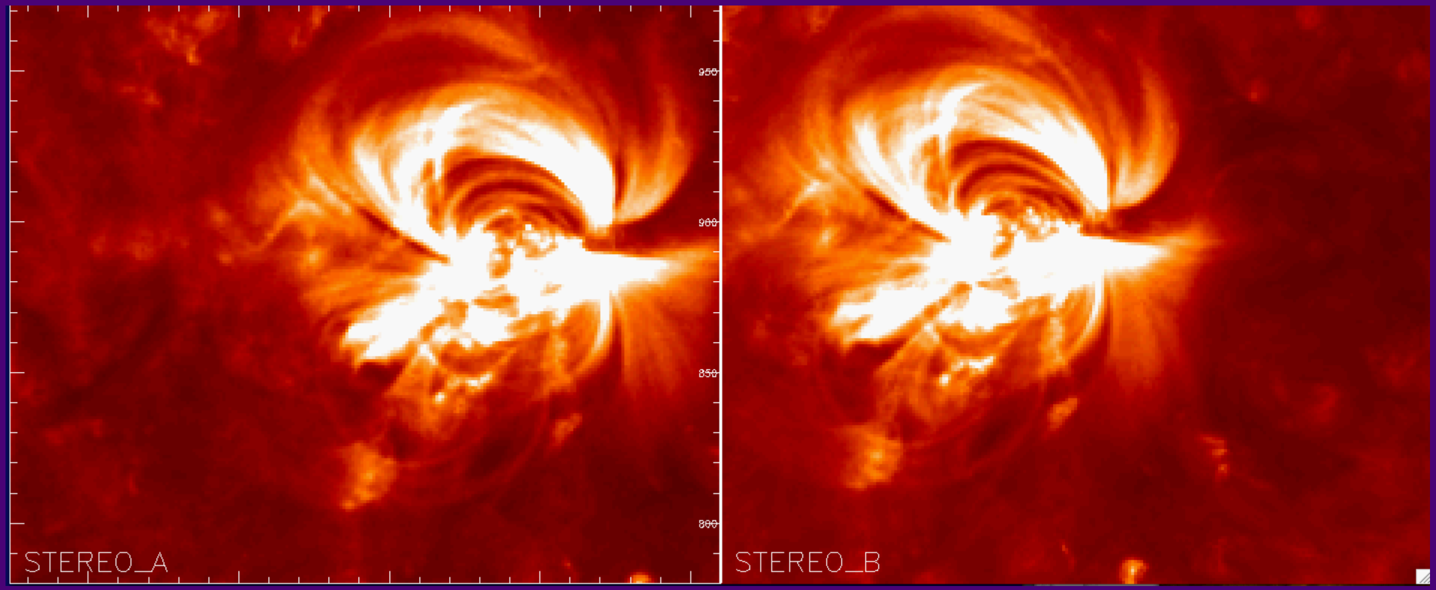

Highpass-filtered STEREO image pair A+B

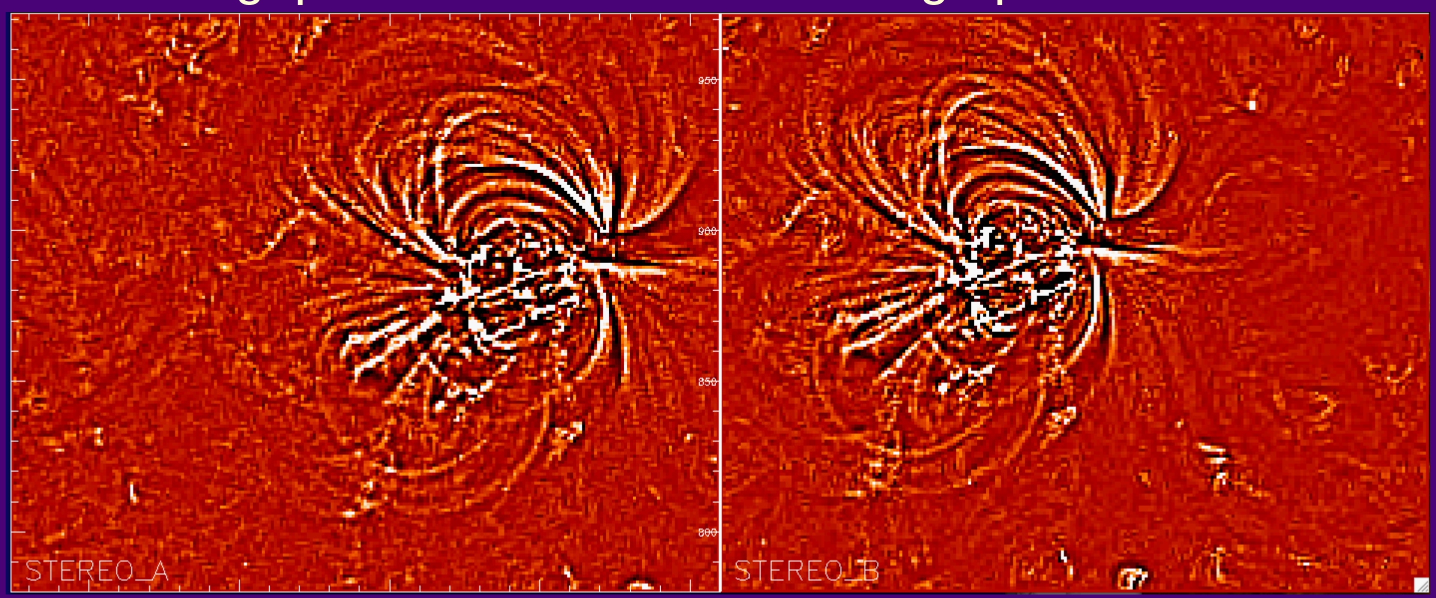

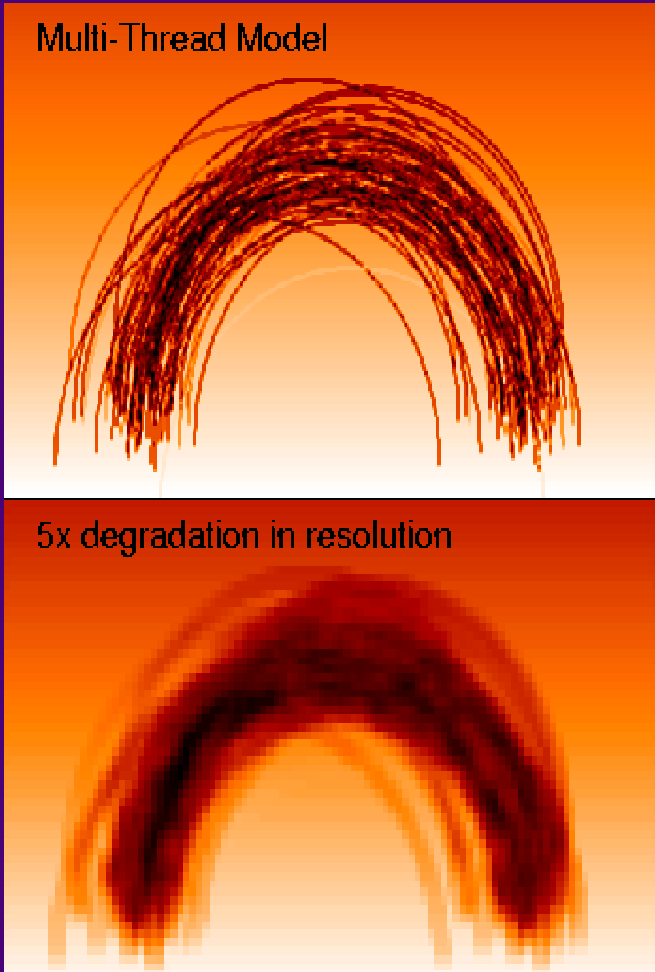

Concept of elementary loop strands and composite loops:

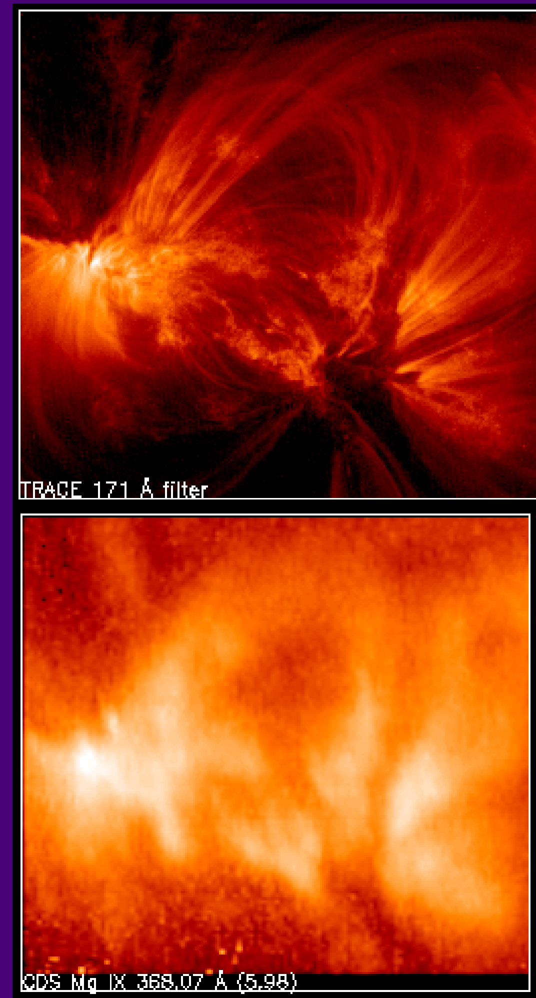

Simultaneous images recorded in EUV in near-identical temperature filters (e.g., TRACE 171 A vs CDS Mg IX, ~ 1.0 MK) reveal that a loop system observed with CDS (with a spatial resolution of ~4" pixel) is composed of at least 10 loop strands when imaged with TRACE (with a pixel size of 0.5" and spatial resolution of ~1").

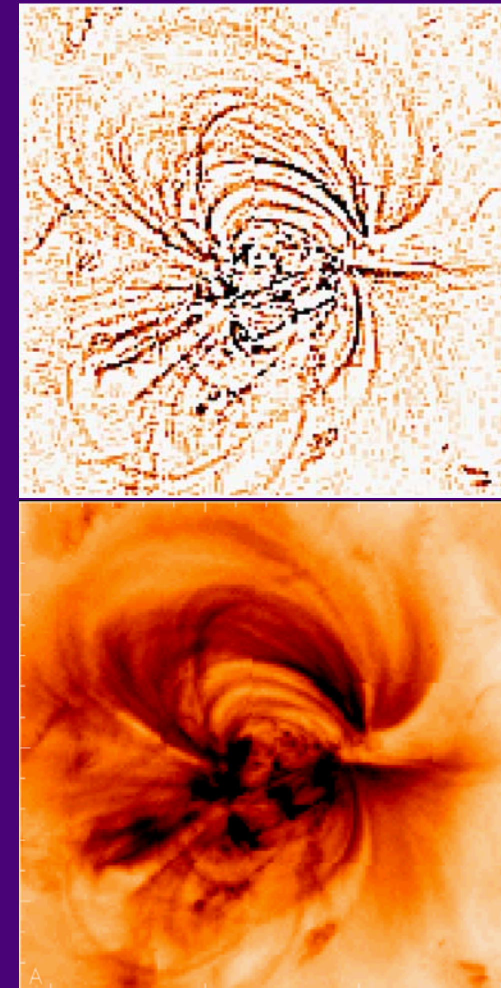

With a highpass filter we enhance the finest loop strands, but EUVI has a spatial resolution of 3.5" (2.2 EUVI pixels = 2500 km), and thus the finest structures seen with EUVI probably correspond to "composite" loops. TRACE found elementary (isothermal) loops for w<1500 km

A4) Automated Loop Tracing

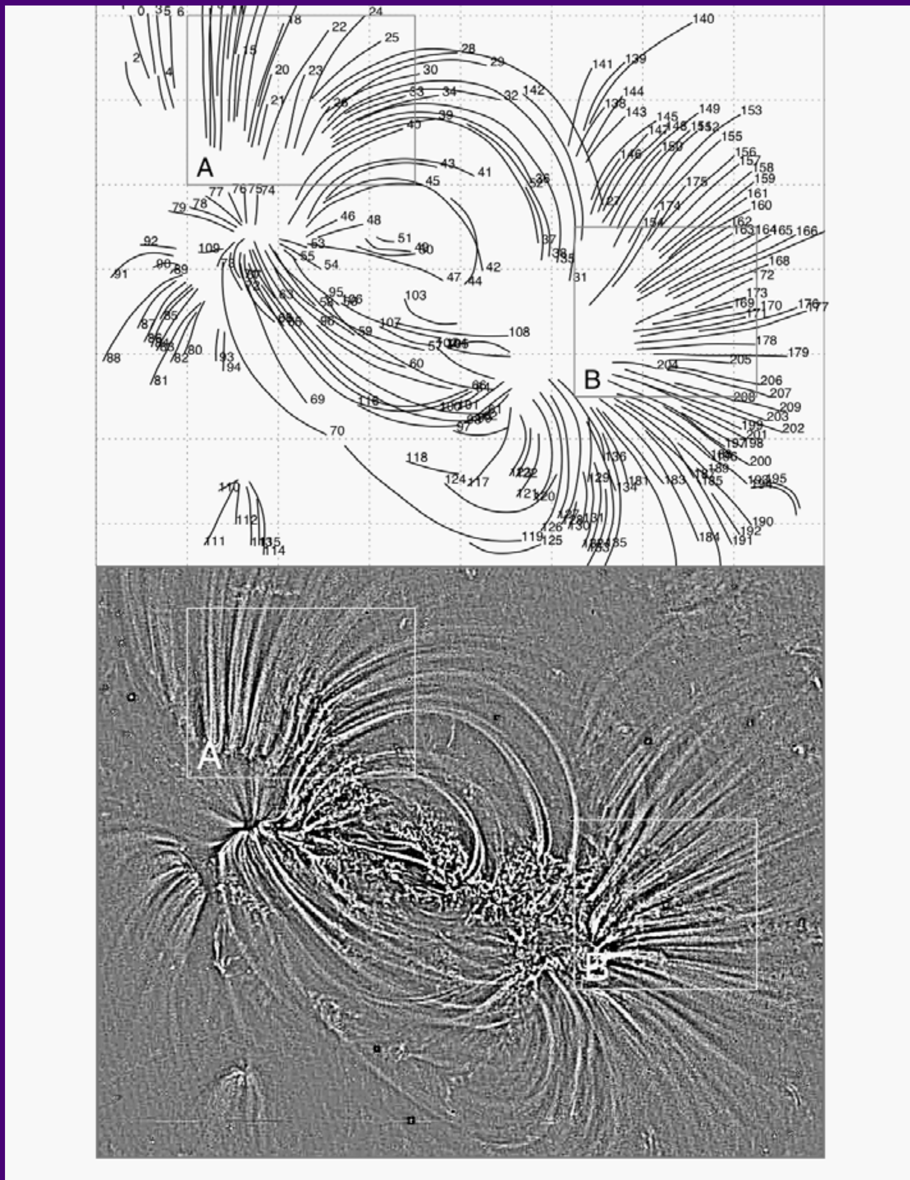

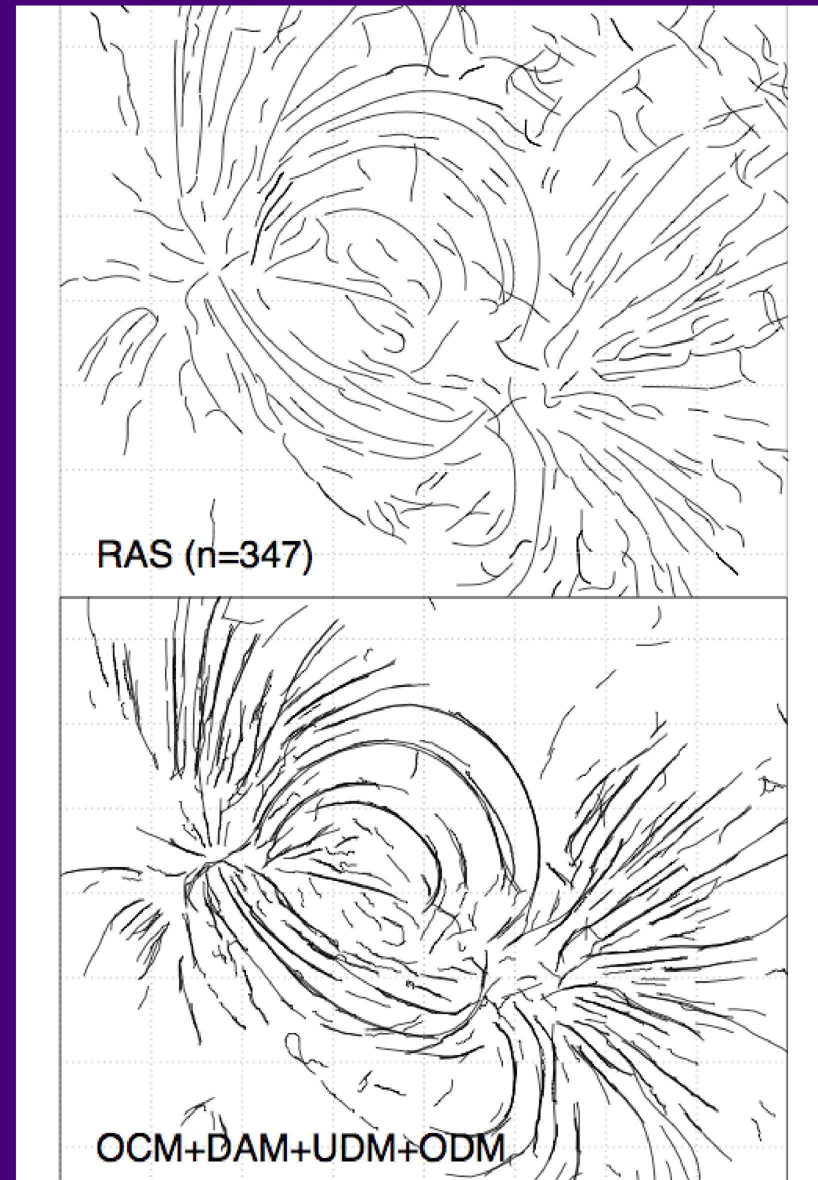

“Comparison of five numerical codes for automated tracing of coronal loops”, Aschwanden, Lee, Gary, Smith, & Inhester (2007), Solar Physics, (in press)

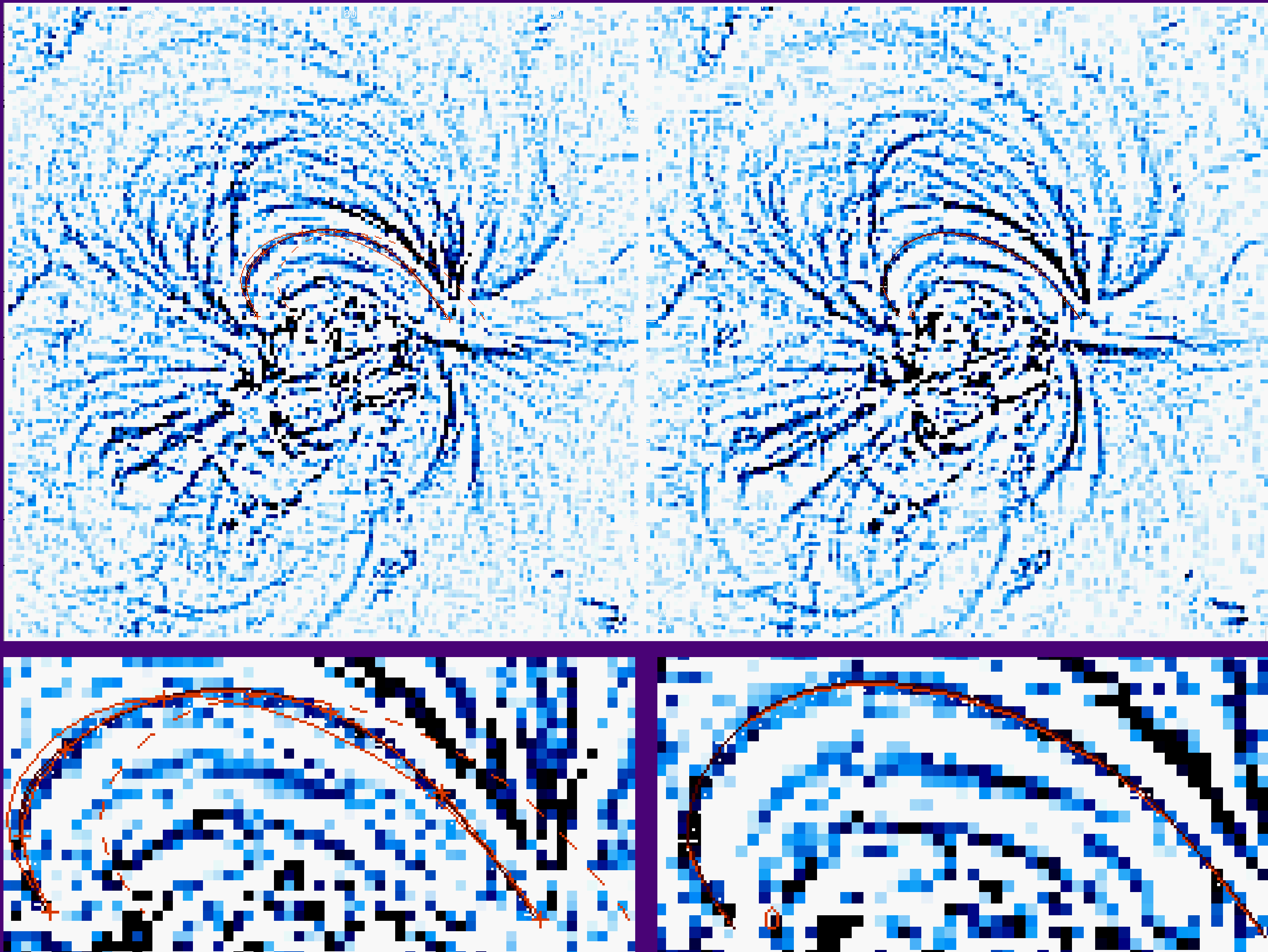

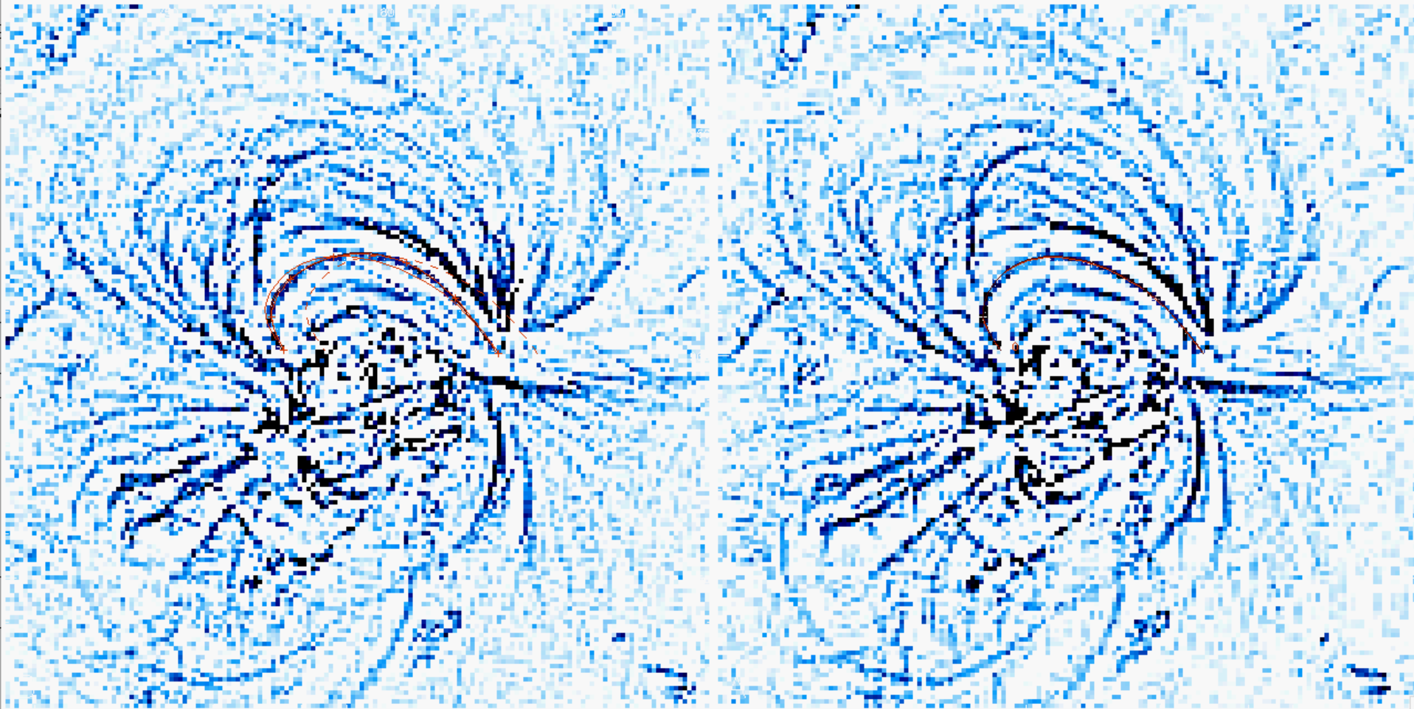

Highpass filter: subtract image smoothed with 3x3 boxcar

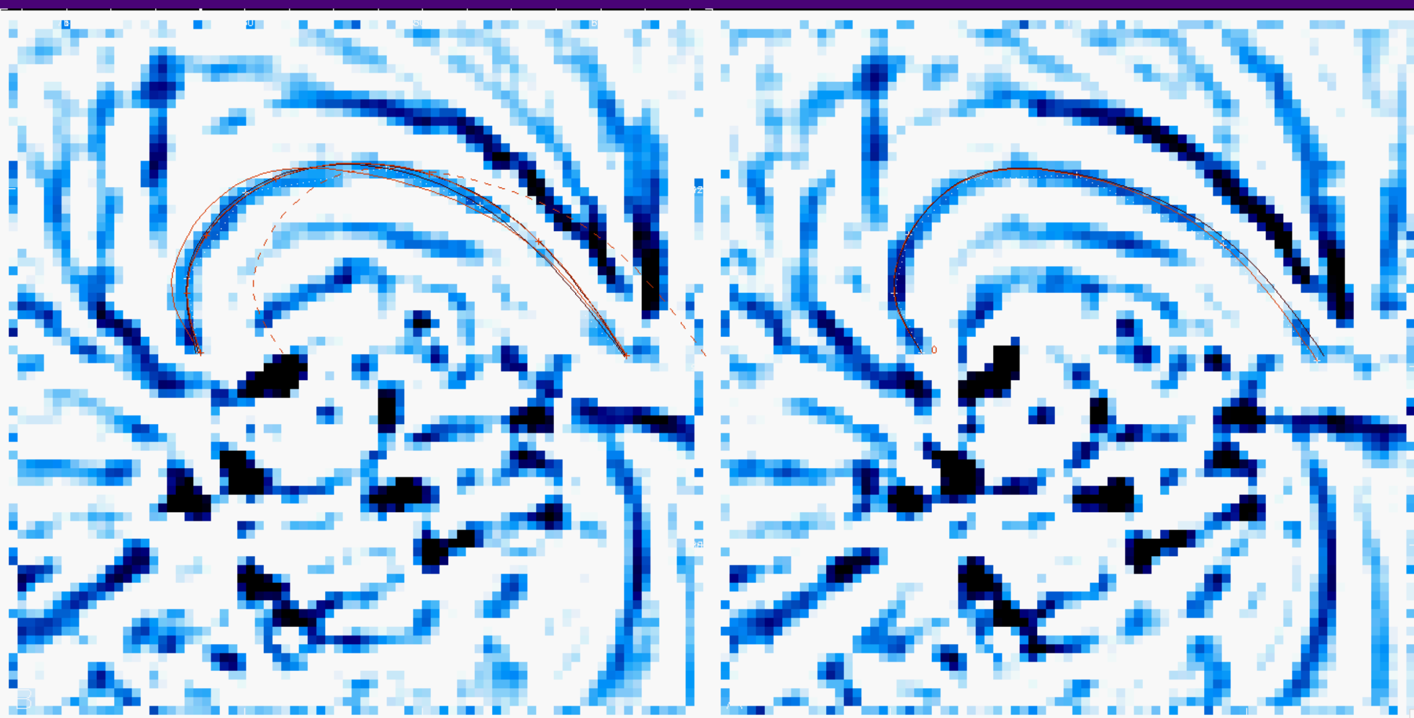

Highpass filter: subtract image smoothed with 5x5 boxcar

A5) Stereoscopic 3D Reconstruction

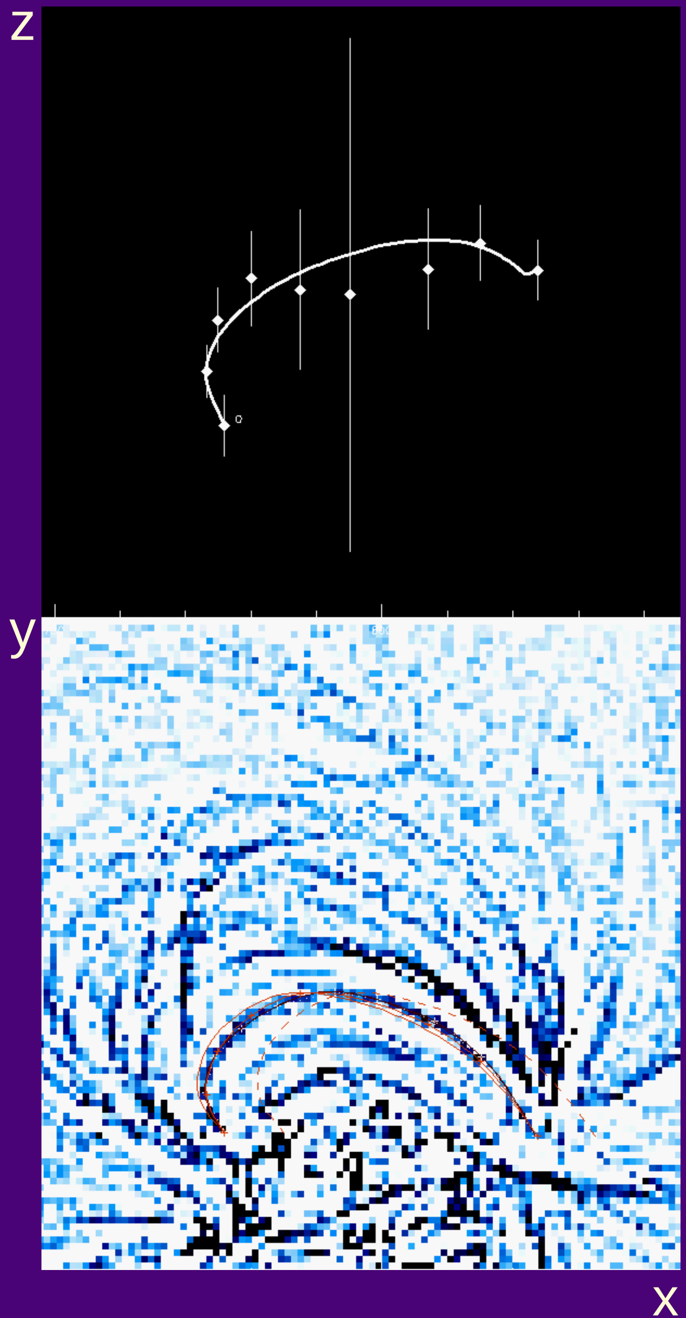

- Manual clicking on 4-8 loop positions in STEREO-A image (x_A,y_A)
- Manual clicking on 4-8 loop positions in STEREO-B image (x_B, y_B)
- Calculating (x,y,z) 3D coordinates from stereoscopic parallax
- Calculate stereoscopic error for each loop point $z \pm \sigma_z$
- Weighted polynomial fit z(s) (2nd-order) with s' the projected loop length coordinate s in [x,y] plane

Stereoscopic error in z-coordinate:

$$\sigma_z = \frac{1}{2}\sqrt{1+\tan(\vartheta[s_i])}$$

$$\tan(\vartheta[s_i]) = \frac{|\alpha_B(s_{i+1}) - \alpha_B(s_i)|}{|\delta_B(s_{i+1}) - \delta_B(s_i)|}$$

Error=1/2 pixel in NS direction
infinite in EW direction

Tracing of 36 individual loops in STEREO-A image

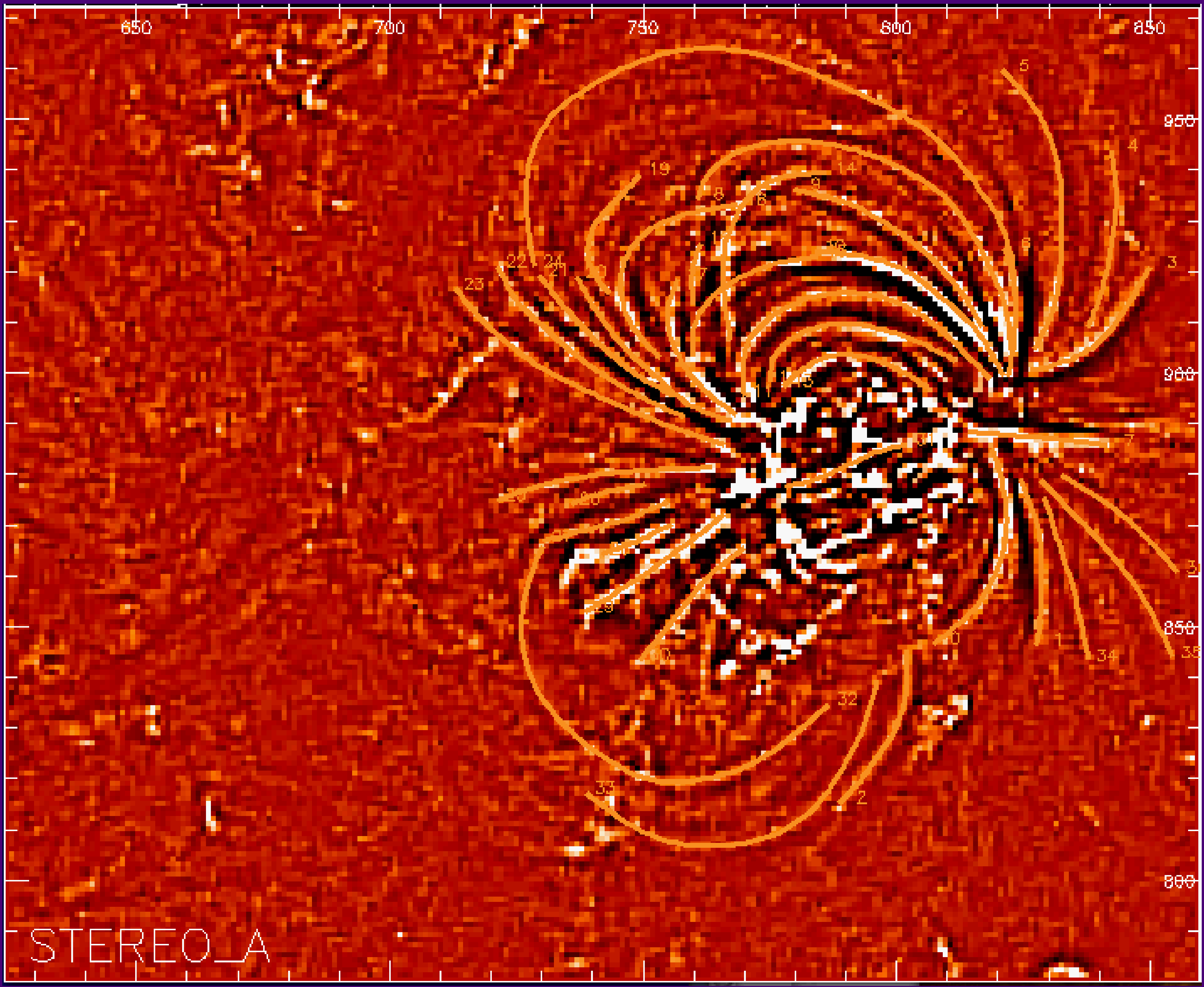

Tracing of 36 individual loops in STEREO-B image

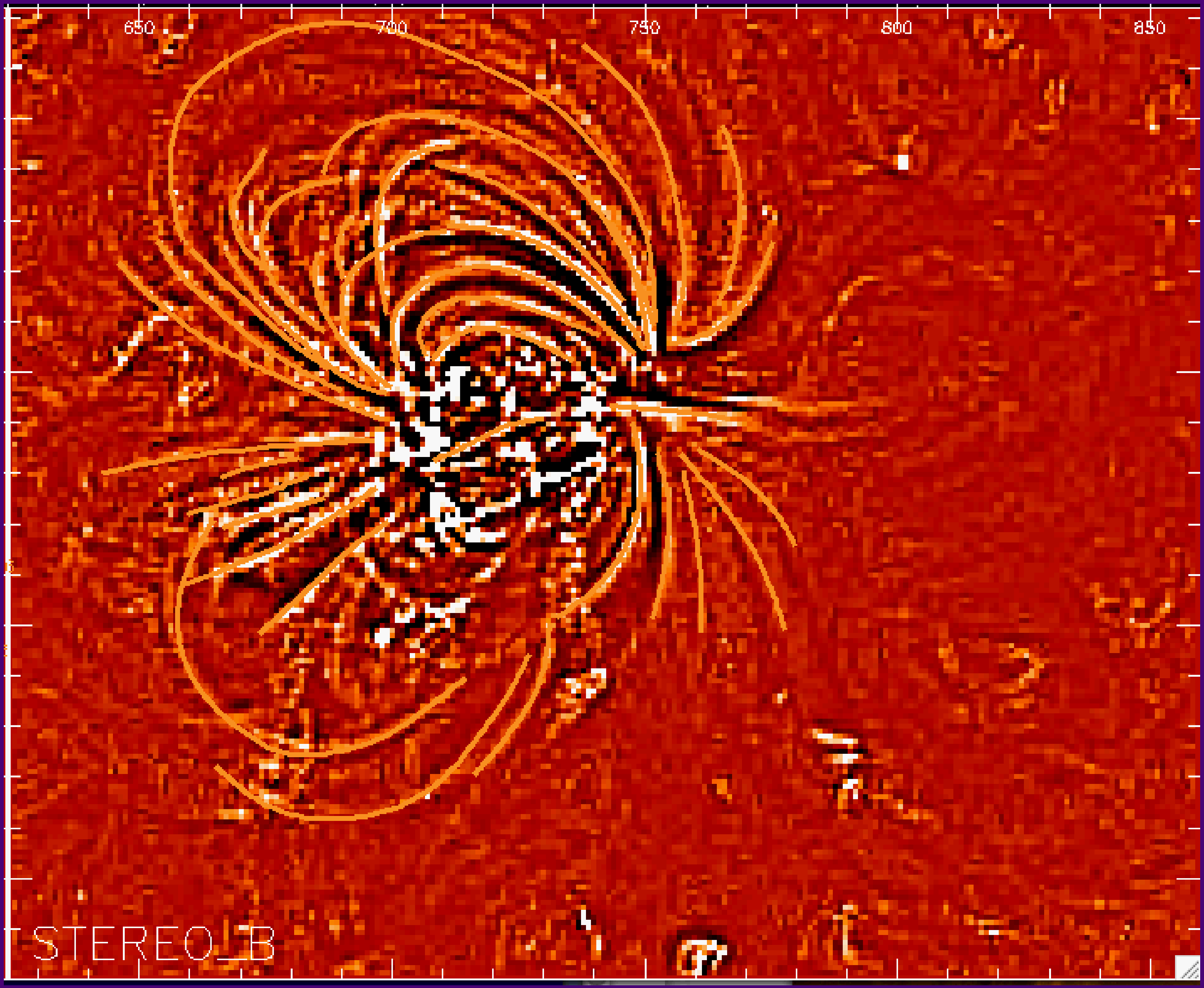

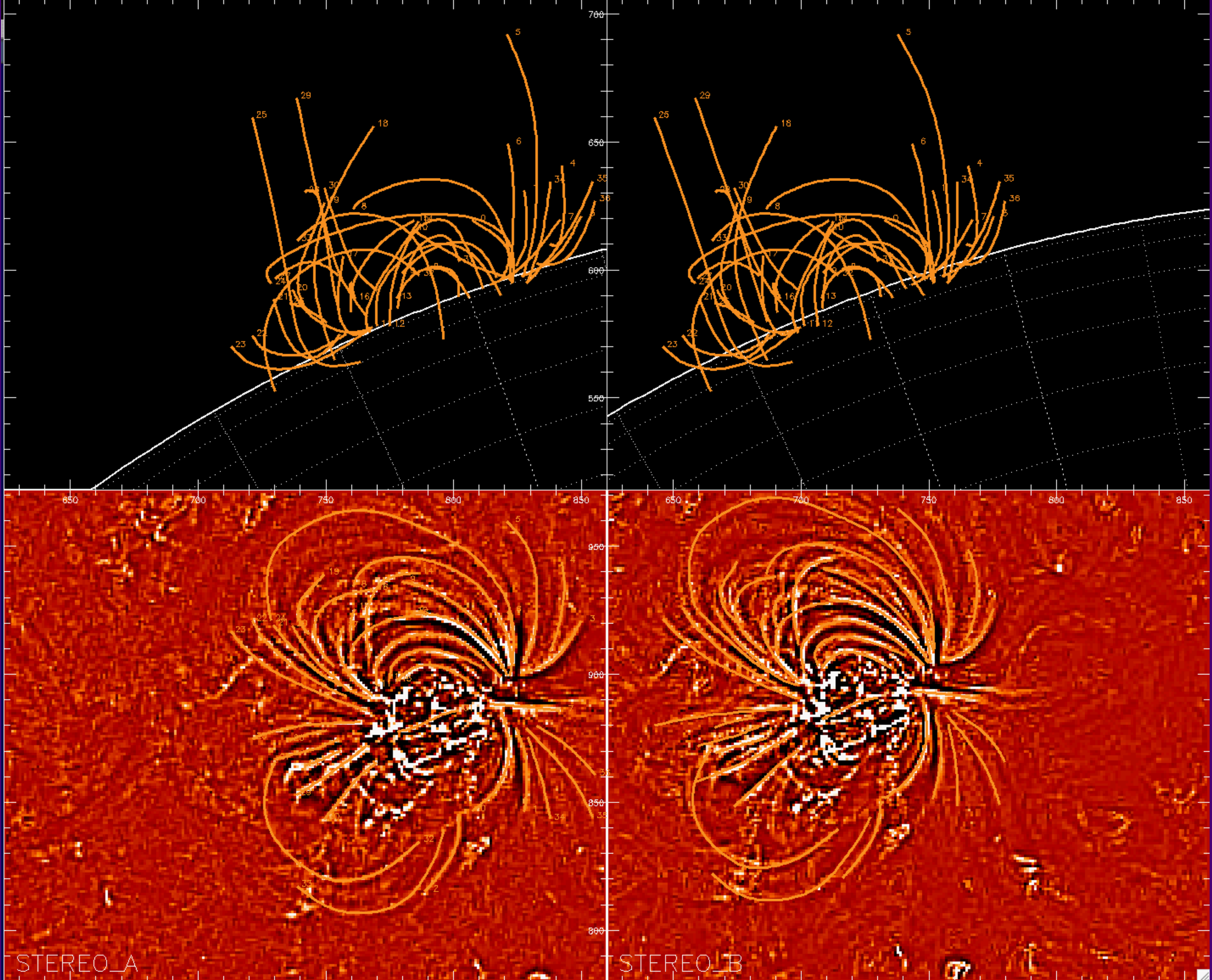
STEREO_A
STEREO_B

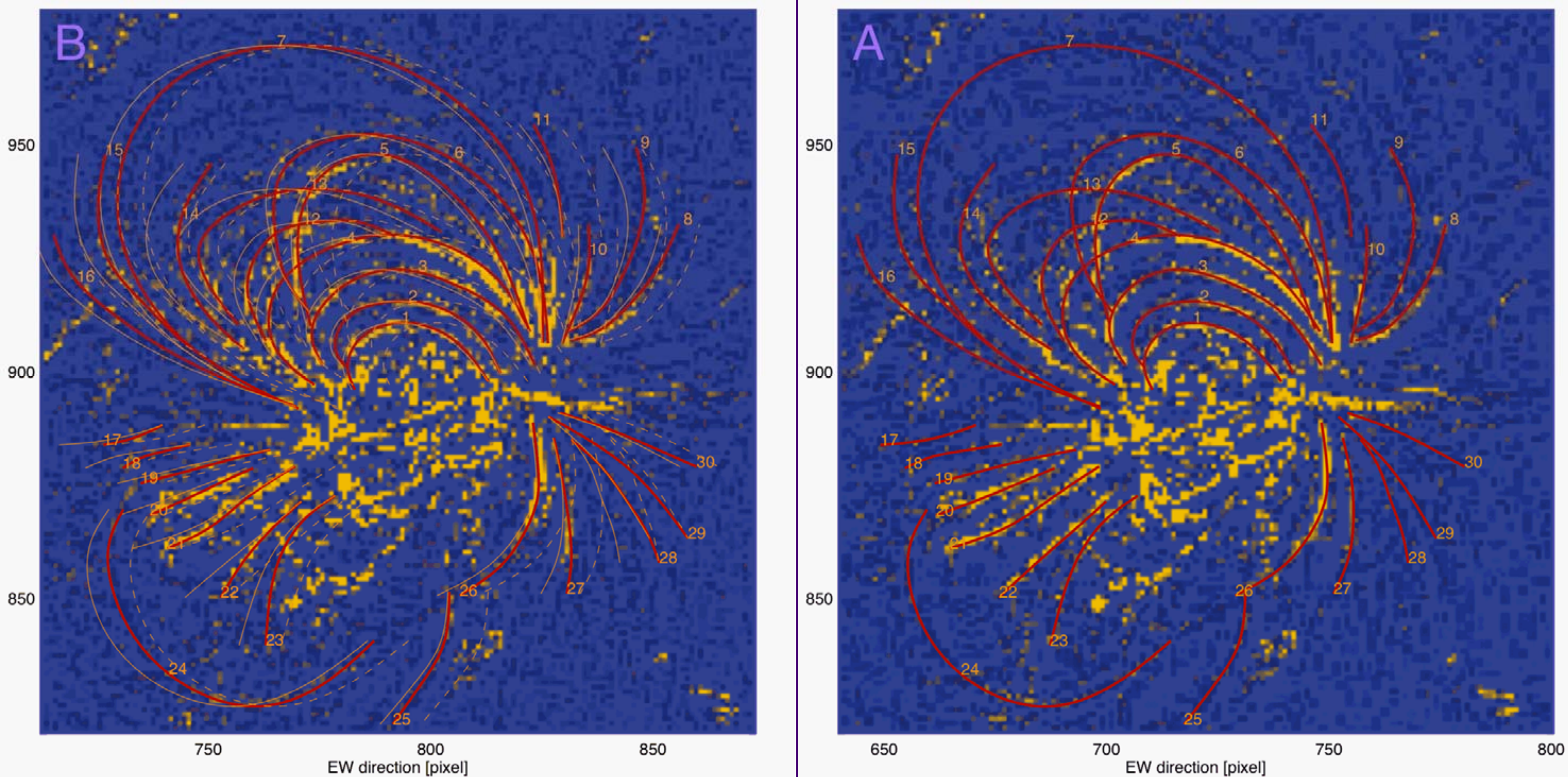

B
950
900
850
750
800
850
EW direction [pixel]
1 2 3 4 5 6 7 8 9 10 11 12 13 14 15 16 17 18 19 20 21 22 23 24 25 26 27 28 29 30
A
950
900
850
650
700
750
800
EW direction [pixel]
1 2 3 4 5 6 7 8 9 10 11 12 13 14 15 16 17 18 19 20 21 22 23 24 25 26 27 28 29 30

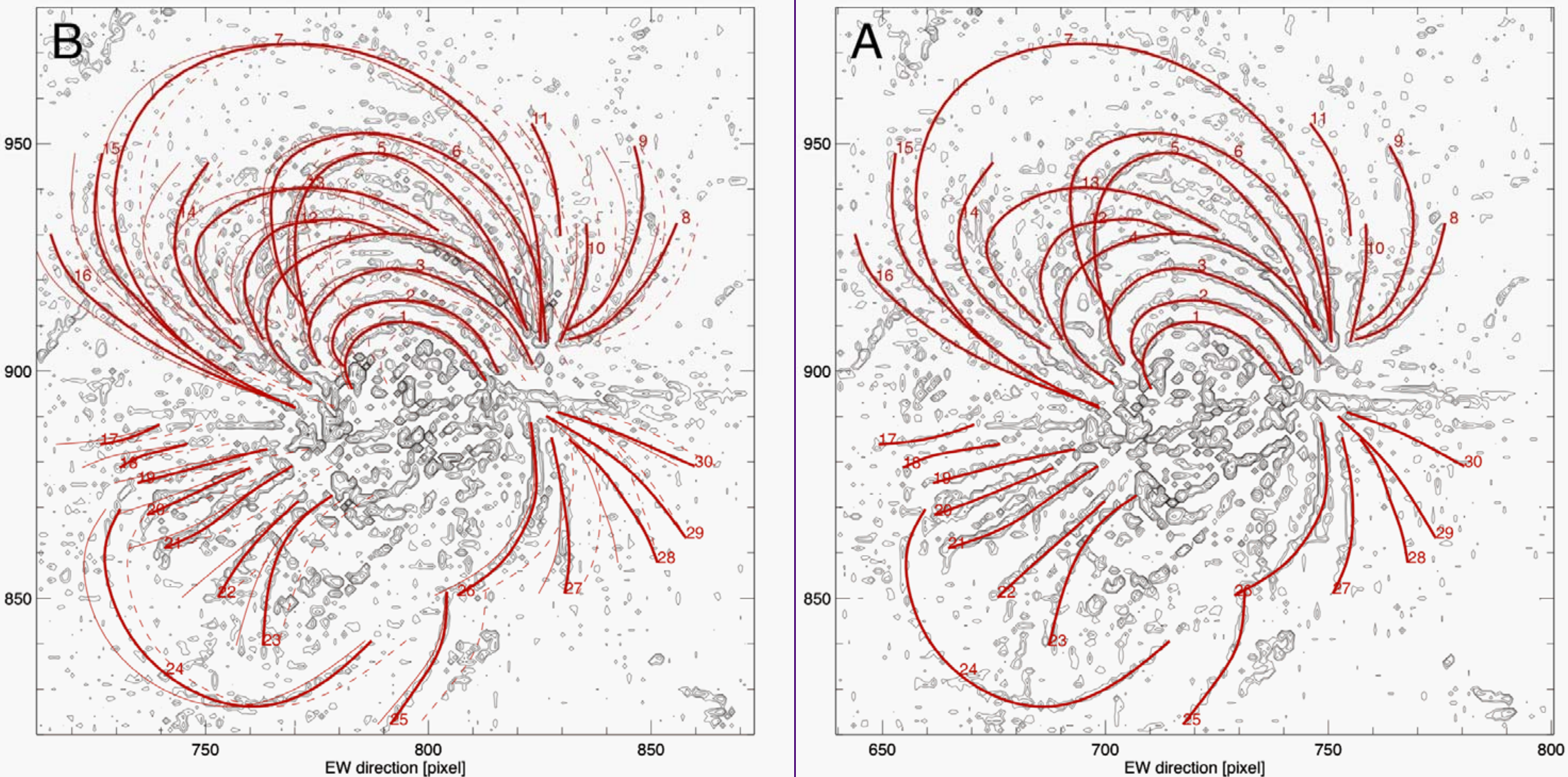
B
950
900
850
750
800
850
EW direction [pixel]
A
950
900
850
650
700
750
800
EW direction [pixel]
1
2
3
4
5
6
7
8
9
10
11
12
13
14
15
16
17
18
19
20
21
22
23
24
25
26
27
28
29
30

3D projections of loop geometries: [x,y] --> [x,z],[y,z]

Color: blue=short loops
red=midsize loops
yellow=long loops
white=longest loop

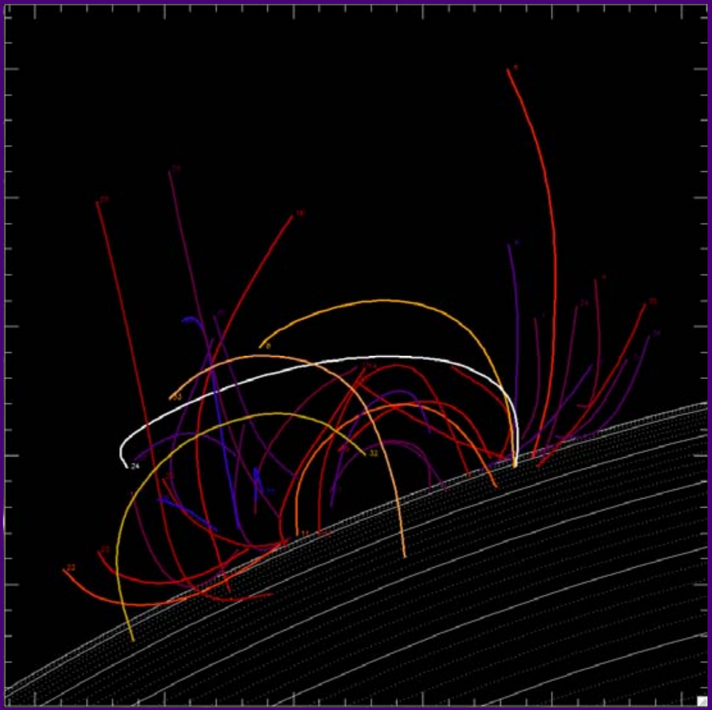

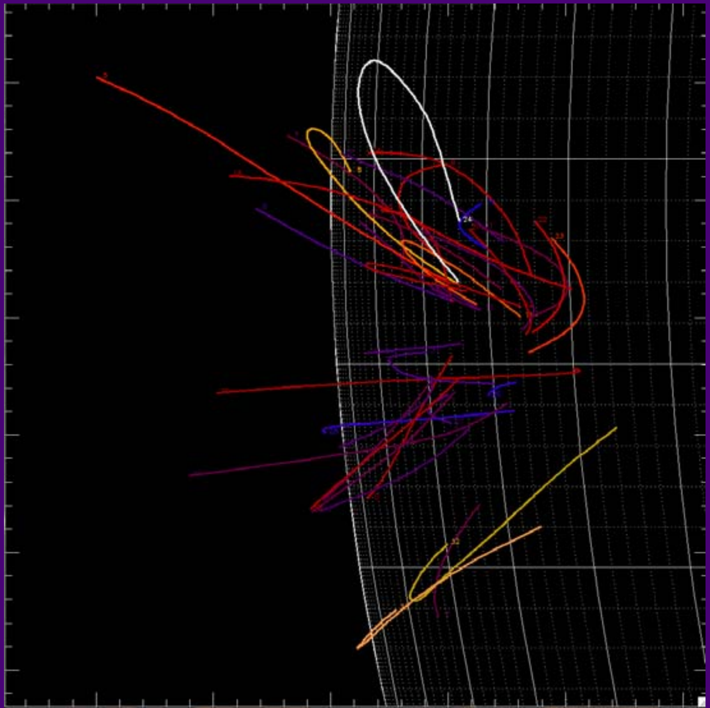

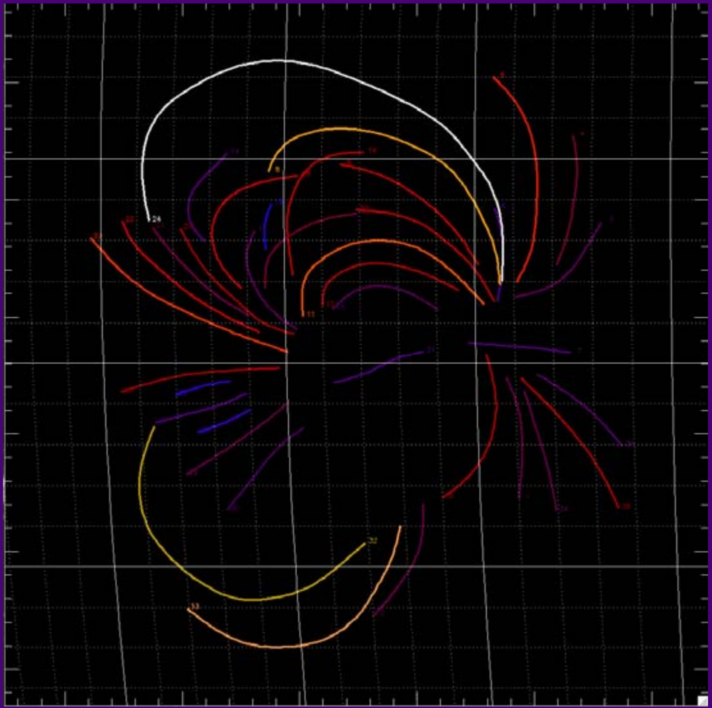

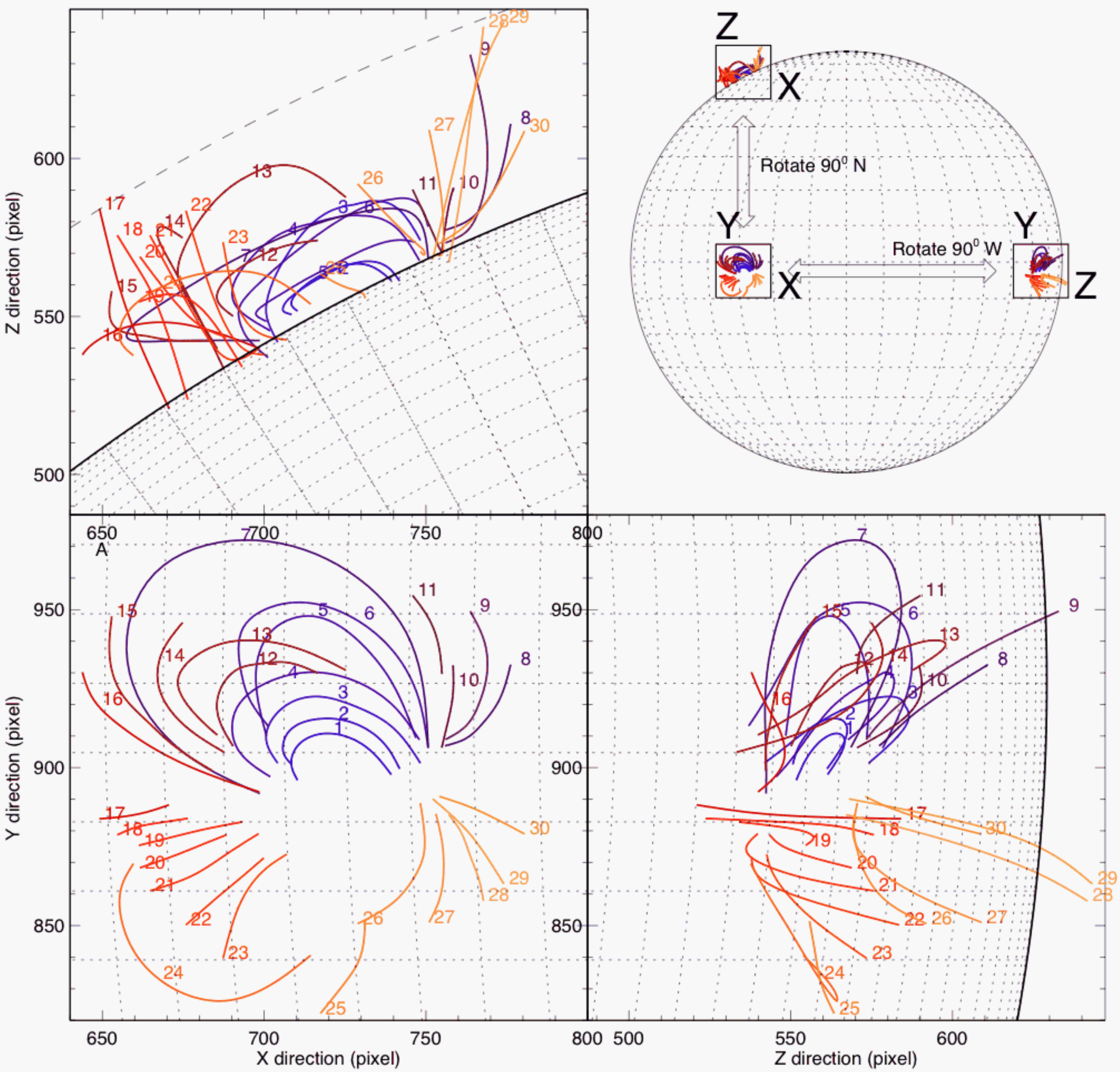
Z direction (pixel)
600
550
500
650
700
750
800
X direction (pixel)
Y direction (pixel)
950
900
850
A
500
550
600
Z direction (pixel)
Z
X
Y
Rotate 90⁰ N
Rotate 90⁰ W
Y
X
Y
Z

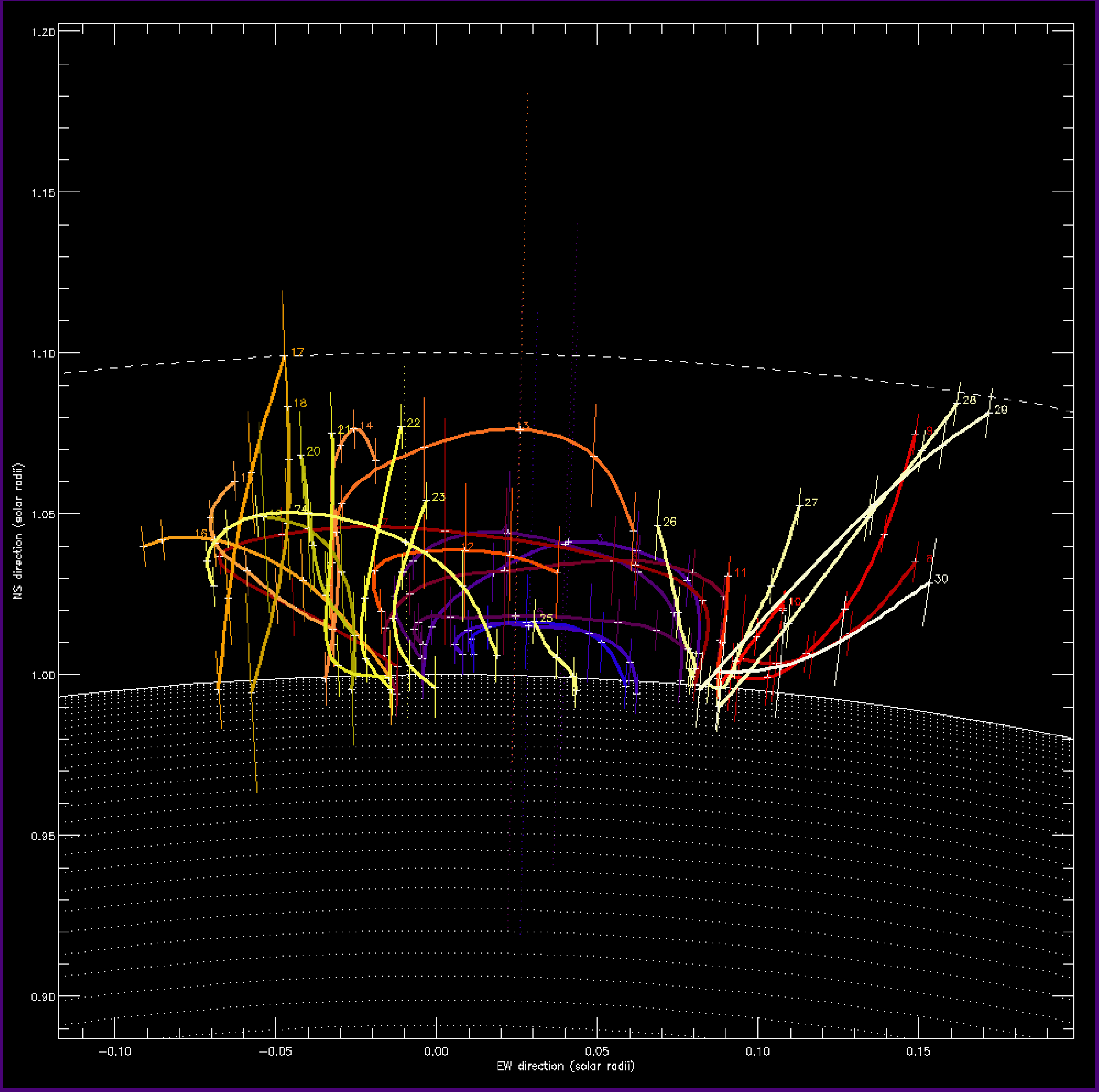

View in NS projection with errors of heights

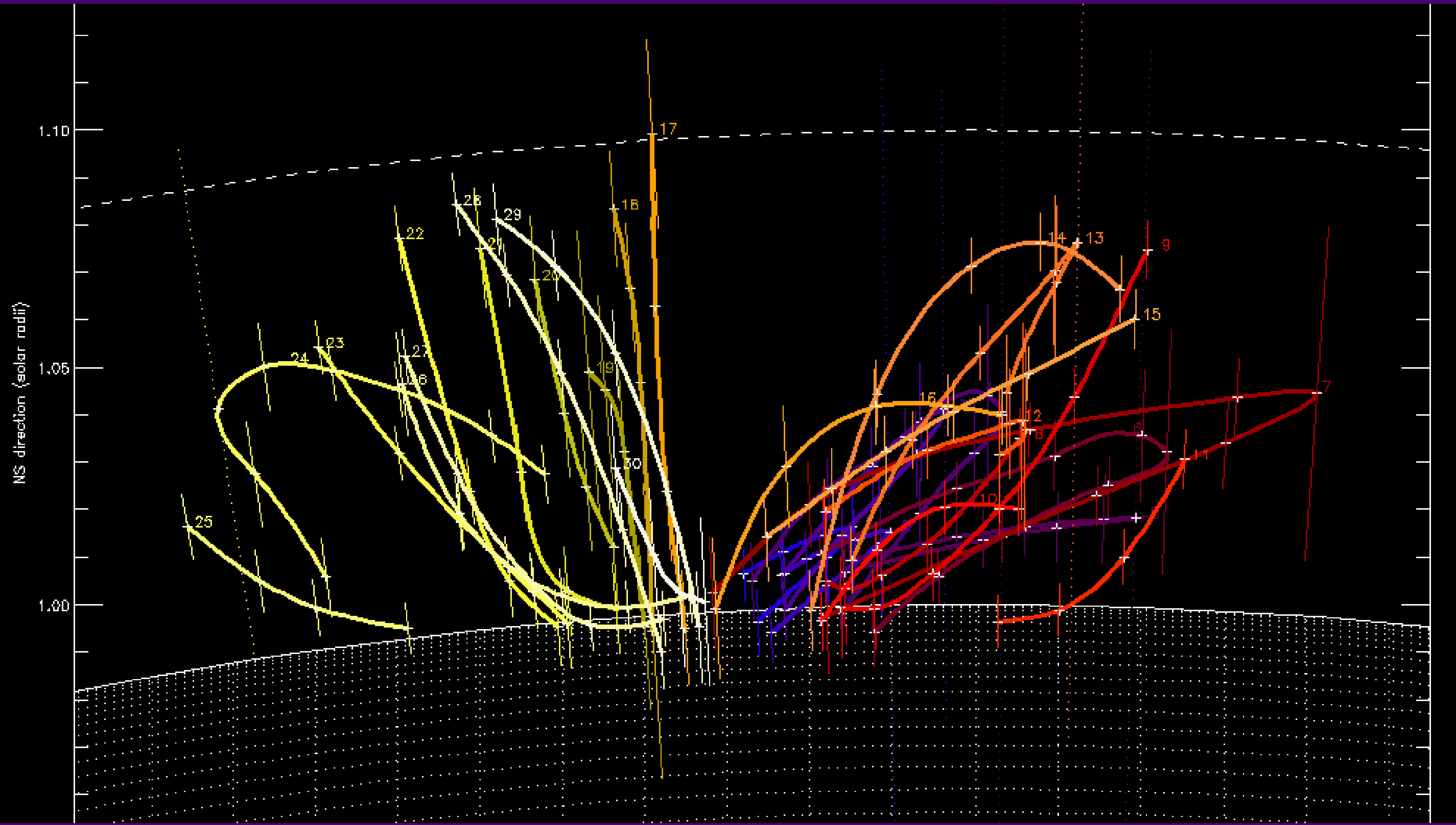

View in EW direction with stereoscopic height errors

A7) Loop Coplanarity and Circularity

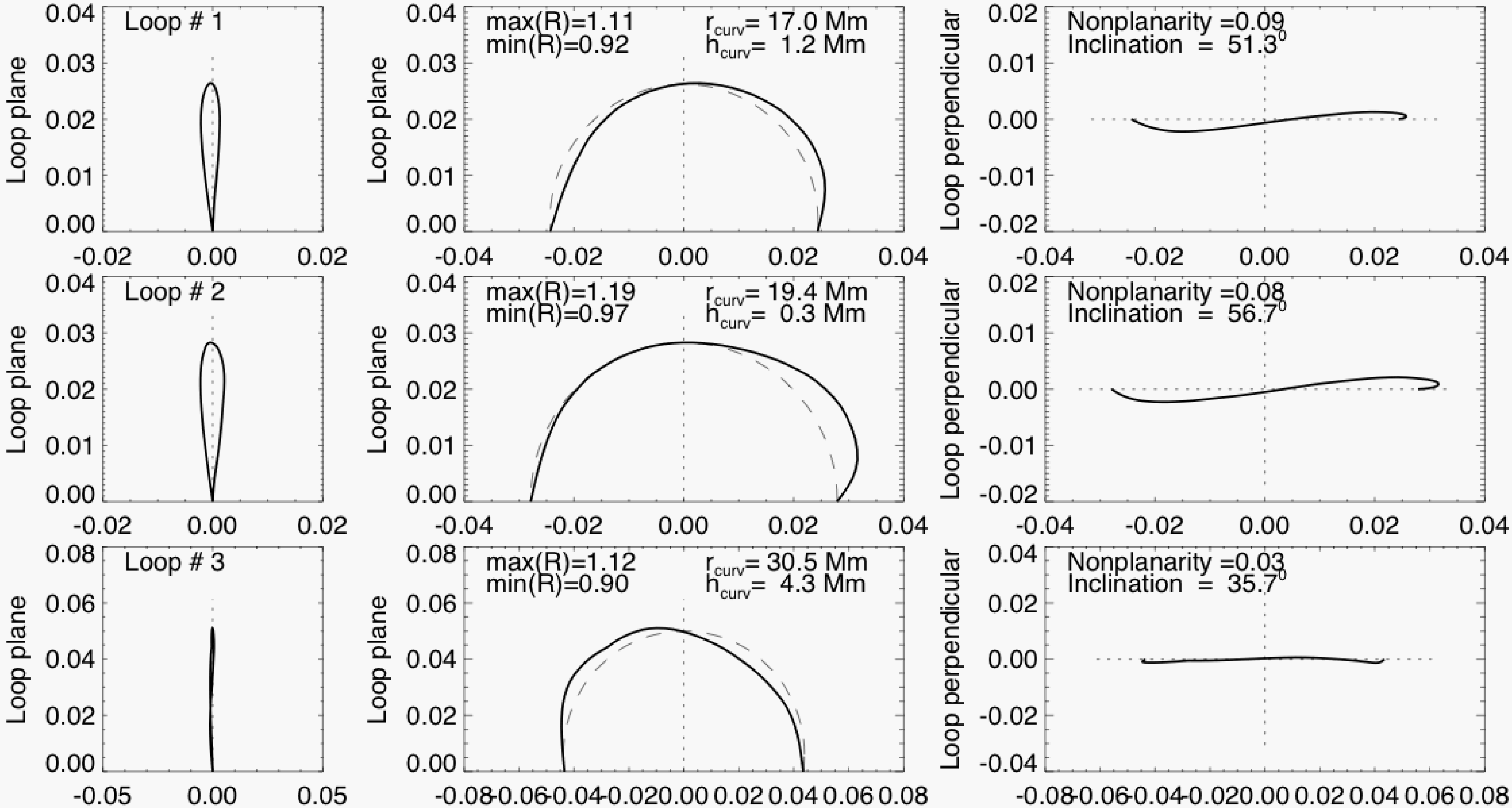

Rotation of 3D [x,y,z] coordinates into cartesian coordinate system of loop plane --> measurement of coplanarity and circularity

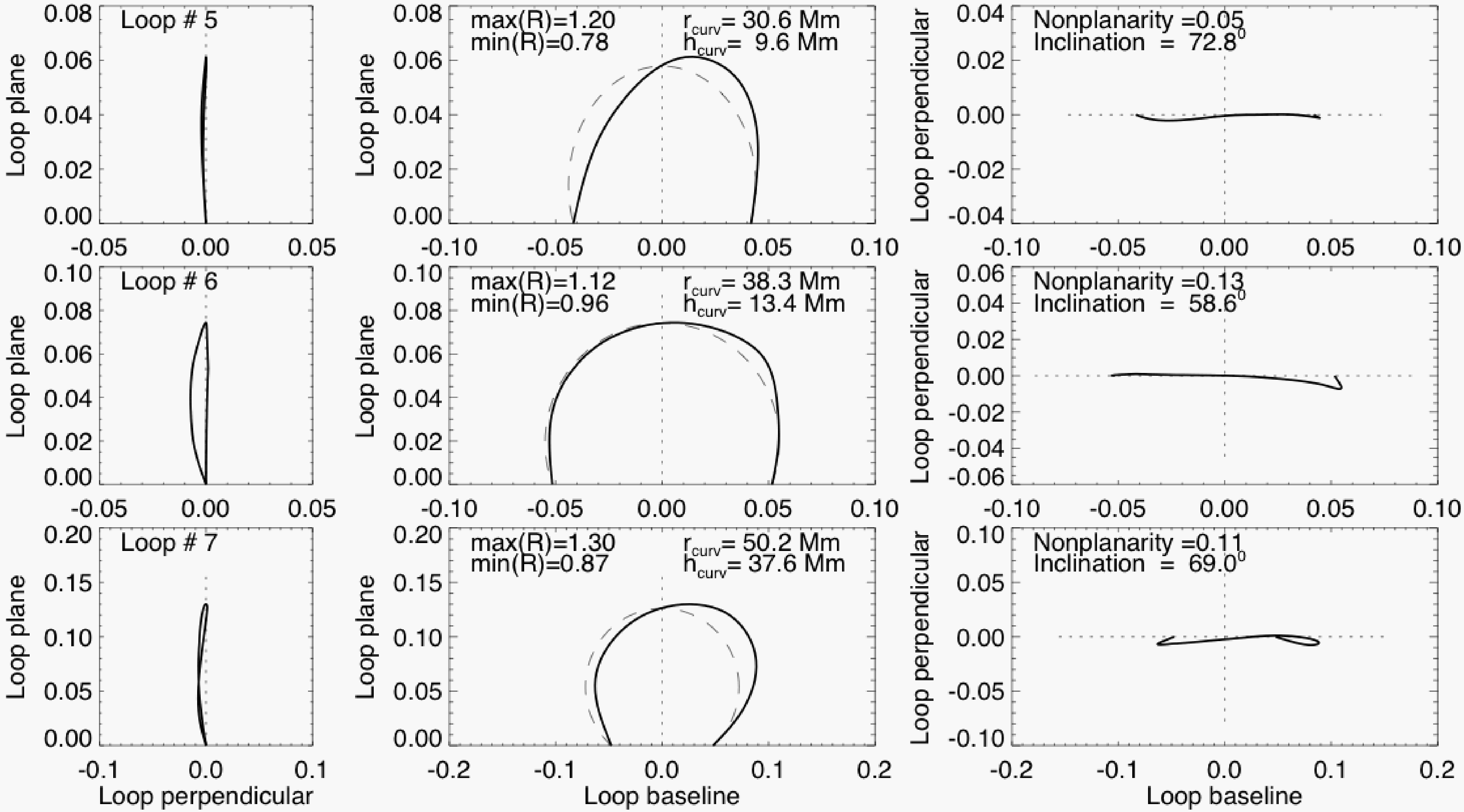

Circularity ratio: $C(s) = R(s)/r_{curv}$

Coplanarity ratio: $P(s)=y_{perp}(s)/r_{curv}$

Loop #	Maximum Height h_{max} [Mm]	Curvature radius r_{curv} [Mm]	Center offset h_{curv} [Mm]	Inclination angle ϑ [deg]	Circularity ratio C	Coplanarity ratio P
1	11.6	17.0	1.2	51.3	0.92−1.11	0.09
2	10.9	19.4	0.3	56.7	0.97−1.19	0.08
3	29.8	30.5	4.3	35.7	0.90−1.12	0.03
4	30.7	30.9	10.7	42.9	0.96−1.11	0.07
5	13.0	30.6	9.6	72.8	0.78−1.20	0.05
6	26.2	38.3	13.4	58.6	0.96−1.12	0.13
7	32.3	50.2	37.6	69.0	0.87−1.30	0.11

Measuring the twist of magnetic field lines from edge-on views

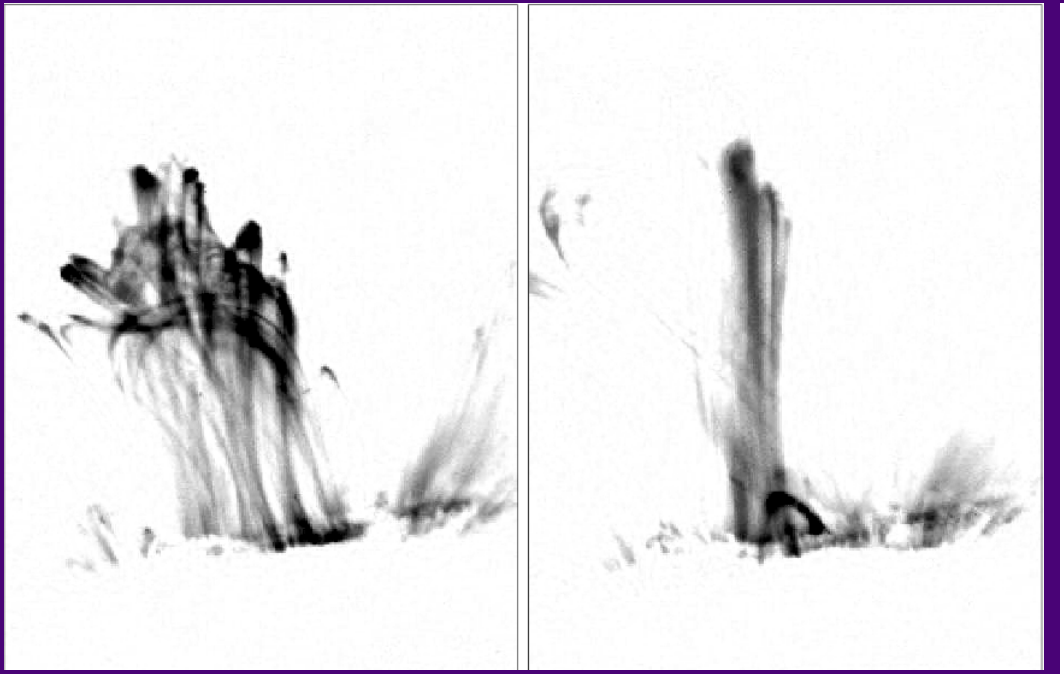

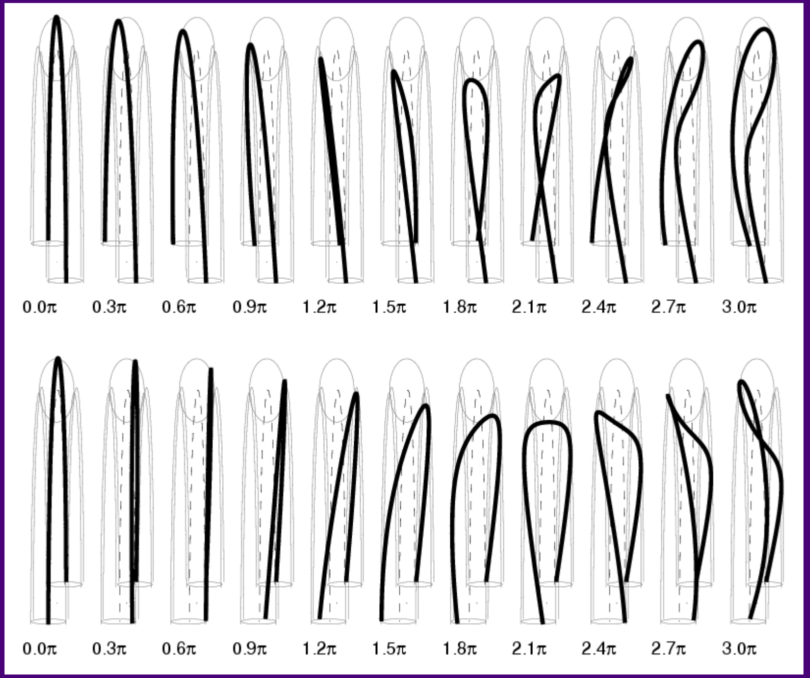

- -Measuring the number of turns in twisted loops
- -Testing the kink-instability criterion for stable/erupting loops
- -Monitoring the evolution of magnetic relaxation (untwisting) between preflare and postflare loops

A8) Hydrostatic Modeling

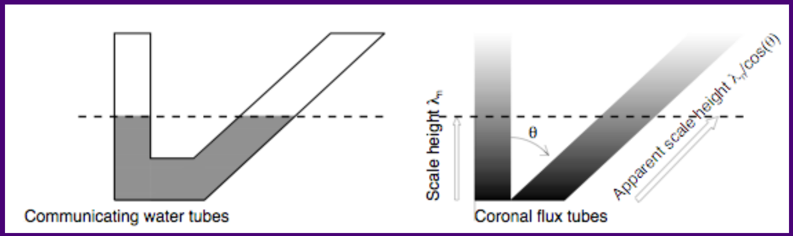

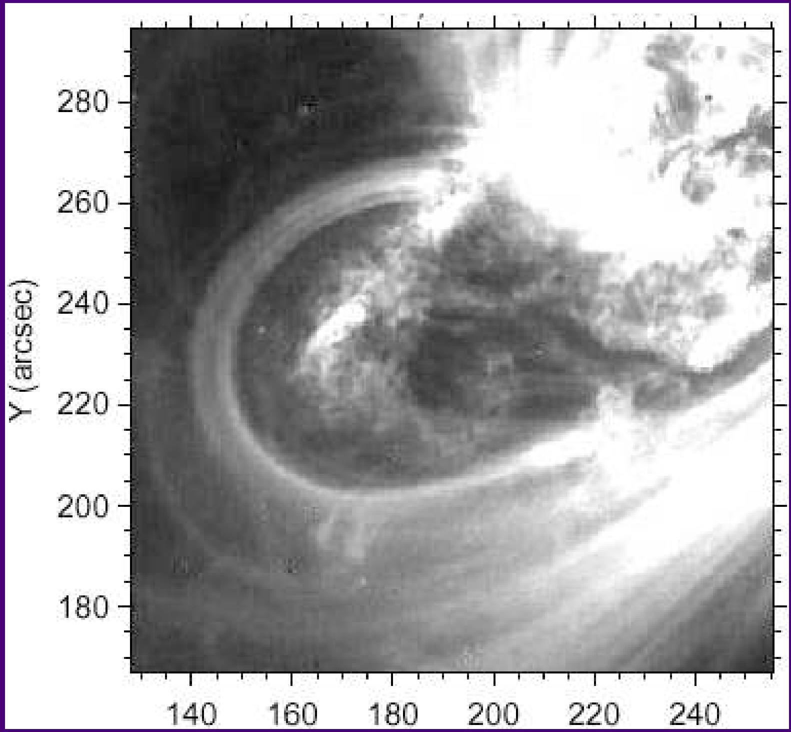

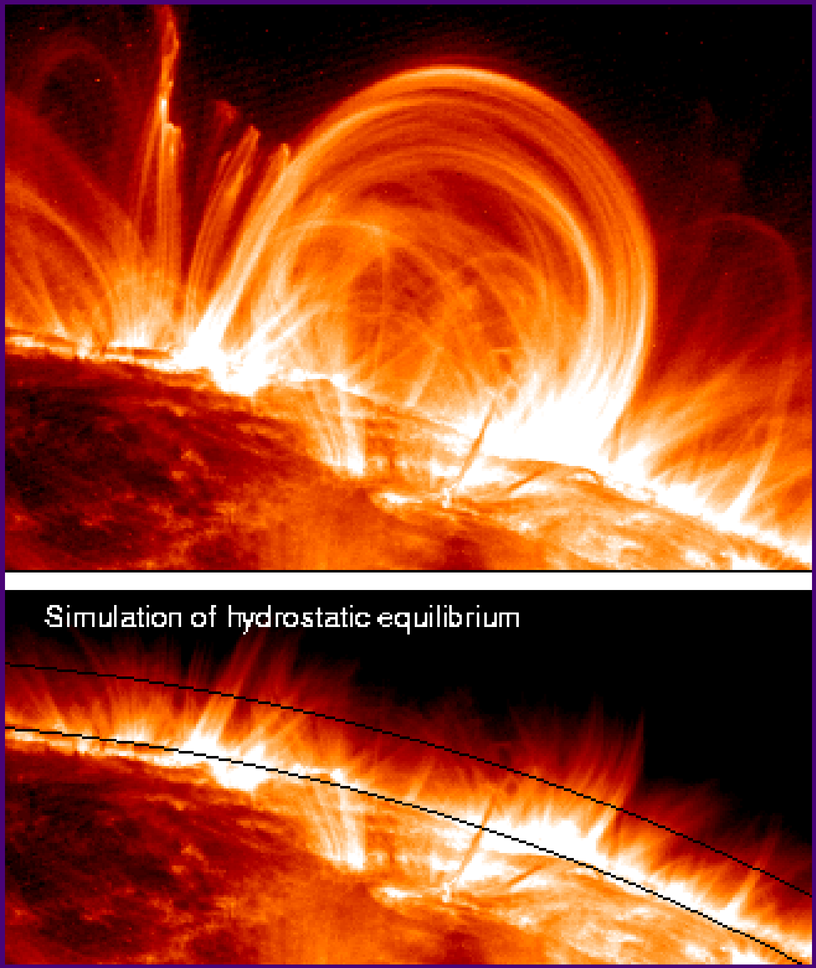

The true vertical scale height can only be determined from proper (stereoscopic) 3D reconstruction of the loop geometry:
--> Tests of hydrostatic equilibrium vs. super-hydrostatic dynamic states

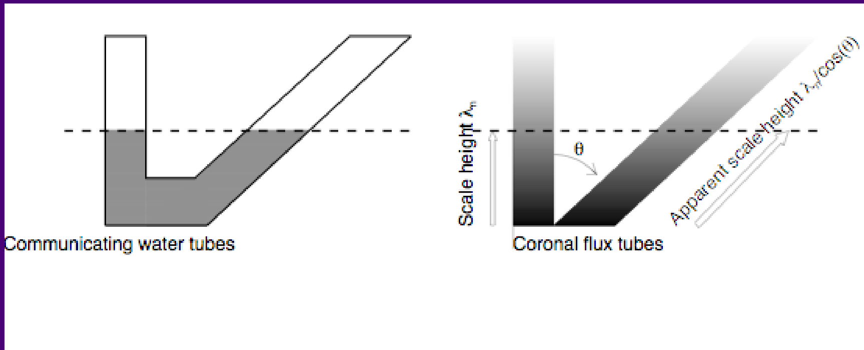

Loop #	Maximum Height h_{max} [Mm]	Curvature radius r_{curv} [Mm]	Center offset h_{curv} [Mm]	Inclination angle ϑ [deg]
1	11.6	17.0	1.2	51.3
2	10.9	19.4	0.3	56.7
3	29.8	30.5	4.3	35.7
4	30.7	30.9	10.7	42.9
5	13.0	30.6	9.6	72.8
6	26.2	38.3	13.4	58.6
7	32.3	50.2	37.6	69.0

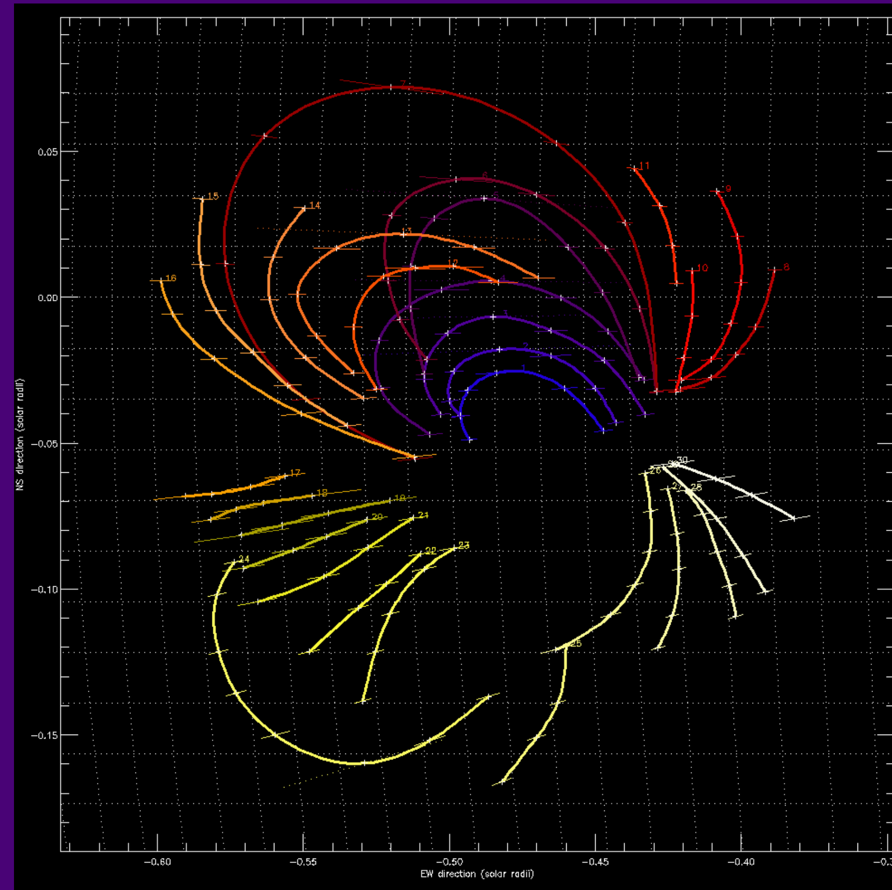

Entire loops are only visible because of the large inclination angles:

θ ~ 51 … 73 deg

so that their apex is in an altitude of less than about a hydrostatic scale height.

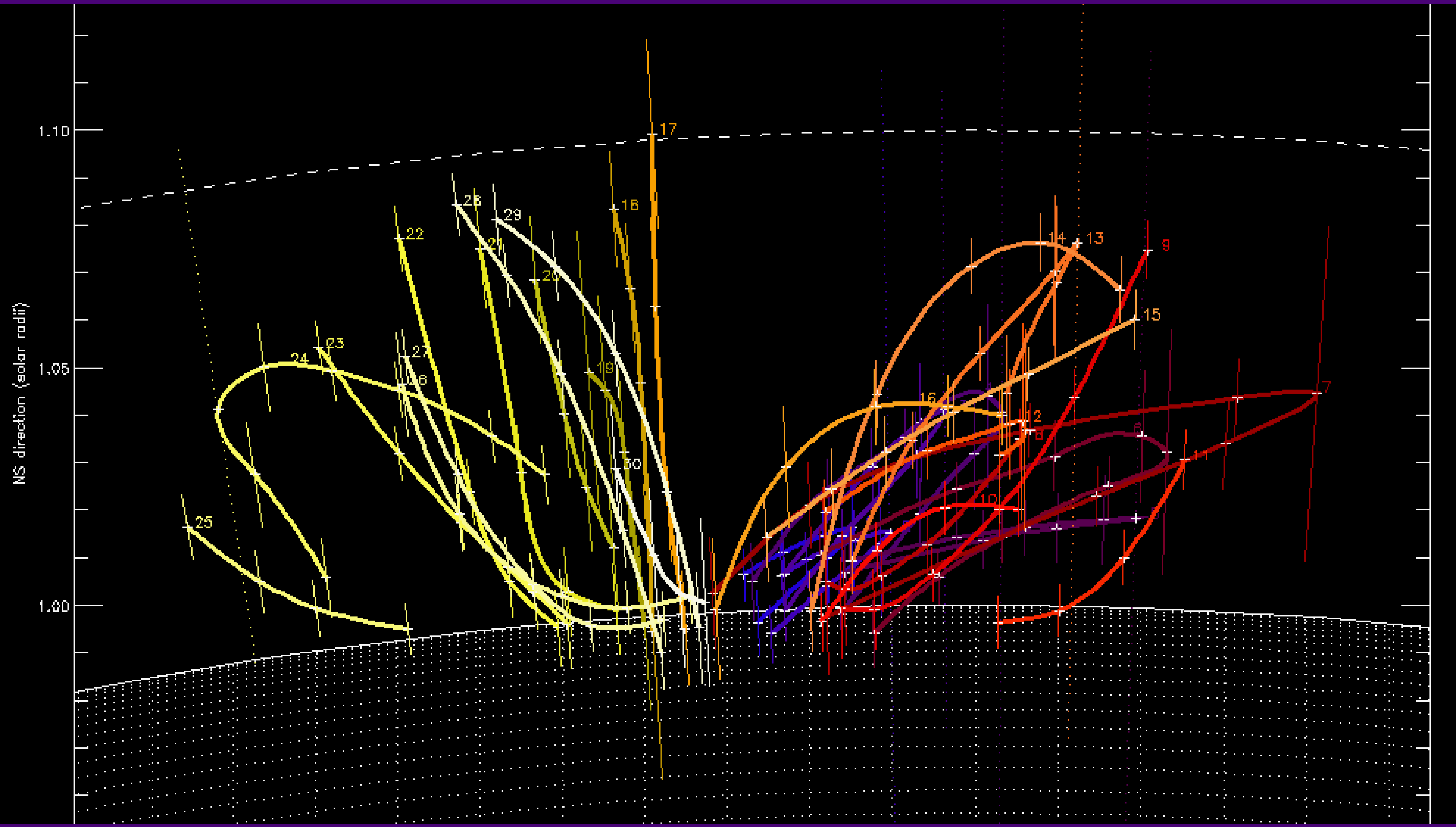

The height limit of detectable loops is given by the dynamic range of the (hydrostatic) emission measure contrast:

$$\frac{EM(h=h_{\max})}{EM(h=0)} = \exp\left(-\frac{h_{\max}}{\lambda_{EM}(T=1MK)}\right) = \exp\left(-\frac{70}{23}\right) \sim 0.05, \lambda_{EM} = \frac{1}{2}\lambda_n$$

A9) Magnetic Modeling

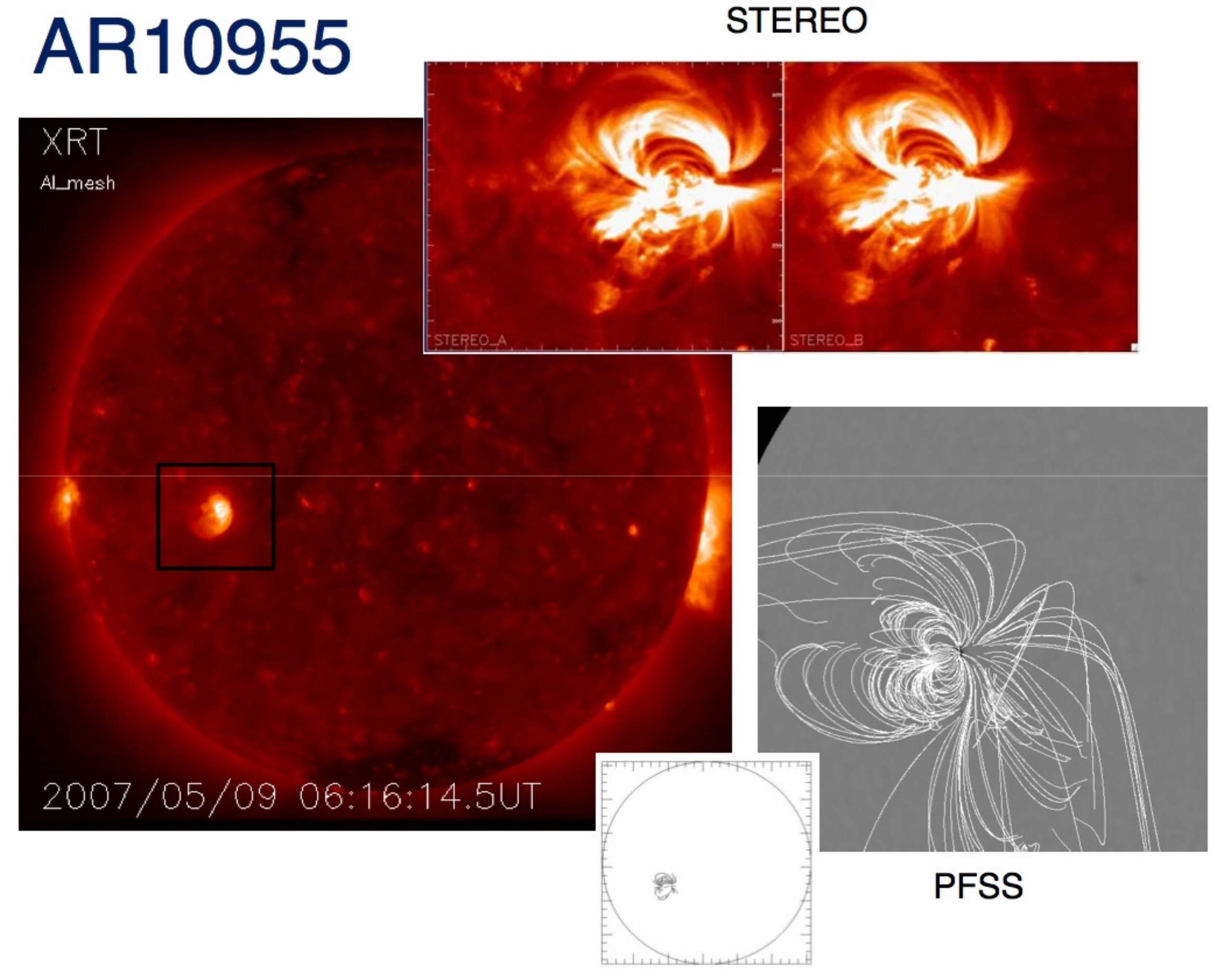

Courtesy of Allen Gary

A potential-field source surface model of AR 10955.
Goal: Minimize difference between theoretical magnetic field model and 3D geometry of EUV loops obtained from stereoscopy.

Schematic Representation of the Parametric Transformation Analysis (PTA)

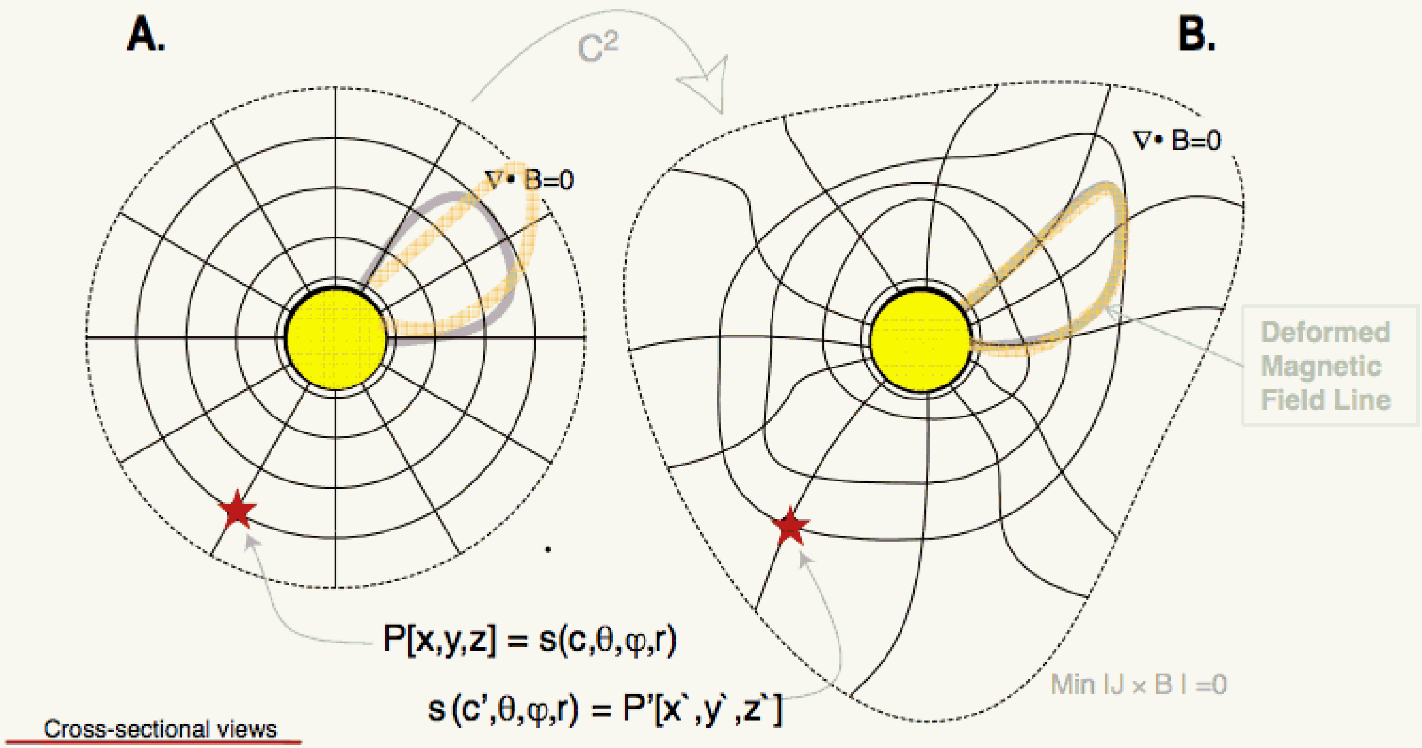

- ***The "coronal" coordinate space points ($\in$ field lines) X[x,y,z] are transformed into X'[x',y',z'].***
- ***The magnetic field is transformed into another magnetic field solution:*** **B'= J B / det(J)**
- ***The new solution is divergent free: the transformed field has C^2 continuity.***

Uniqueness constraints:

(i) The photospheric magnetic vector field

(ii) The field satisfies the observed coronal loop structure

(iii) The magnetic field minimizes the Lorentz forces in the volume

PTA conserves initial model topology, i.e., does not employ reconnection

Courtesy of Allen Gary (2007)

AR 10955
9 May 2007

PERSPECTIVES

Long=-24.92 Lat=-10.32
B0=-3.30 L0=201.39

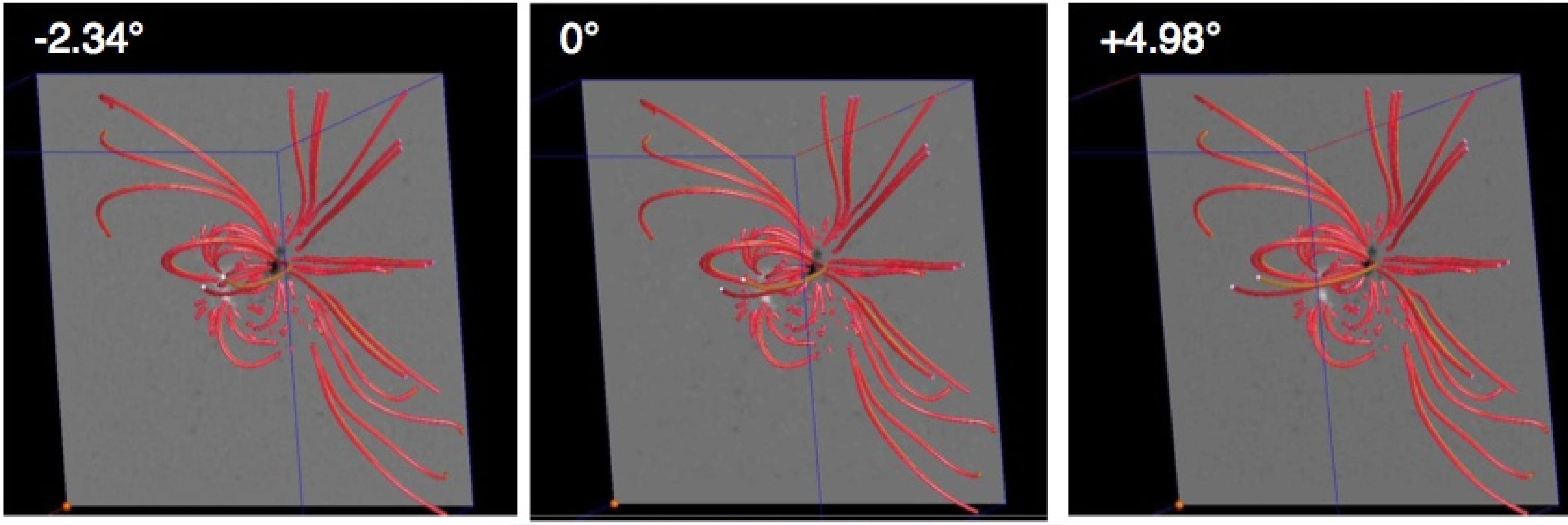

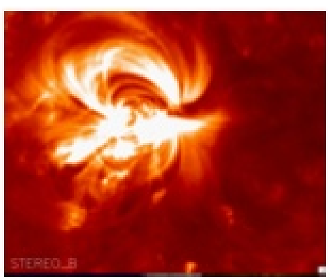

STEREO B

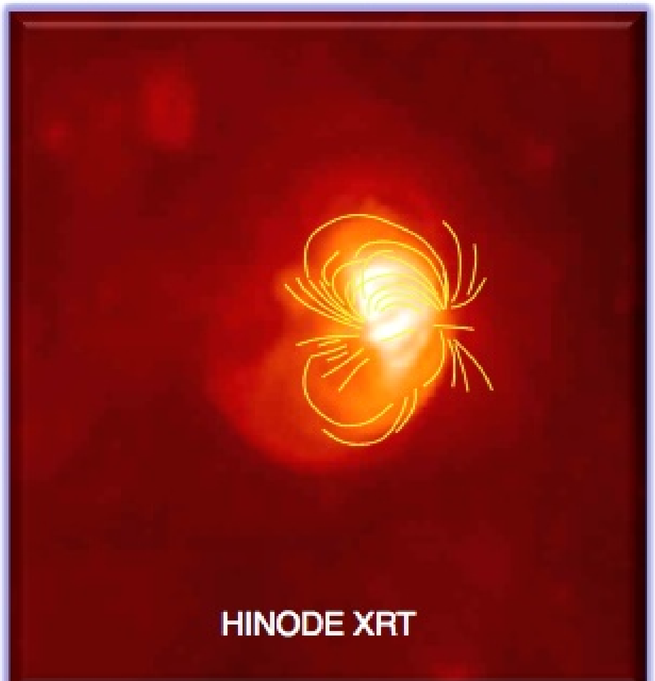

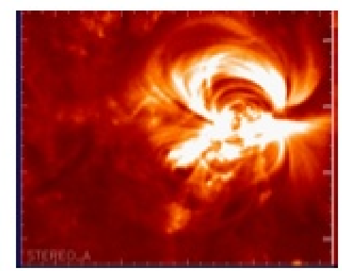

STEREO A

STEREO reconstruction
M.J. Aschwanden,
AAS, 2007

Comparison of Potential Model & Observation

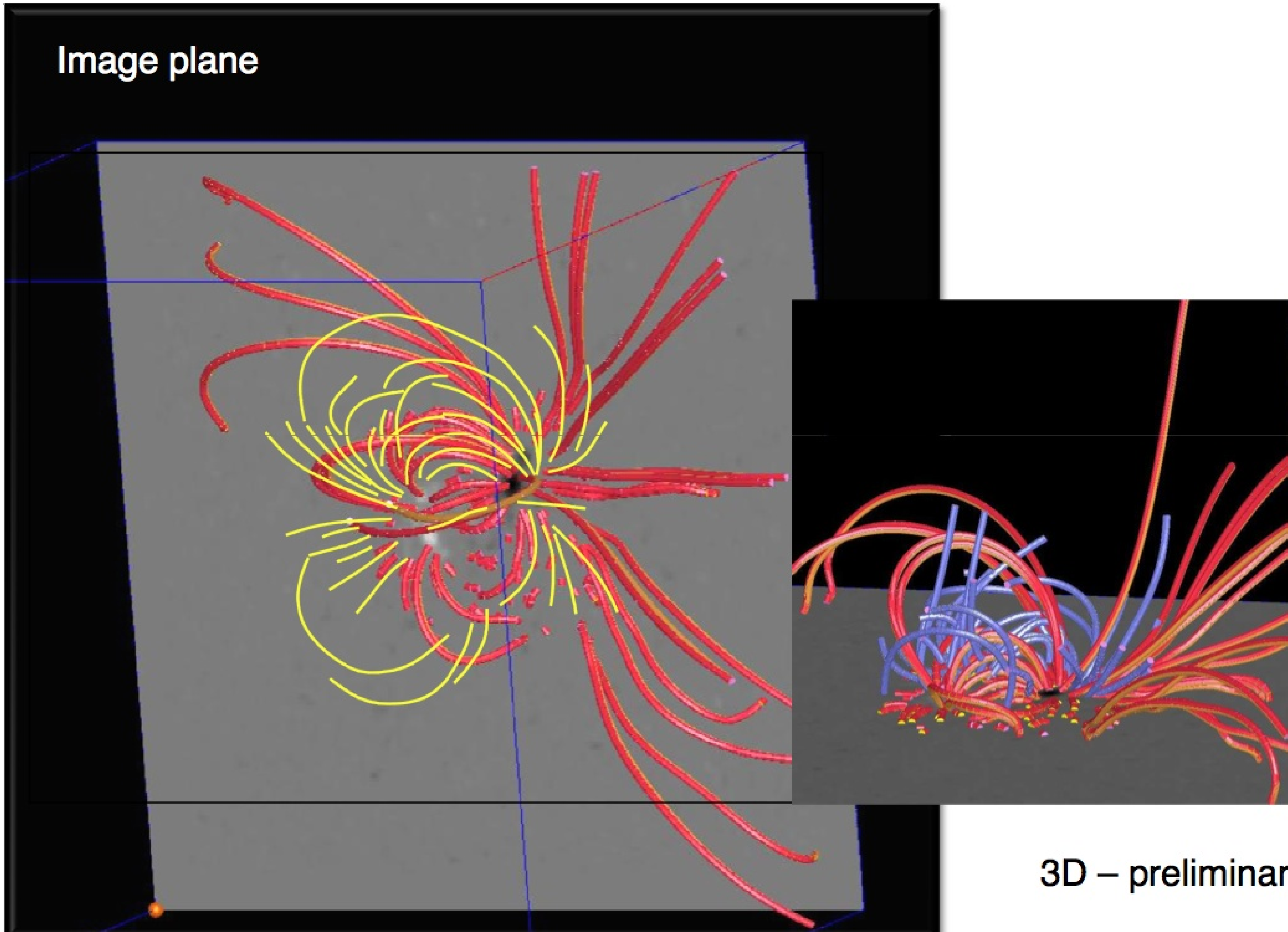

3D – preliminary

Magnetic field radial stretching method (Gary & Alexander 1999)

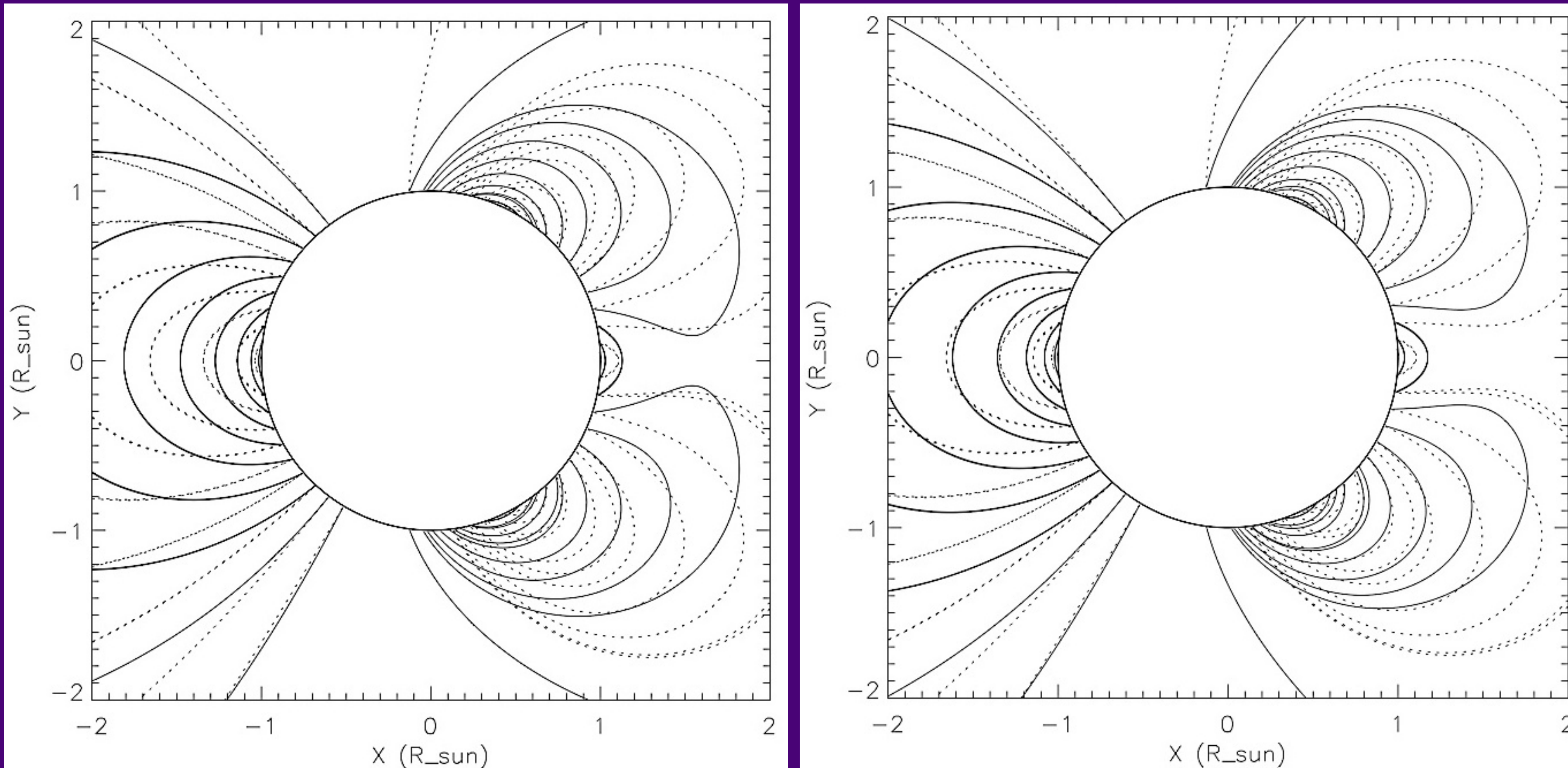

Sandman (2007; Master Thesis) -
Radial stretching of potential field model (____) to match analytical magnetostatic model (…..) of Bogdan & Low (1986)

The observed 3D magnetic field is fitted with a parametric transformation of a theoretical magnetic field model, e.g. by radial stretching of potential field solutions, a transformation that conserves the divergence-free condition.

Comparison of PTA Models & Observation

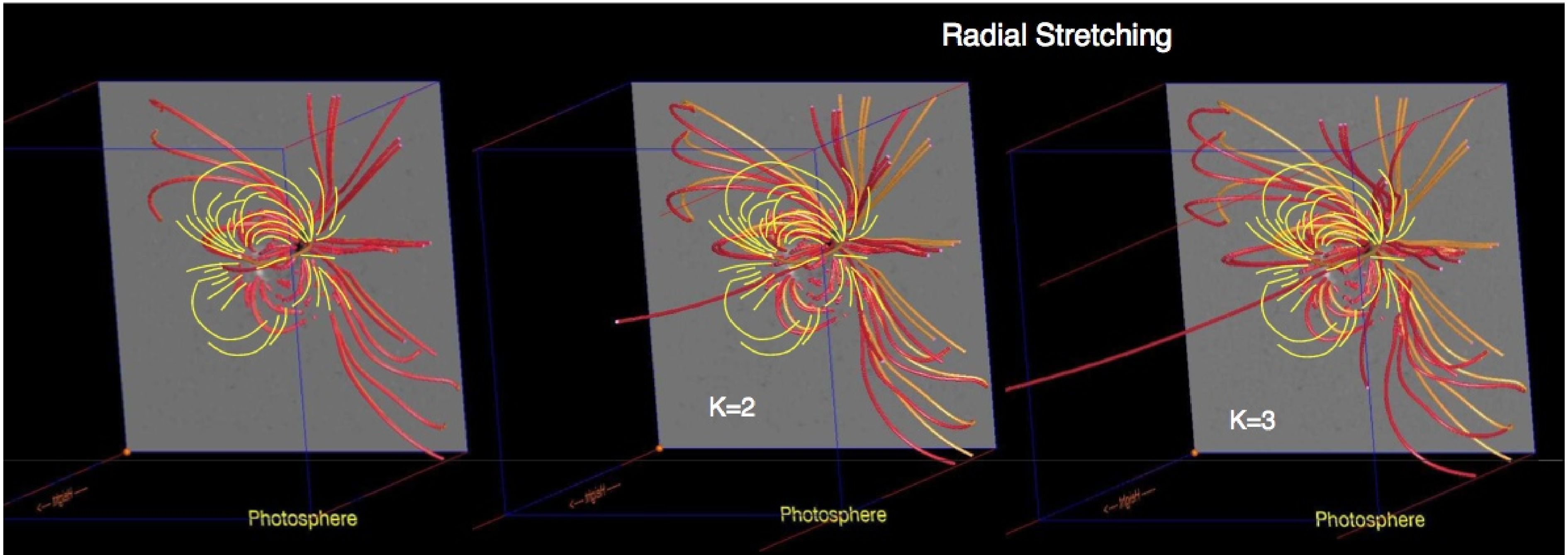

Development items to be included

1) Identify EIS/XRT loops
2) Employ vector magnetograms and NLFFF models
3) Complete L_F minimization process
4) Use STEREO results in a 3D implementation

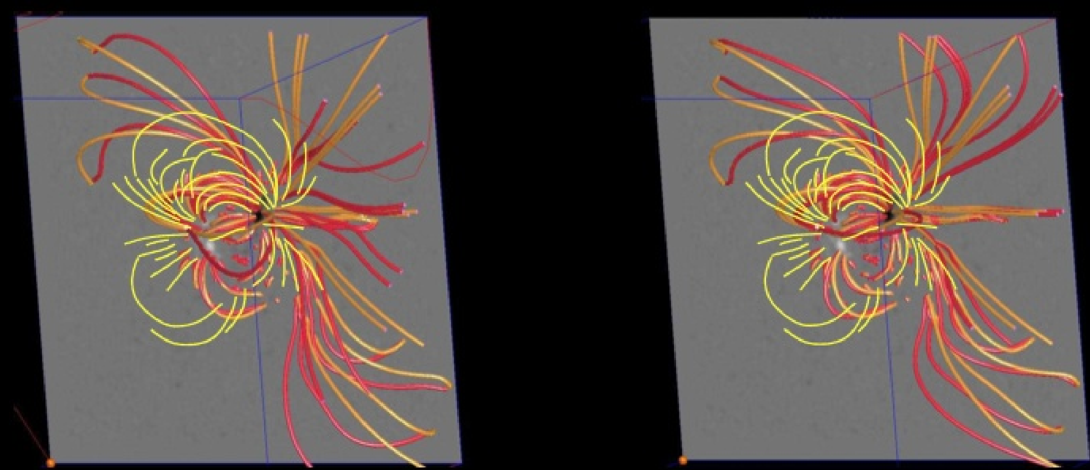

Center Twist (60°)

Longitudinal Sheared

Goal and significance of magnetic modeling:

- Minimize difference between observed 3D coordinates of loops and theoretical magnetic field extrapolation models to provide the magnetic field solution B(x,y,z). - [MHD solutions do not correct for flows, evolution of photosphere, source surface, reconnection, heating, etc.)

- Improves magnetic field energy calculation $$E_B = \left(\frac{1}{8\pi}\right)\iiint_V B^2(x,y,z)\,dxdydz$$

- Provides the magnetic current density $$j = \left(\nabla \times B\right)/\mu$$

- Allows the Lorentz forces and cross-field current density to be calculated $$L_F = j \times B = (\nabla \times B) \times B/\mu$$

- Determines the necessary pressure gradients to balance Lorentz forces. $$(\nabla \times B) \times B/\mu = \nabla p + \rho \nabla \psi$$

- Snap-shots the dynamic evolution B(x,y,z,t) of non-forcefree magnetic field in AR.

Contents :

(A) Triangulation and 3D reconstruction of active region loops
- A1) Image coalignment
- A2) Triangulation and 3D geometry
- A3) Image highpass filtering & loop definition
- A4) Loop tracing
- A5) Stereoscopic 3D coordinates and error of z(x,y)
- A6) Loop inclination, coplanarity, & circularity
- A7) Hydrostatic modeling
- A8) Magnetic modeling

(B) Outlook for 3D reconstruction of other EUV phenomena
- B1) Moss
- B2) Filaments and prominences
- B3) CMEs

Conclusions

B1) Moss structure

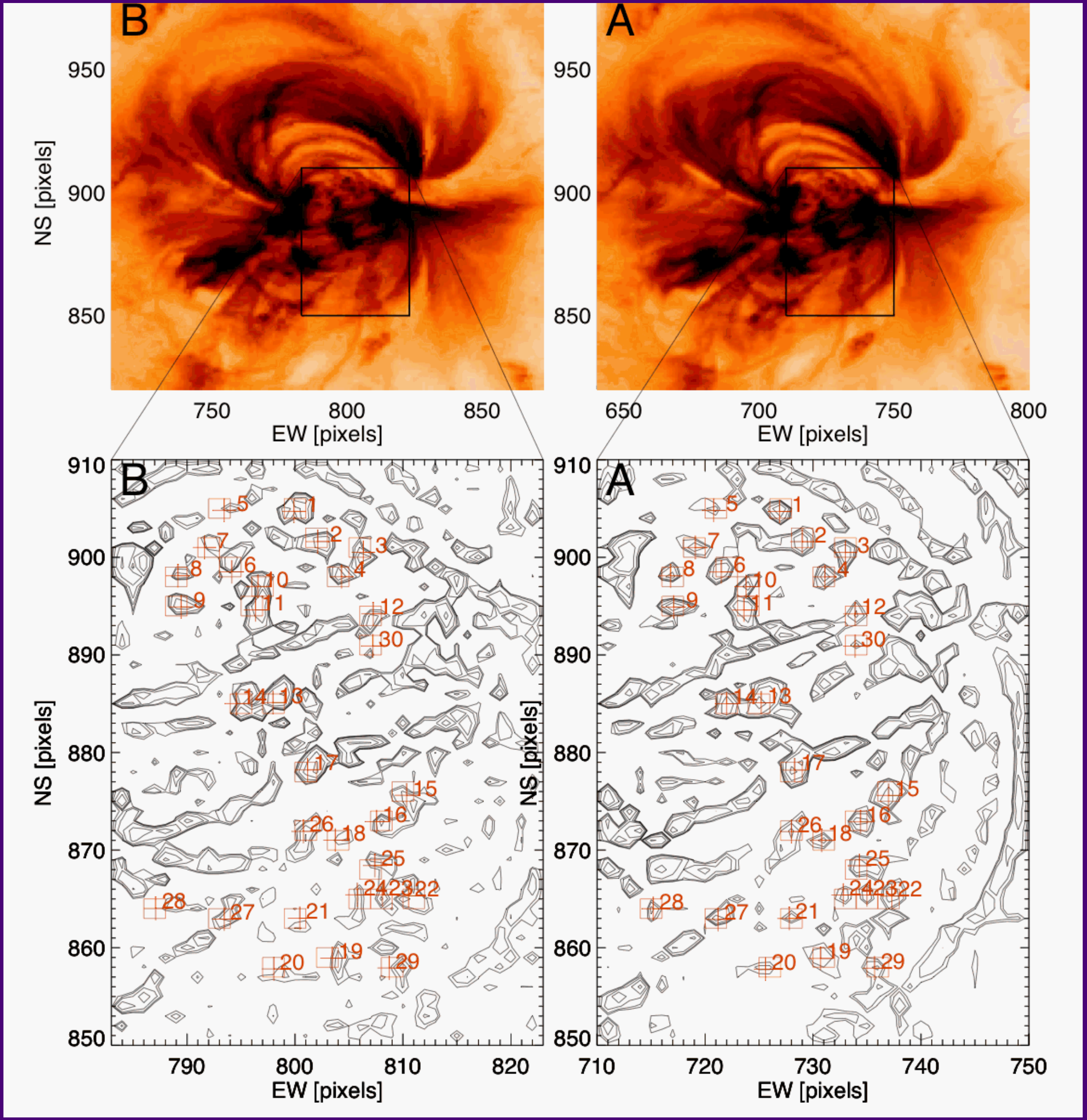

Stereoscopic correlation of 30 moss features yields a height distribution of:

$\langle h_{moss} \rangle = 1.2 \pm 2.8$ Mm

Estimated error of height stereoscopic measurement (if unresolved):

$\sigma_h = 3.8$ Mm

Moss is the footpoint TR zone (T~1MK) of hotter loops (T>2 MK)

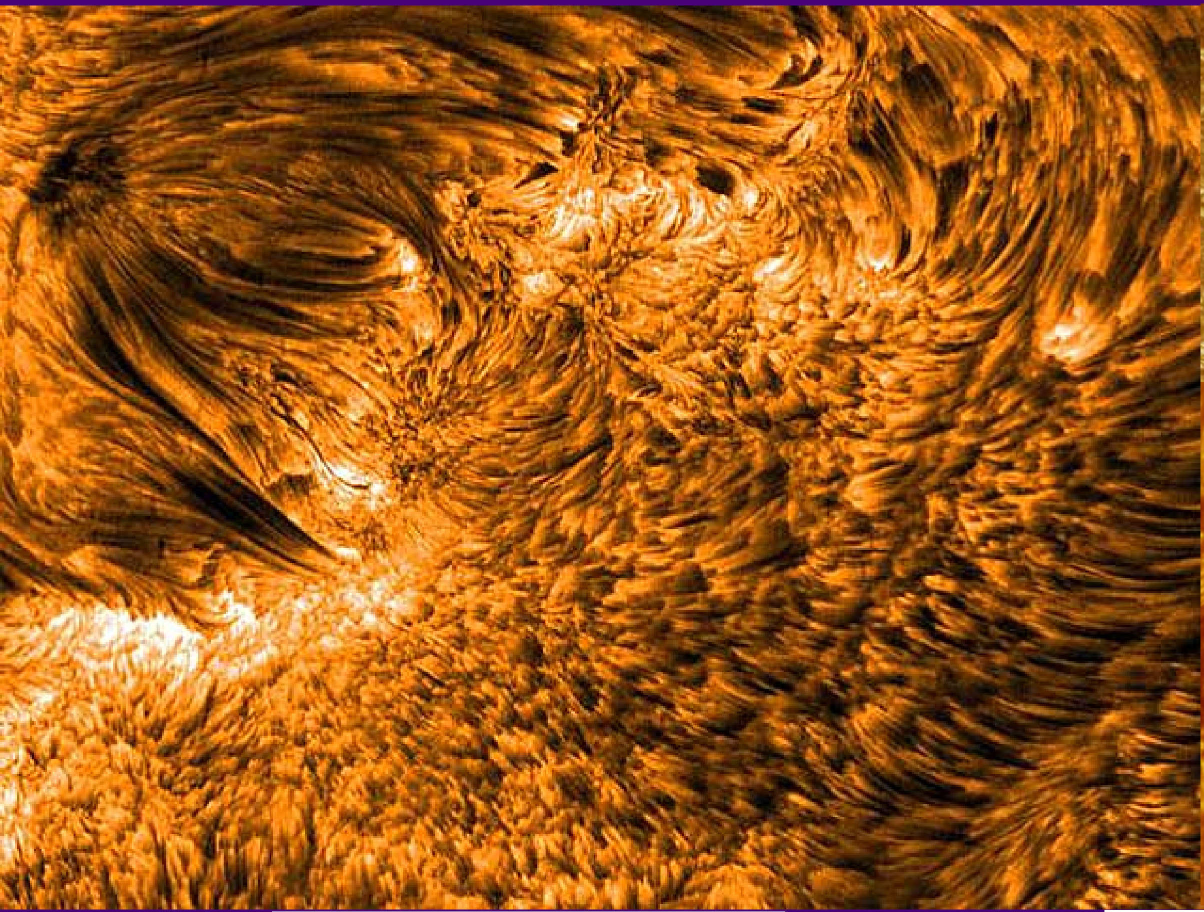

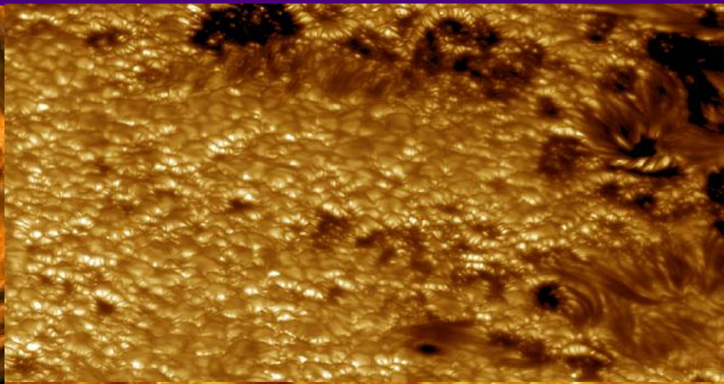

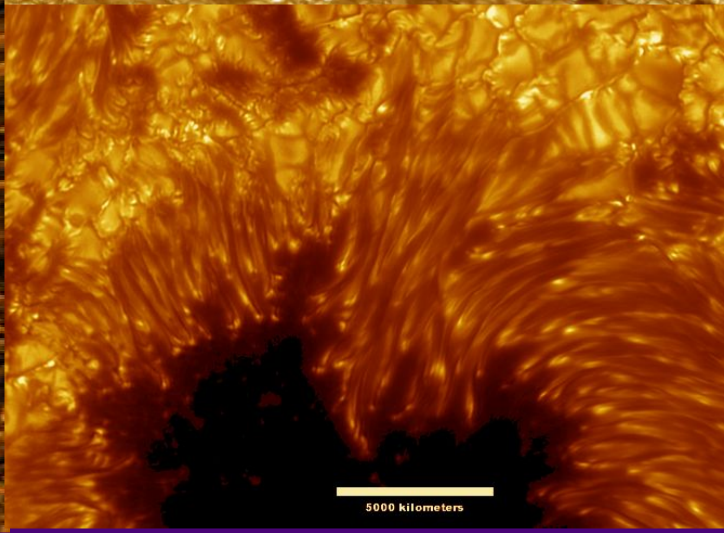

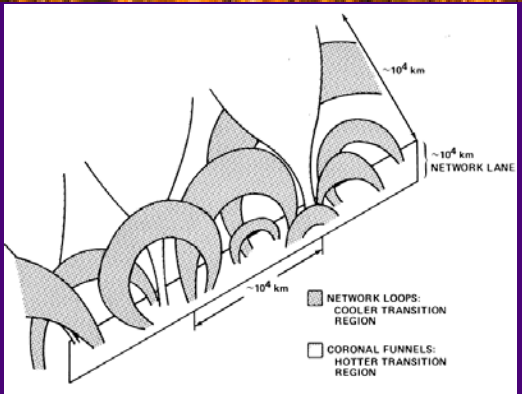

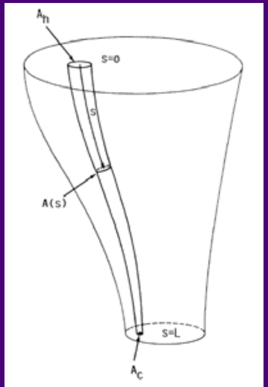

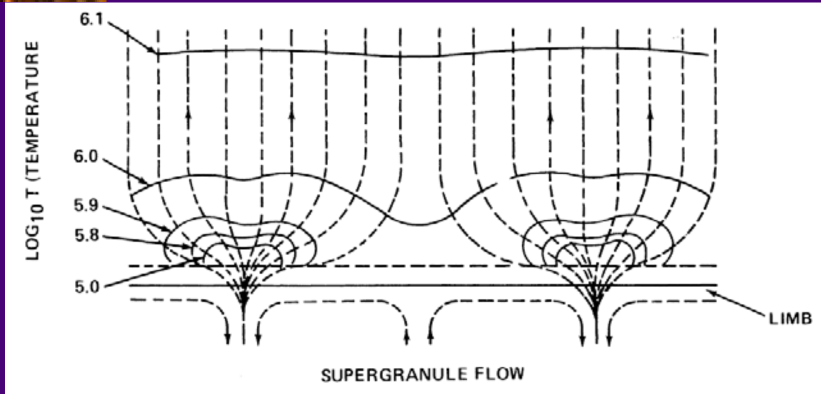

Stereoscopic probing of the transition region at h~1-4 Mm:

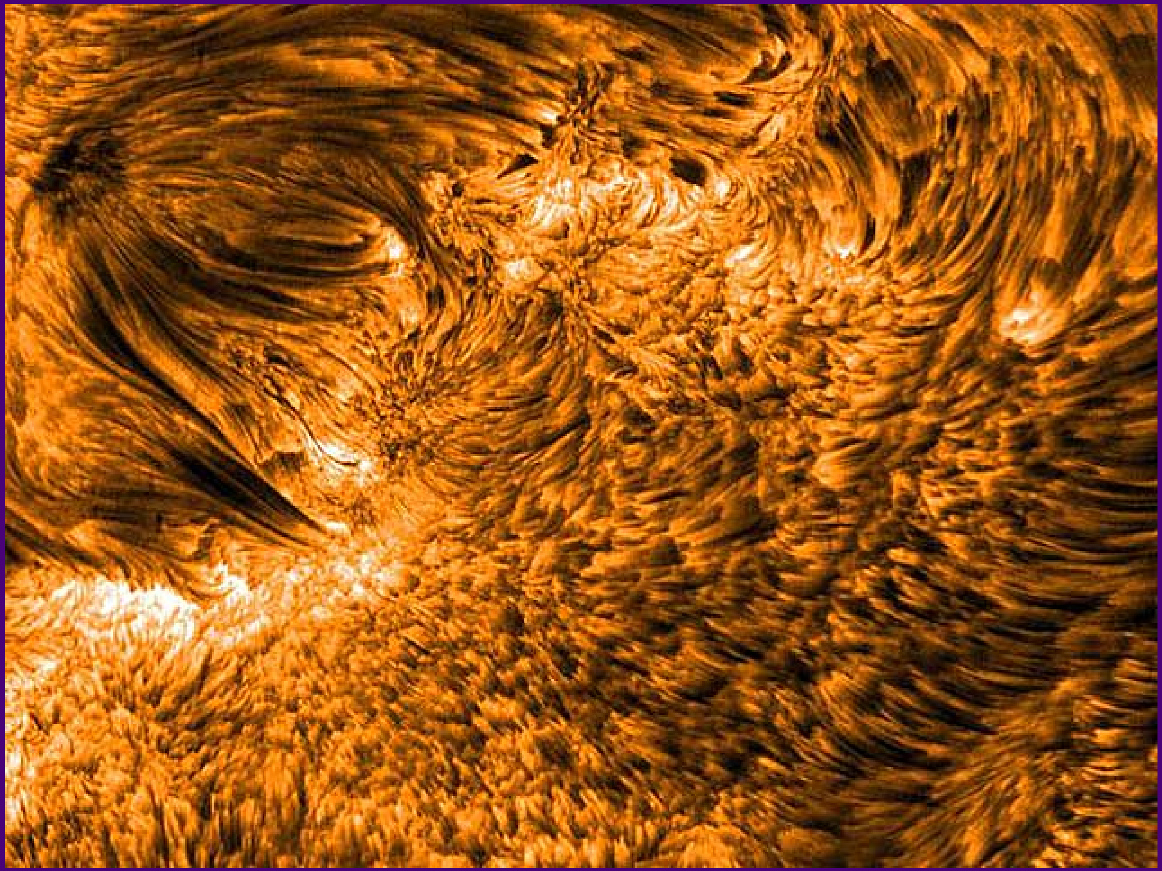

Swedish 1-m Solar Telescope at La Palma, Spain

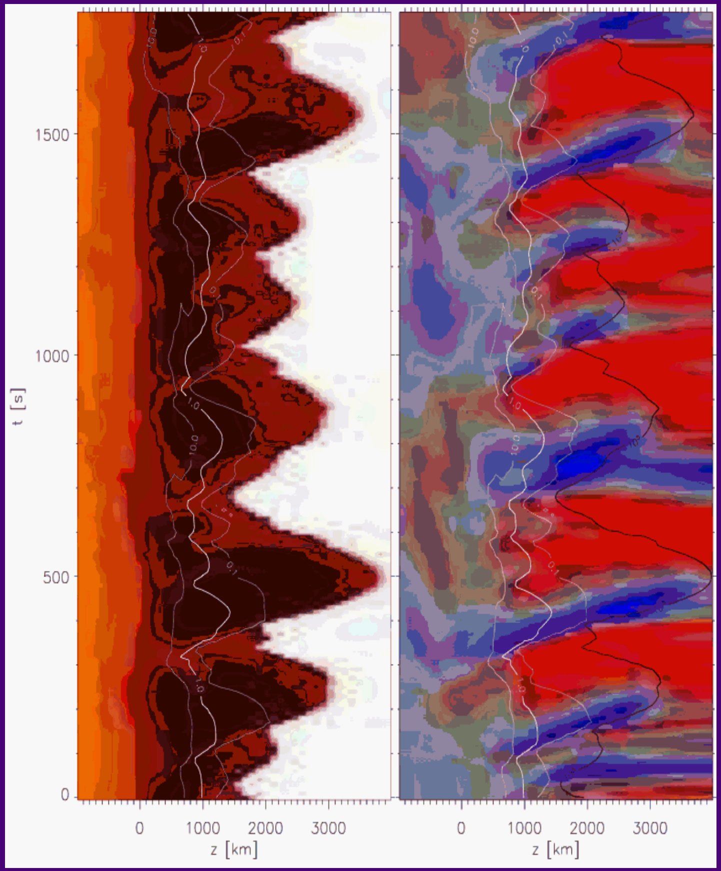

DePontieu et al. (2007, ApJ 655, 624)

High-resolution Ha images reveal for the first time, spatially and temporally resolved dynamic fibrils in active regions. These jet-like features are similar to mottles or spicules in the quiet-Sun. Their 3D structure can be reconstructed from the parabolic path trajectory of chromospheric shock waves, which can be reproduced by radiative MHD simulations (right frame).

B2) Filaments and Prominences

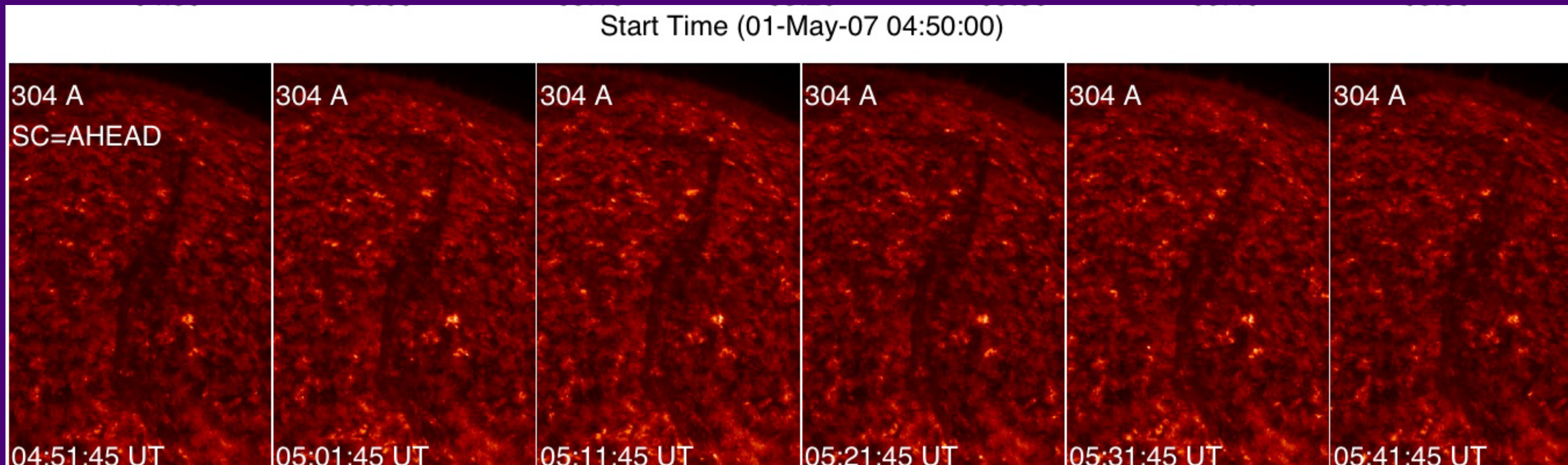

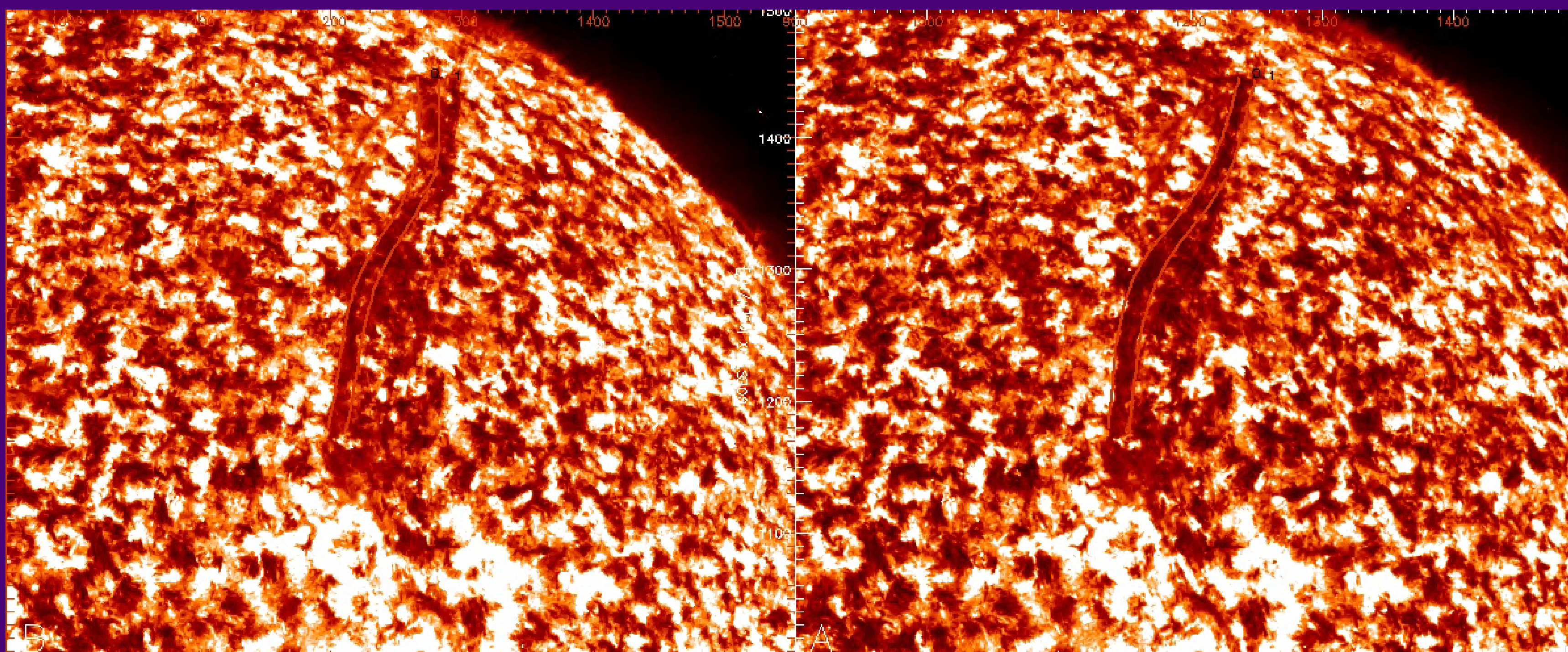

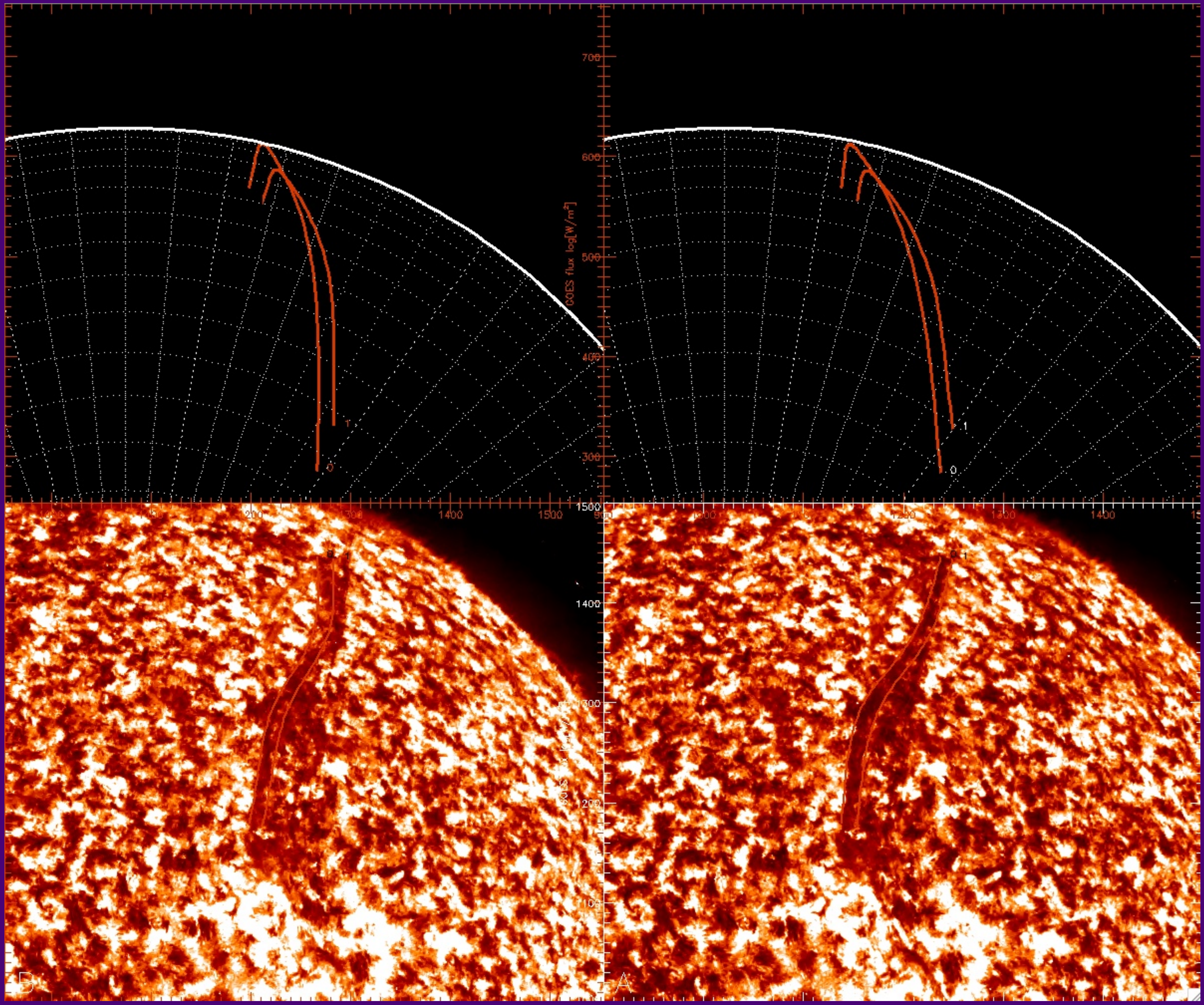

Stereoscopic correlation depends on identification of corresponding edges

Projections [x,y],[x,z],[y,z]

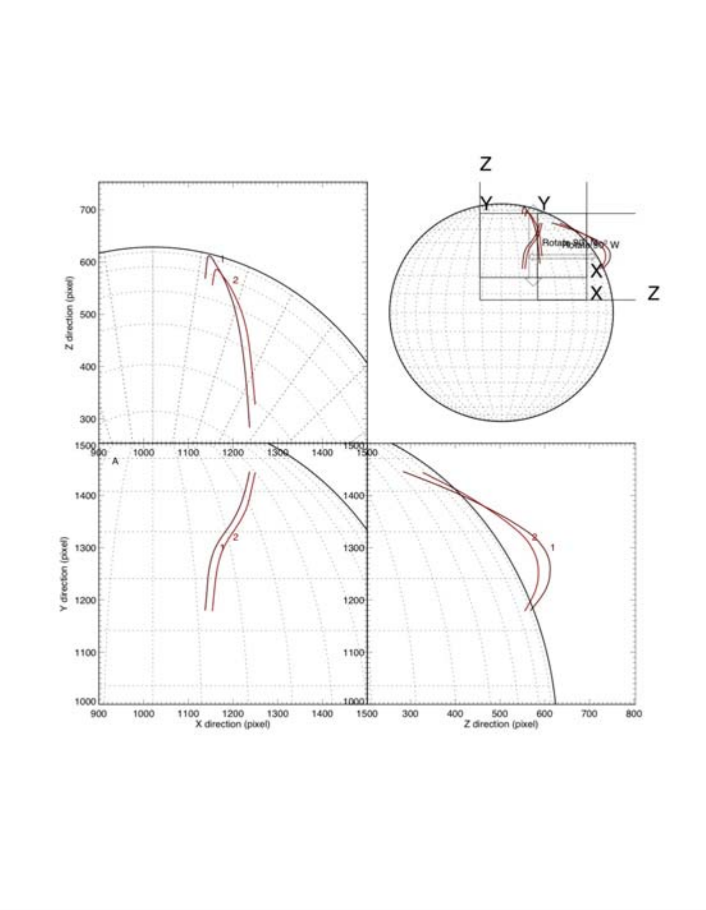

Limb view from 70^0 E

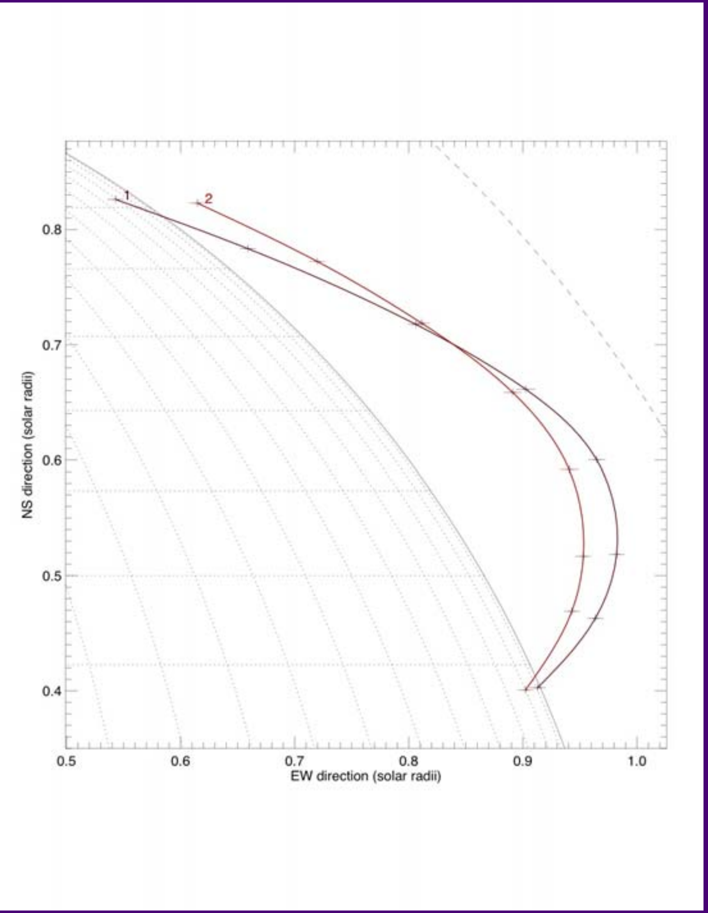

Stereoscopic height error of curvi-linear feature is small, but identification of corresponding curvi-linear features in A and B bears some uncertainty.

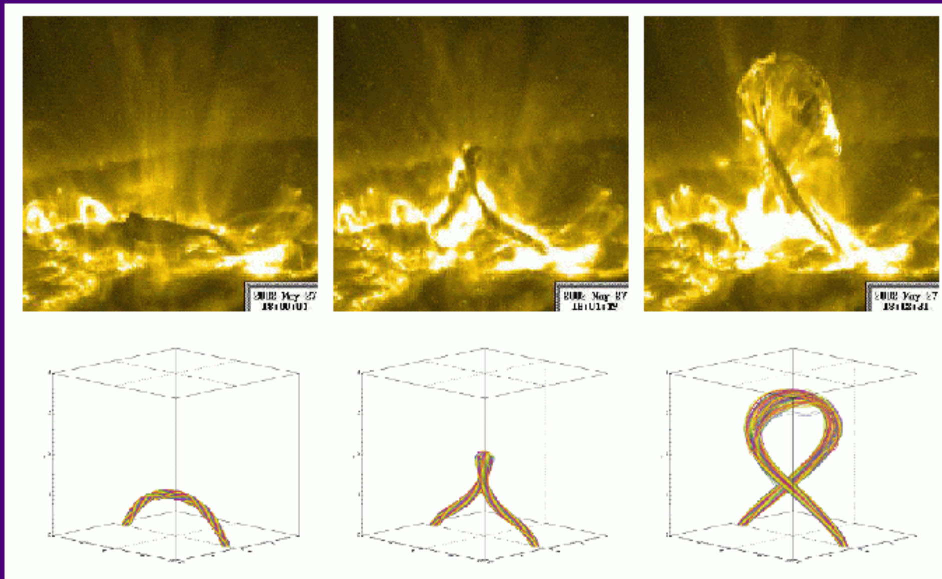

Figure 9. **Top:** TRACE 195 Å images of the confined filament eruption on 2002 May 27. The right image shows the filament after it has reached its maximum height. **Bottom:** magnetic field lines outlining the kink-unstable flux rope reproduced with 3D MHD simulations (Török & Kliem 2004).

Torok & Kliem (2004)

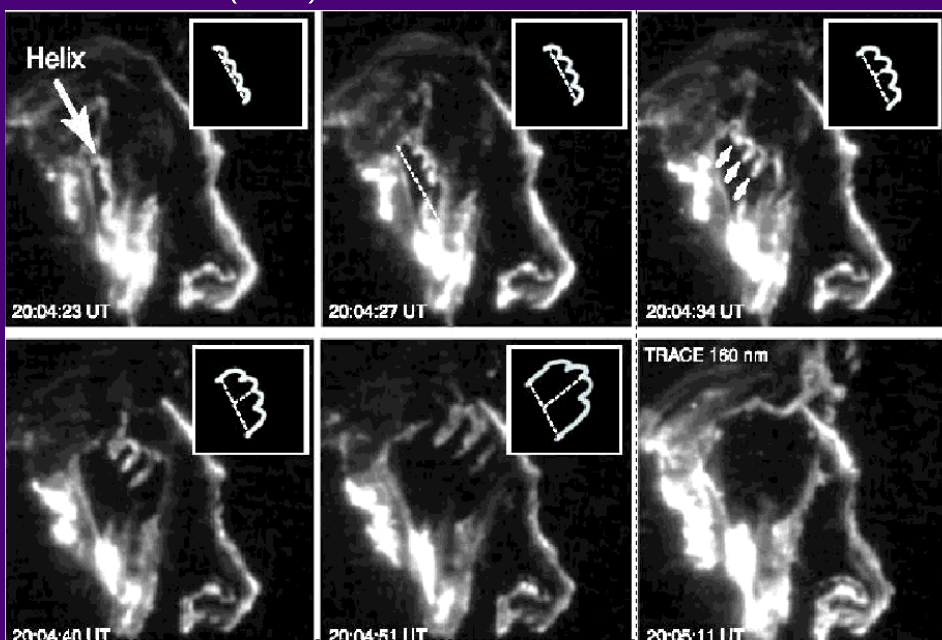

Gary & Moore (2004)

Identification of CME drivers: Sigmoids and Fluxropes

Twisted magnetic field lines become unstable to the kink-mode instability at >1.5 turns

→filament eruptions
→confined eruptions

Helicity of sigmoidal loops and eruptive filaments can predict helicity of Interplanetary fluxrope

→CME magnetic field
→geoeffective predictions

B3) CMEs

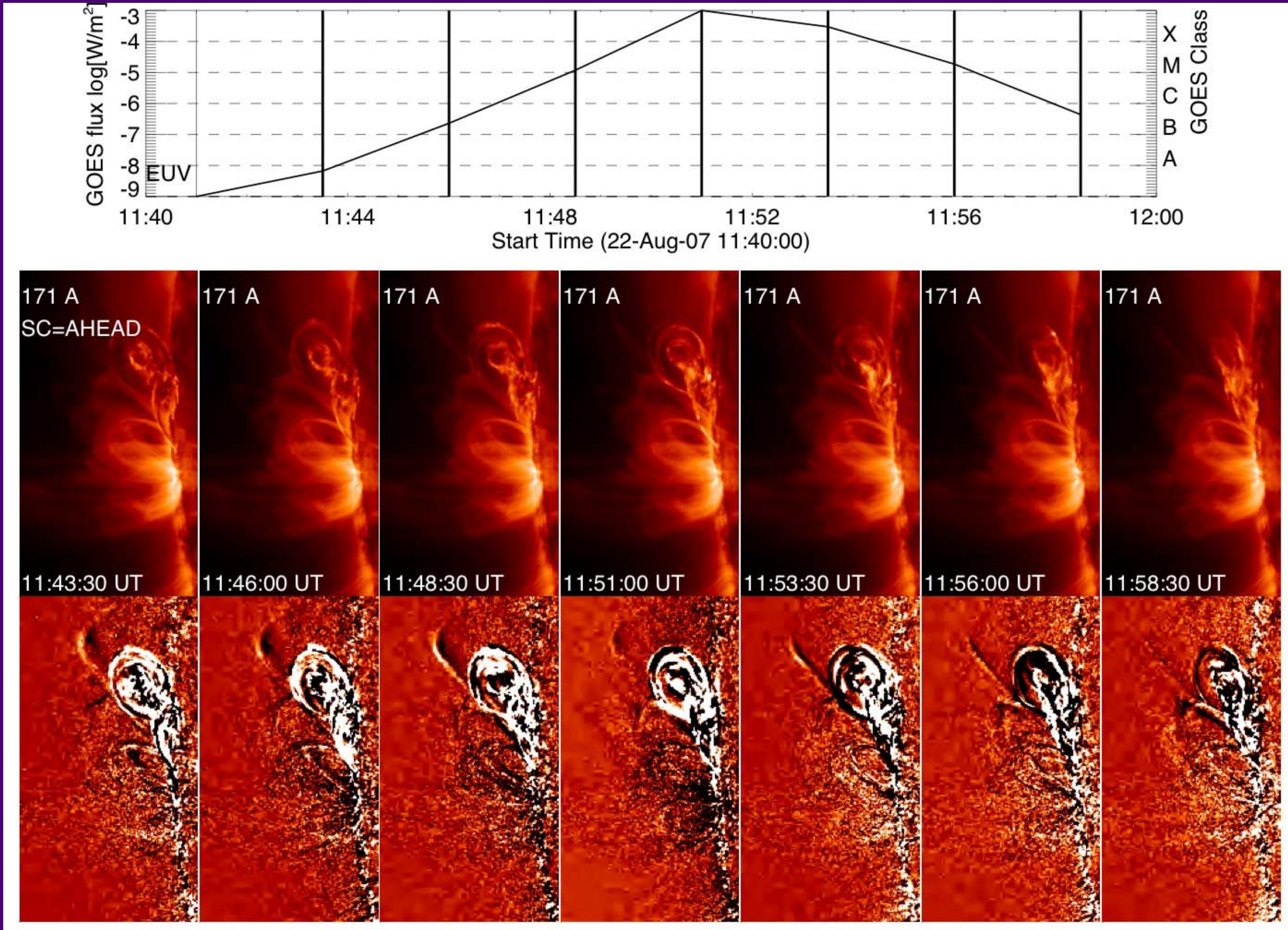

GOES flux log[W/m²]
-3
-4
-5
-6
-7
-8
-9
EUV
X
M
C
B
A
GOES Class
11:40
11:44
11:48
11:52
11:56
12:00
Start Time (22-Aug-07 11:40:00)
171 A
SC=AHEAD
11:43:30 UT
171 A
11:46:00 UT
171 A
11:48:30 UT
171 A
11:51:00 UT
171 A
11:53:30 UT
171 A
11:56:00 UT
171 A
11:58:30 UT

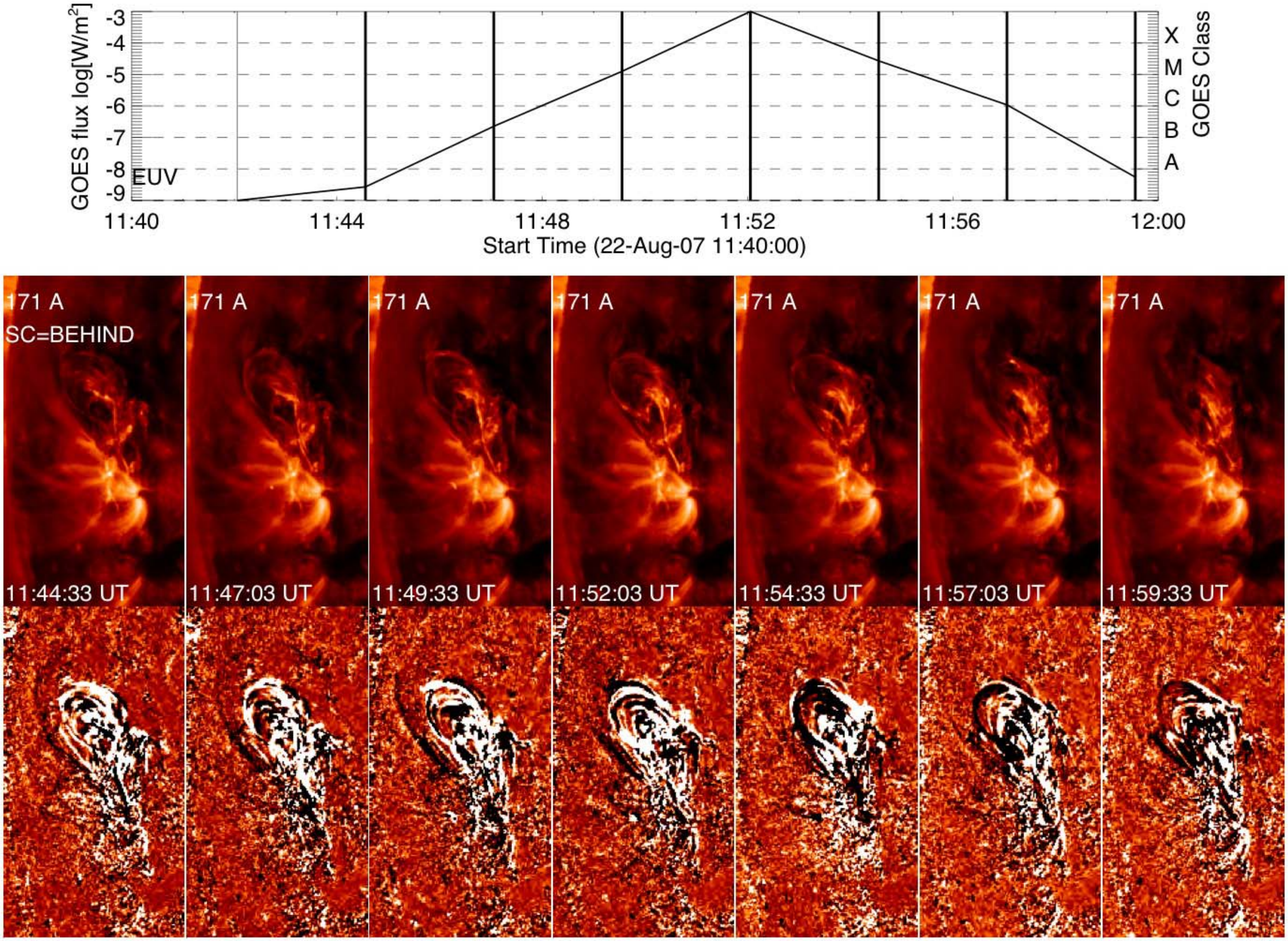

GOES flux log[W/m²]
-3
-4
-5
-6
-7
-8
-9
EUV
X
M
C
B
A
GOES Class
11:40
11:44
11:48
11:52
11:56
12:00
Start Time (22-Aug-07 11:40:00)
171 A
SC=BEHIND
11:44:33 UT
11:47:03 UT
11:49:33 UT
11:52:03 UT
11:54:33 UT
11:57:03 UT
11:59:33 UT

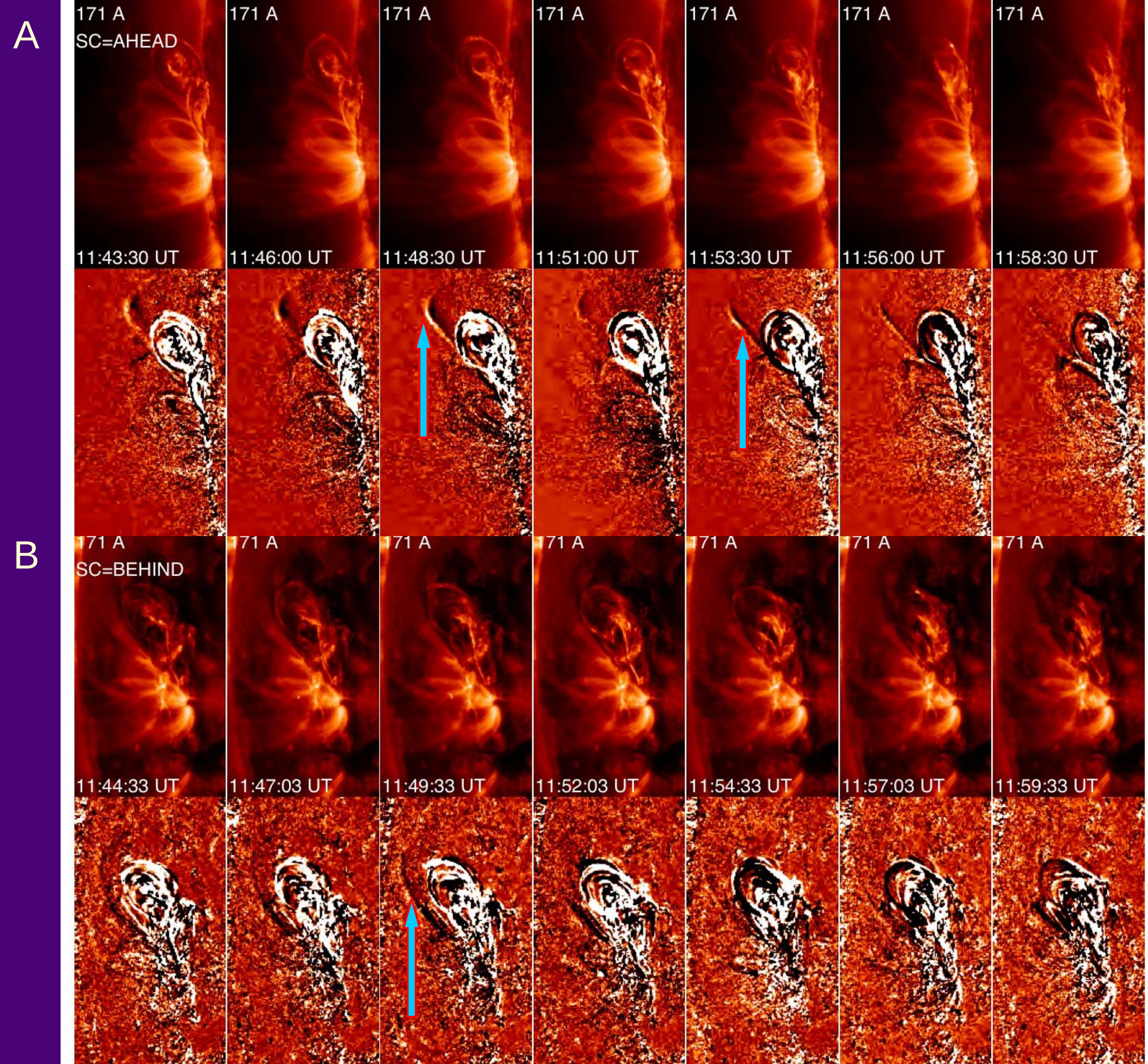

Does an untwisting fluxrope drive an eruption or CME ?

Erupting parts

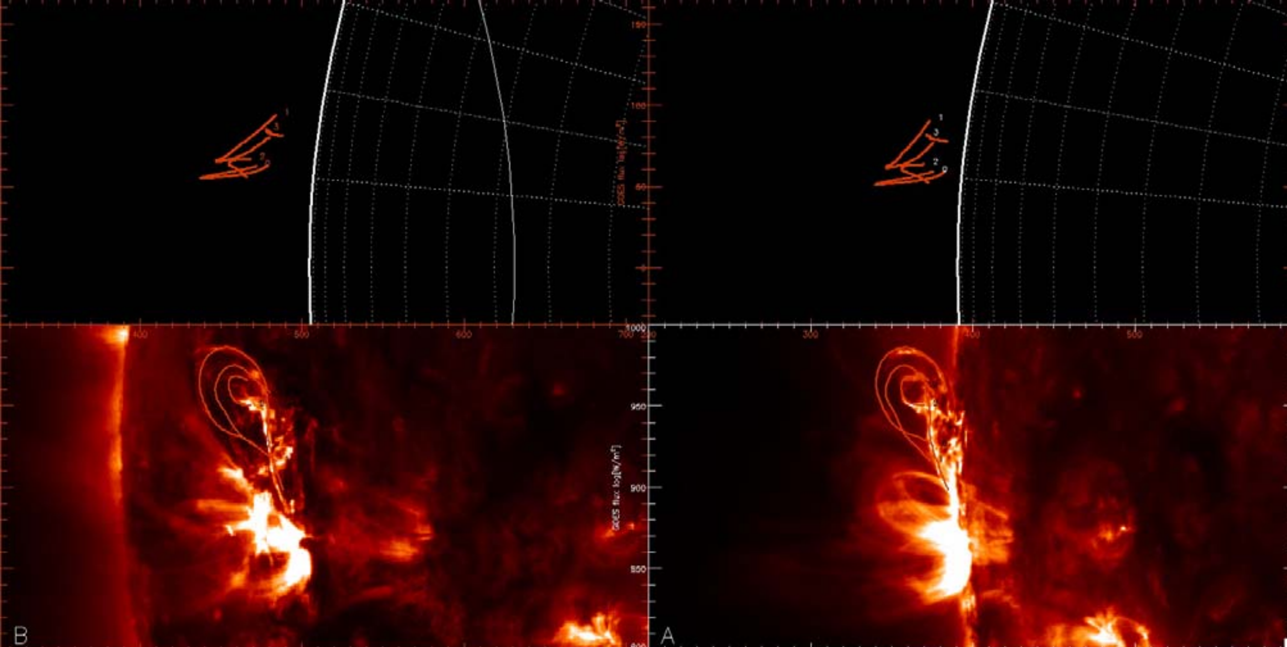

3D reconstruction shows geometry of twisted field lines relative to the horizontal filament

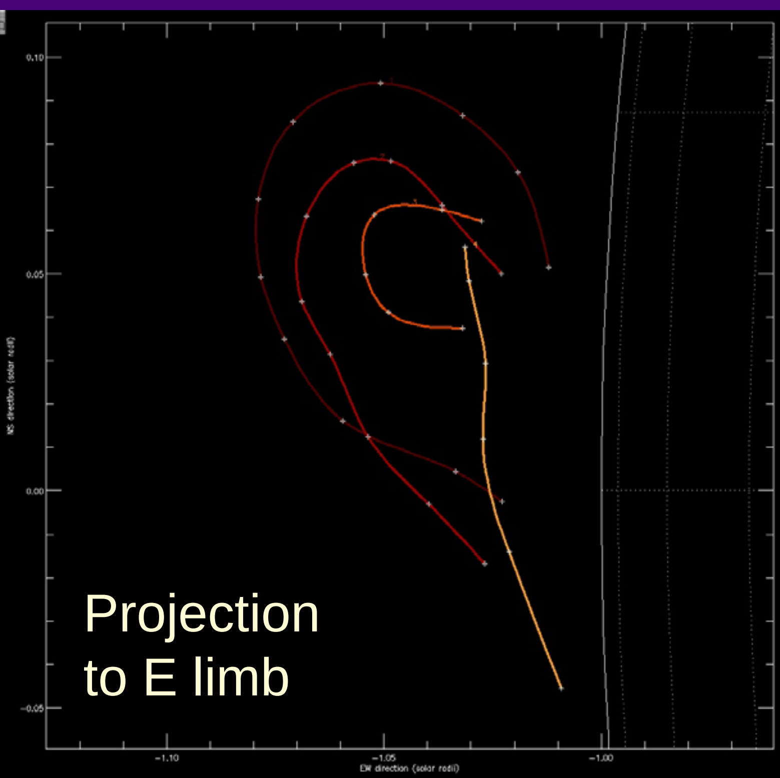

Projection to E limb

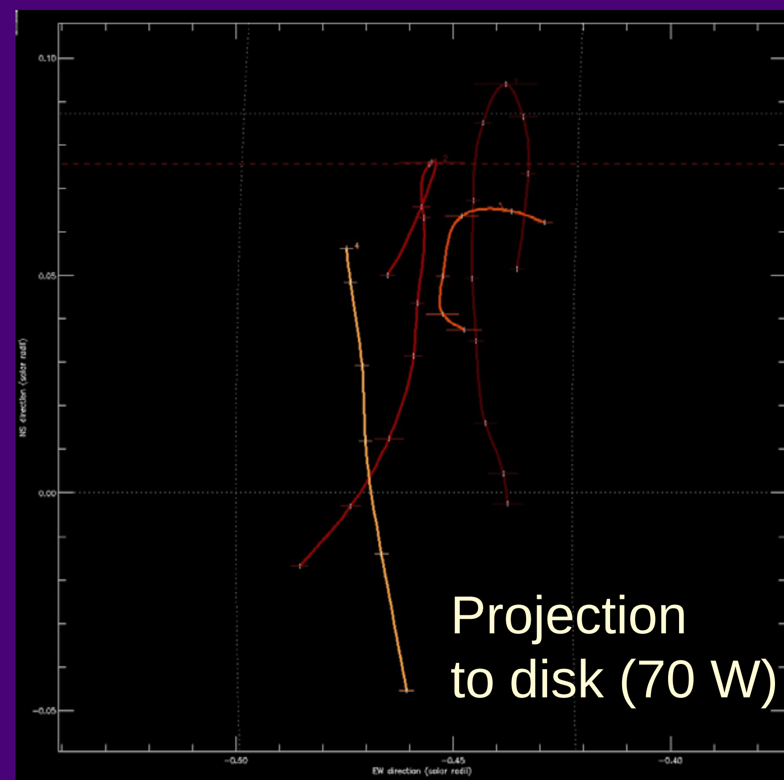

Projection to disk (70 W)

Goal: Disentangling the 3D geometry of twisted CME structures

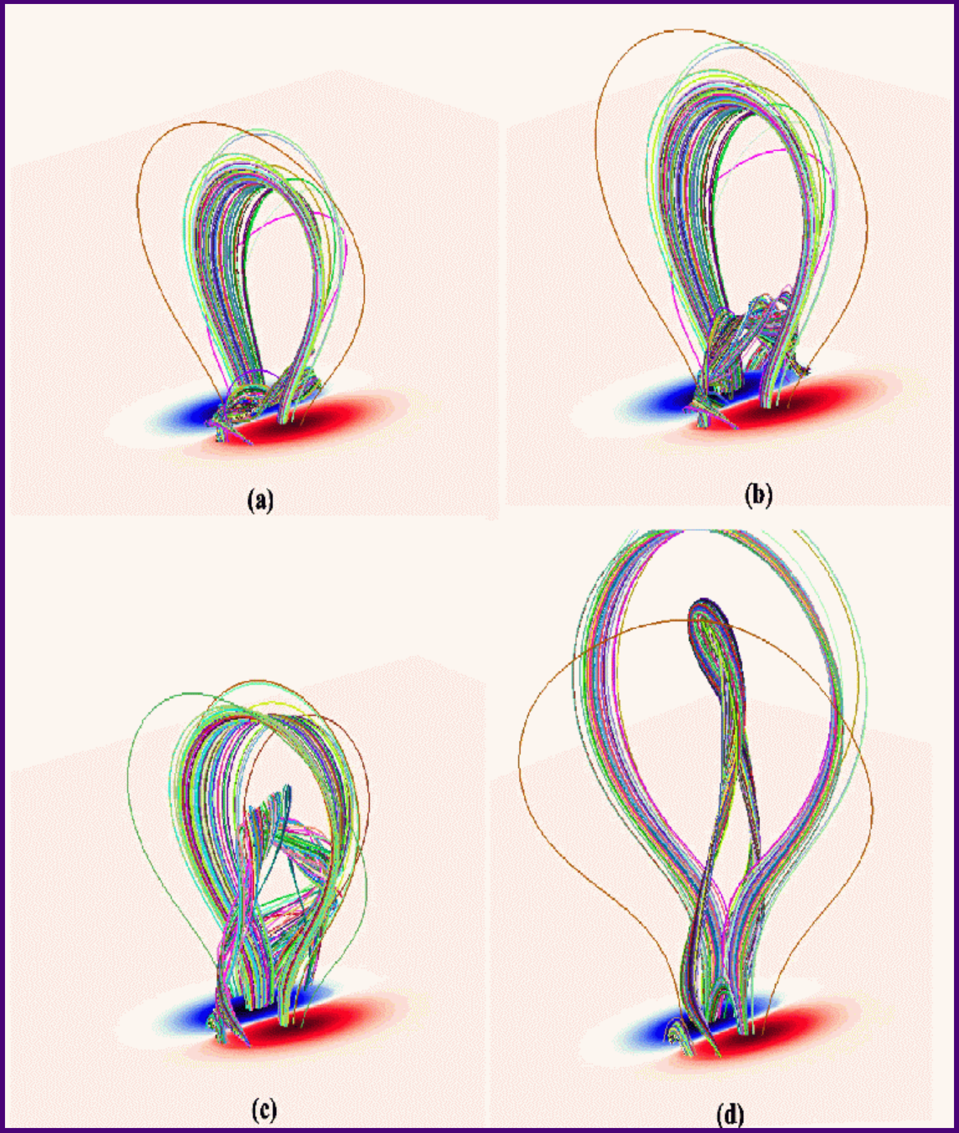

Amary et al. (2003)

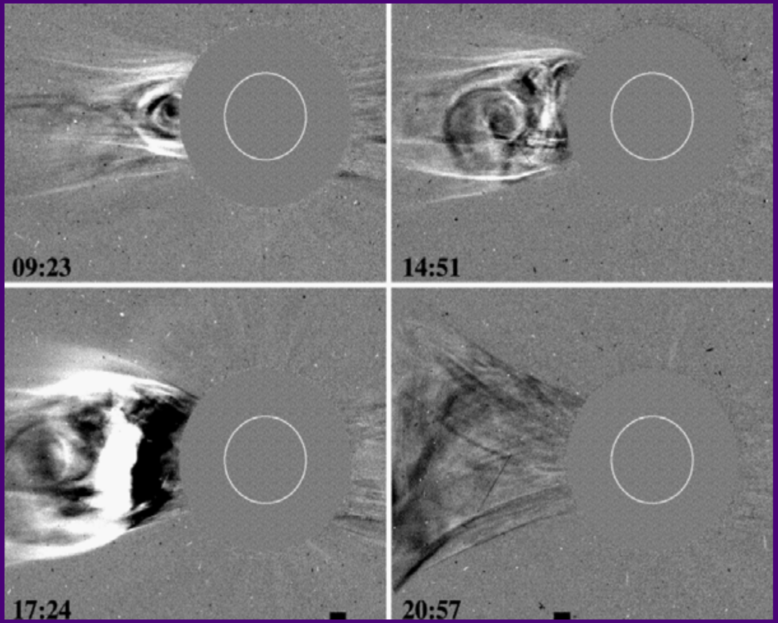

Dere et al. (1999)

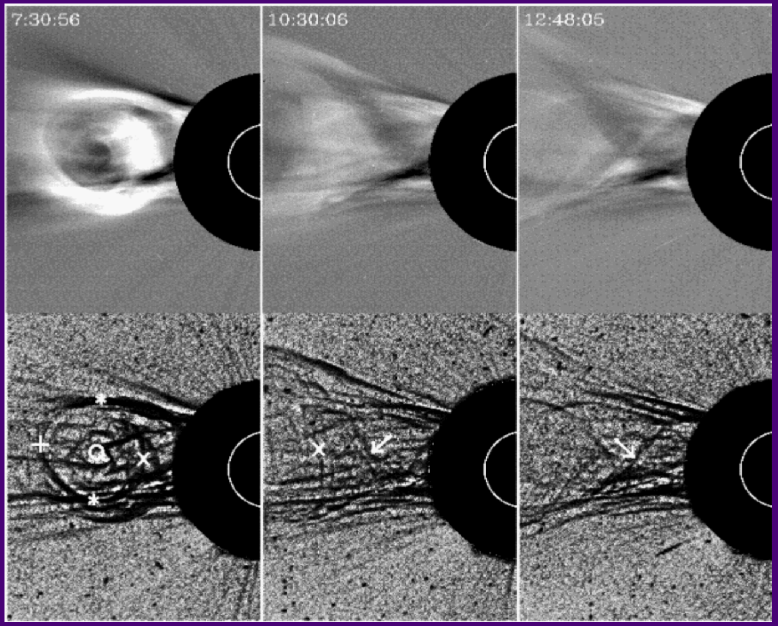

(Wood et al. 1999)

Conclusions:

(1) 2007 is the prime mission time for classical stereosocopy with small separation angles ($<40^0$). EUVI image quality is excellent and coalignment is known with subpixel accuracy.

(2) Stereoscopic triangulation of an active region on 2007-May-9 provided the 3D loop coordinates [x,y,z] of 7 complete AR loops and 23 incomplete loop segments. Maximum height of detectable loops restricted by hydrostatic scale height ($<0.1\ R_0$). Complete loops have either small curvature radius or large inclination angle. Inclination angles: 35^0-73^0, loop circularity $R(s)/R_{curv} \sim 0.8$-1.3, loop coplanarity $y_{perp}/R_{curv} < 0.13$. Future physical modeling:

- Magnetic field modeling (param.transforms, radial stretching)
- Hydrodynamic modeling (press.scale height, non-equilibrium)

(3) Moss height $h=1.2 \pm 2.8$ Mm (hydrostatic modeling of TR in hot loops)

(4) Filaments threads: 3D geometry measurable with stereoscopy

- Measurement of twist, helicity, and kink instability criterion

(5) CME topology derivable from 3D stereoscopy of erupting filaments.

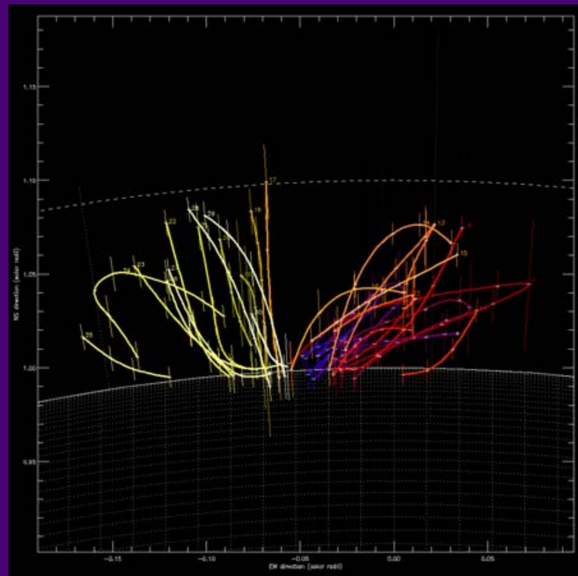

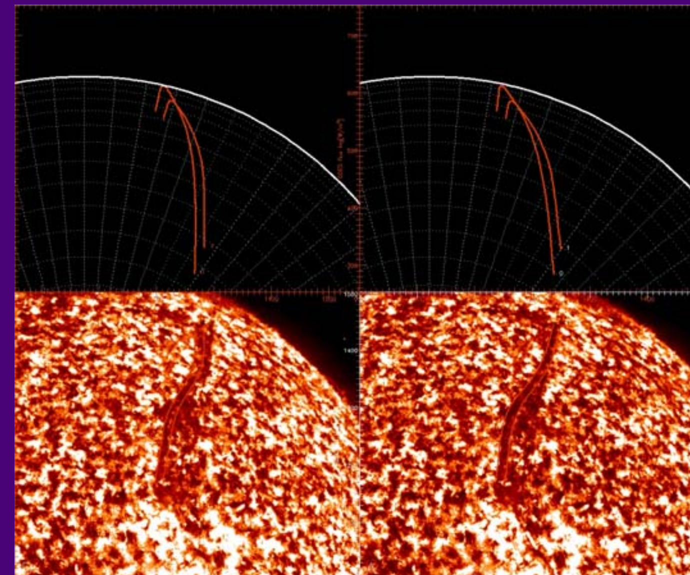

http://www.lmsal.com/~aschwand/ppt/2007_STEREO_SWG_Pasadena.ppt